# Quantum dots for multiplexed biological imaging


UNIVERSITY *of the*
WESTERN CAPE

**By**

**Alungile Mtotywa**

**(MSc Nanoscience)**

A mini thesis submitted in fulfilment of the requirements for the degree of

Magister Scientiae Nanoscience in the Department of Chemistry,

The University of the Western Cape.

Faculty of Science

University of the Western Cape

Cape Town / South Africa

**Supervisor**: Prof M.O Onani

**Co-supervisor**: Dr N.R Sibuyi

March 2023

## DECLARATION

I hereby **declare** that "***Quantum dots for multiplexed biological imaging***" is my work, that it has not been submitted for any degree or examination in any other university, and that all sources I have used or quoted have been indicated and acknowledged by complete references.

**Alungile Mtotywa** **Date: March 2023**

**Signature:** 

## DEDICATION

This work is dedicated to my daughter Ngcwalisa Buncwane Mtotywa and to myself.

## ACKNOWLEDGEMENTS

I would like to thank the Almighty God for his guidance and for giving me much-needed strength to complete this project. "*God is faithful, and he will not let you be tested beyond your strength but with your testing, he will also provide the way out so that you may be able to endure it*", (1 Corinthians 10:13).

I want to thank my supervisor, Prof. Onani, for trusting me with this work. Thank you for the support and words of encouragement. I truly appreciate you.

To my co-supervisor Dr. Nicole, thank you for your help with the write-up and analysis of results, I really appreciate you.

I would like to show my appreciation to Ms Miche Meyer, thank you for helping with the cytotoxicity studies.

I would also like to acknowledge the DST for funding this work through the Nanoscience program.

To my partner, Simosethu Shaun Mangaliso, I appreciate and recognize your consistent motivation and dedication to everything. The year 2022 was very difficult for me, but you kept me pushing. I pray that God will keep you as you are and bless you.

Last but not least, I'd like to thank the Organometallics and Nanoscience research group for making my research enjoyable and for assisting me throughout. Most importantly, Zimkhitha Bianca Nqakala, you've taken on the role of my co-supervisor in the chemistry department, and I greatly appreciate your assistance, constant check-ups, and advice. Miss Shonny Nkuna and Zuraan Paulsen thank you very much for showing me how to synthesize my quantum dots, your assistance, and advice, I appreciate your help.

## Abstract

Over the past two decades, indium phosphide (InP) colloidal quantum dots (QDs) have attracted substantial interest as a possibly less hazardous alternative to cadmium-based QDs. The improvements in their colloidal synthesis techniques have made it possible to synthesize a wide range of compositions, and ligands with perfect quantum yields close to unity, spectrum tunability from blue to near-infrared, and narrow emission linewidths. Additionally, InP QDs have better optical stability than cadmium chalcogenides due to their higher covalency. Modern InP QDs have demonstrated superior performance in a wide range of applications, including solar cells with strong commercial potential, luminescent solar concentrators (LSCs), and light-emitting diodes. The use of non-cadmium-based quantum dots (QDs) as highly effective, non-toxic optical probes for bioimaging is discussed in this study. Core/ shell InP/ZnS and InP/ZnSe QDs were synthesized using tris (dialkylamino) phosphines via one-pot synthesis. Water compatibility was achieved through ligand exchange with 3- mercaptopropionic acid. Chitosan was further added to make the QDs more stable and less toxic. All the synthesized QDs were characterized with UV-Vis, PL, FTIR, and HRTEM.

In a one-pot synthesis of the InP-based QDs, tris (diethyl amino) phosphine $(DEA)_3P$ and tris (dimethyl amino) phosphine $(DMA)_3P$ were utilized as phosphorus precursors. While InP/ZnSe was prepared using both $(DEA)_3P$ and $(DMA)_3P$, InP/ZnS QDs were prepared with $(DEA)_3P$. InP/ZnSe-based QDs had a larger absorption wavelength than InP/ZnS QDs, according to UV-Vis, and 3MPA quenched their fluorescence while Chitosan only did so for InP/ZnSe-based QDs. The PL of 3MPA-based and chitosan-based QDs had the same emission wavelength when excited at 445 nm as expected. The FTIR of the core-shell QDs showed no hydrophilicity in the region of 3200 -2700 $cm^{-1}$, while the FTIR of the 3MPA capped QDs showed no thiol bond and O-H functional group, proving the bonding of 3MPA onto the surface of the QDs and that they are water-soluble. The chitosan QDs FTIR showed an amide and amino from the chitosan molecule, confirming the presence of this polymer in the QDs sample. Chitosan increased the size of the QDs since this polymer is bulkier than 3MPA, and the HRTEM revealed a size drop in the 3MPA QDs compared to the core/shell QDs. As the InP/ZnSe QDs synthesized with $(DEA)_3P$ and $(DMA)_3P$ followed the same pattern, demonstrating that there is no variation in their physiochemical properties, the effect of modifying the phosphorus precursor on the InP/ZnSe QDs did not exhibit any significant differences. The cytotoxicity studies showed that when the QDs are modified with 3MPA and CHT, InP/ZnS-CHT and InP/ZnS-3MPA demonstrated no considerable toxicity to the cells.

Using the two led to a biologically intriguing action of boosting cell development, a trait that is highly sought after in wound healing, in addition to preventing the toxicity of the QDs. The combination of 3MPA and CHT was also able to limit cancer cell growth while enhancing cell viability on the normal cells. This shows that these QDs can be employed as both bioimaging and anti-cancer medicines. Further research is, therefore, necessary to investigate the intriguing bioactivities, such as bioimaging, wound healing, and anticancer activities, that these QDS have shown.

**Keywords**

Quantum dots

Indium Phosphide

Bioimaging

Cytotoxicity

Precursor

## Table of Contents

## List of Abbreviations

| | |
|---|---|
| 3MPA | 3- mercaptopropionic acid |
| ACS | Aqueous colloidal synthesis |
| AFM | Atomic force microscopy |
| ATP | Adenosine triphosphate |
| CAT | Computed tomography |
| Cd | Cadmium |
| CdSe | Cadmium selenide |
| CdTe | Cadmium telluride |
| CHT | Chitosan |
| CdS | Cadmium sulphide |
| CdSe/ZnS | Cadmium selenide/ zinc sulphide |
| DMEM | Dulbecco Modified Eagle medium |
| $(DEA)_3P$ | Tris (diethyl amino) phosphine |
| DLS | Dynamic light scattering |
| $(DMA)_3P$ | Tris (dimethyl amino) phosphine |
| EDC | 1-ethyl-3-(3-dimethyl aminopropyl) carbodiimide |
| EAC | Enrichment ascites cells |
| FBS | Foetal Bovine Serum |
| FRET | Fluorescence resonance energy transfer |
| FTIR | Fourier- transform infrared spectroscopy |
| GlcA | Glucuronic acid |
| HAD | Hexadecyl amine |
| HEK-293 | Human embryonic kidney cell |

| | |
|---|---|
| HepG2 | Human hepatoma cell |
| HK-2 | Human kidney 2 cell |
| $InCl_3$ | Indium chloride |
| $InI_3$ | Indium iodide |
| InP | Indium phosphide |
| InP/ZnS | Indium phosphide/ zinc sulfide |
| InP/ZnSe | Indium phosphide/ zinc selenide |
| LSCs | Luminescent solar concentrators |
| MCF-7 | Michigan cancer foundation-7 |
| MDCK | Madin-Darby canine kidney |
| MSA | Mercaptosuccinic acid capped |
| MIP | Molecularly imprinted polymer |
| MRI | Magnetic resonance imaging |
| MTT | 3-(4,5-Dimethyl-2- thiazolyl)-2,5-diphenyl-2H-tetrazolium bromide |
| NANA | N-acetylneuraminic acid |
| NIR | Near-infrared |
| NPs | Nanoparticles |
| OCS | Organometallic colloidal synthesis |
| ODE | Octadecene |
| $P_4$ | Tetra phosphorus tetramer |
| PAG | Poly acrylic acids |
| PBS | Phosphate buffered saline |
| $PCl_3$ | Phosphorus trichloride |
| PDMS | Polydimethylsiloxane |

| | |
|---|---|
| PET | Positron emission tomography |
| PEG | Polyethylene glycol |
| $PH_3$ | Hydrogen phosphine gas |
| PL | Photoluminescence |
| PLQY | Photoluminescence quantum yield |
| QDs | Quantum dots |
| RT | Room temperature |
| SAED | Selected area diffraction. |
| SDGs | Sustainable development goals |
| SEM | Scanning electron microscope |
| SPECT | Single-photon emission computed tomography |
| STM | Scanning tunnelling microscope |
| TEM | Transmission electron microscopy |
| TGA | Thioglycolic acid |
| $(TMS)_3P$ | Tris (trimethyl silyl) phosphine |
| TOP | Trioctylphosphine |
| TOPO | Trioctylphosphine oxide |
| UWC | University of the Western Cape |
| UV-Vis | Ultraviolet visible |
| XRD | X-ray diffraction |
| $ZnBr_2$ | Zinc bromide |
| $ZnCl_2$ | Zinc chloride |
| ZnS | Zinc sulphide |

## List of Figures

## List of Tables

## Thesis Overview

The thesis is divided into the following five chapters:

### Chapter 1

This introductory chapter provides background information on how quantum dots and bioimaging are related. It starts by defining bioimaging, listing different kinds of bioimaging techniques, and then focusing on optical imaging, a form of bioimaging that employs quantum dots. It provides additional justifications for why optical imaging—rather than another form of bioimaging technique—is the subject of this research. This provides more information about optical imaging and the image-capturing source used in this method. This is where the classifications of fluorophores used in optical bioimaging, along with the advantages of quantum dots over other fluorophores are explained. Explaining the characteristics of quantum dots highlights the significance of multiplexed bioimaging. In several sections of this chapter, the topics of synthesis, characterization, functionalization, biofunctionalization, and the toxicity of quantum dots are further discussed. The study's motivation and suggestions are presented as the chapter ends.

### Chapter 2

The use of quantum dots for bioimaging applications is covered in this chapter, citing literature examples that demonstrate how to modify quantum dots for bioimaging. That includes the use of quantum dots in general and narrows the use of indium phosphide-based quantum dots for bioimaging.

### Chapter 3

The materials, reagents, and analytical methods utilized throughout this investigation are listed in the first paragraph of this chapter. The chapter describes the process used to create the quantum, which was then capped with 3MPA and chitosan. This chapter also describes the analytical techniques employed to characterize the synthesized quantum and what information they will provide upon characterization.

### Chapter 4

The outcomes of this research and discussion of the results are presented in this chapter followed by their characterization techniques using i.e., UV- Vis, PL, FTIR, TEM, SAED, and EDS. The cytotoxicity results will also be presented and discussed in this chapter.

## Chapter 5

This chapter summarizes the findings obtained from the synthesis, characterization, and biological applications of the indium-based quantum dots. It also links the specific aims and objectives to the outcomes of the study. Furthermore, recommendations and future works are briefly discussed.

# Chapter 1

## 1. Introduction

Quantum dots are spherical colloidal fluorescent semiconductor nanocrystals with sizes ranging from 2 to 10 nm. They frequently have distinct optical, electronic, and photophysical properties that make them appealing for use in future biological labelling, imaging, and detection applications (Dios & ElenaDíaz-García, 2010). These nanocrystals are utilized as fluorophores in medicine because when energy is supplied to them, they produce light of a certain wavelength (Gil, *et al*., 2021). The use of two or more fluorophores with different emission wavelengths is known as multiplex bioimaging (Pandey & Bodas, 2020). Bioimaging is a term used to describe techniques and tools for acquiring, processing, and visualizing structural or functional images of living things or systems at chosen spatial and temporal scales (Georgia Tech, 2022). Because they allow for the early detection, diagnosis, and treatment of cancer cells, multiplexed fluorophores have been employed in bioimaging with considerable success (Beloglazova, *et al*., 2017).

### 1.1.Bioimaging

This is a non-invasive method of observing biological activity across time (Malik, *et al*., 2019). Methods for seeing into the body or viewing cells are critical for monitoring illnesses, diagnosis, and treatment, as well as a study into the fundamental processes of life. The procedures utilized should not be invasive, as a result, tools for visualizing physiological or pathophysiological changes in the body and cells have grown in importance in biomedical sciences (Nagano, 2010). This method allows for accurate tracking of metabolites that can be utilized as biomarkers for illness detection, progression, and therapy response (Luc, *et al*., 2010). This technique is used to obtain information on the 3-D (Offenhäusser & Rinaldi, 2009) structure of the observed specimen. Existing bioimaging approaches include magnetic resonance imaging (MRI), single-photon emission computed tomography (SPECT), positron emission tomography (PET), and optical imaging (Frangioni, 2008, Grumezescu, 2016). Images for these approaches are obtained from different sources. PET, for example, uses a radioactive drug tracer, SPECT uses a gamma camera, and optical imaging employs a light source (Ueno, 2020, Anon., 1995).

For the diagnosis and treatment of human illnesses, biomedical imaging has turned out to be one of the most trusted technologies in healthcare. Medical imaging has evolved from simple radiography through x-ray imaging, magnetic resonance imaging (MRI), ultrasound imaging, and (Allied Market Research, 2022) computer-assisted tomography (CAT scans). These approaches, however, are primarily fixated on anatomical and structural imaging at the organ or tissue levels. There is an obvious need to expand imaging to the molecular and cellular biology levels to create advanced imaging approaches for early diagnosis, screening, detection, and image-guided therapy of life-threatening illnesses such as cancer. Only cellular and molecular information can lead to the discovery of early stages of illness or cancer development, as well as early molecular differences throughout intervention or therapy (Prasad, 2003).

There are various limits to the present medical procedures of x-ray imaging, CAT scans, radiography, ultrasound imaging, and MRI. For example, MRI cannot offer particular chemical information or any dynamic information, such as changes that occur in real-time in response to therapy. The X-ray cannot differentiate between gentle and malignant tumours and is not appropriate for imaging young individuals or thick breasts. Ionizing radiation has enough energy to damage DNA and causes cancer (National Cancer Institute, 2019) in the case of CAT scans and x-ray imaging. Radiation is harmful in radioisotope imaging and ultrasound's incapacity to produce resolution lesser than millimetres and to discriminate among benign and malignant tumours limits its use (Prasad, 2003). Optical imaging fills up a lot of the limitations experienced by these bioimaging techniques. Optical imaging does not only include imaging of cells and molecules, but it also makes use of the spatial variation in the optical characteristics of a bio specie, whether it is a cell, organ tissue, or a complete living entity. Reflection, scattering, absorption, and fluorescence are examples of optical characteristics. As a result, an optical picture may be obtained by monitoring the spatial fluctuation of transmission, reflection, or fluorescence. The use of lasers as a strong and suitable light source to create an optical response, whether reflection, transmission, or emission, has significantly enlarged the bounds of optical imaging, making it a valuable technology for both fundamental research and clinical diagnostics (Prasad, 2003). Compared to other bioimaging modalities, optical imaging methods provide high-resolution, straightforward, non-hazardous, and cost-effective benefits. Additionally, optical imaging is the molecular and cellular imaging method that is employed the most in preclinical applications (Kang, *et al.*, 2022).

## 1.2.Optical Imaging

This is often known as fluorescence imaging which is a non-invasive method that employs light to explore cellular and molecular activity in living organisms (Serrao, *et al.*, 2021) This approach makes use of light and the unique characteristics of photons to produce comprehensive pictures of organs, tissues, cells, and even molecules (Ueno, 2020, National Institute of Biomedical Imaging and Bioengineering, 2020). By using non-ionizing radiation like visible, ultraviolet, and infrared light, optical imaging reduces the amount of dangerous radiation that patients are exposed to (National Institute of Biomedical Imaging and Bioengineering, 2020). This technique has several advantages, including the ability to image *in vitro*, *in vivo*, and *ex vivo* specimens. It may also be integrated with other imaging methods, such as ultrasound and it offers great sensitivity and selectivity to image molecular events, portability, real-time capability and is free of the difficulties associated with the use of radiolabelled probes or ionizing radiation. It may also be used throughout a wide spectral range, from visible to near-infrared (NIR) (Zhang, *et al.*, 2015), allowing for multi-colour imaging, and the fluorescence signal, resulting in a high target-to-background ratio (Ueno, 2020, Prasad, 2003).

Optical imaging uses light to view cellular and molecular functions in the living body, as well as in animal and plant tissue (The Society of Nuclear Medicine, 2016). The contrast or vision of optical imaging is generated from fluorescent probes (Thermo Fisher Scientific, 2021). Fluorescent probes are molecules that absorb a certain wavelength of light and emit a different, sometimes longer wavelength of light, a process known as fluorescence, is used to evaluate biological material. Fluorescent molecules are widely used in biological research, and their popularity is growing due to their variety, sensitivity, and quantitative capabilities. These compounds, often known as fluorophores, can be linked to a target molecule and used as a marker for fluorescence microscopy research (Nature Journal, 2021). In general, imaging probes are targeted to biomarkers for particular viewing of targets, helping to achieve precision medicine by increasing diagnostic performance for early illness diagnosis, tumour staging, and surgical guiding. Today's large array of fluorophores offers greater versatility, variety, and fluorophore performance than ever before for research purposes (Thermo Fisher Scientific, 2021). Organic dyes, biological fluorophores, and quantum dots are the three types of fluorophores commonly utilized in optical imaging for biological research. Each fluorophore has unique properties that should be considered when selecting a fluorophore for a specific application or experimental setting (Pandey & Bodas, 2020).

The earliest fluorescent substances employed in the biological study were synthetic organic dyes. To increase these compounds' photostability and solubility, derivatives of organic dyes have been created. Because they can be crosslinked to macromolecules, these fluorophores' tiny size has an advantage over biological fluorophores for bioconjugation techniques (Thermo Fisher Scientific, 2021). Although these organic fluorophores are preferred, they are prone to photobleaching, low signal intensity, biocompatibility, and spectral overlapping, (Pandey & Bodas, 2020) (Smith, *et al.*, 2006) thus limiting the possibilities for multicolour labelling. Additionally, the organic dyes have a broad fluorescence emission that is comparable to the background fluorescence lifetime of many naturally occurring compounds, which lowers the signal-to-noise ratio in fluorescent bioimaging (Yordanov & Dushkin, 2011). Furthermore, most organic fluorophores have poor photostability. Their usage in bioimaging, and more especially in multiplexed applications, is restricted by these disadvantages. Contrarily, quantum dots (QDs) have enormous promise because of features like size-tunable narrow emission, single UV- Vis excitation, biocompatibility, an easy technique for surface modification, multiplexed bioimaging applications, etc (Pandey & Bodas, 2020). QDs are nanocrystals with special chemical properties that allow for control over the fluorophore's spectrum characteristics. QDs were created in the 1980s, and since the 1990s, they have been employed more often in biological research for fluorescent applications (Thermo Fisher Scientific, 2021). The use of QDs for various biological applications has increased during the last two decades (Karakoti, *et al.*, 2015). Due to the limitations posed by organic dye fluorophores, QDs have been vastly investigated to replace organic fluorophores as fluorescence labels. According to reports, QDs also feature high quantum effectiveness, prolonged photostability over molecular fluorophores for long-term imaging and preventing photobleaching, and the ability to simultaneously image several colours with a single light source and are simple to modify (Li et al. 2015).

### 1.3.Nanotechnology in Bioimaging

Quantum dots (QDs) are spherical nanocrystals with a diameter of 2–10 nm made of semiconductor materials. These nanocrystals are composed of groups II-VI (Zn, Cd, In, P, C, etc) or III–V (P, C, In, Si, etc) elements in a periodic table (Karakoti, *et al.*, 2015, Fleisher & Oliveira, 2019, Yordanov & Dushkin, 2011). Quantum dots are also nanomaterials classified as inorganic materials in terms of chemical composition and as zero-dimensional nanomaterials in terms of structural dimensionality. The use of synthetic nanoparticles in biomedical applications, particularly in biomedical imaging, is growing in popularity. Nanoparticles with

diameters from 1 to 100 nm are equivalent in size to biological functional units. Nanotechnology has arisen as multidisciplinary research endeavours focused on understanding and controlling materials by bringing together ideas from engineering, chemistry, biology, medicine, and other disciplines. Recent technical advancements in the production of many types of nanoparticles demonstrate the significance of nanoparticles in biological imaging applications. For a variety of reasons, the use of engineered nanoparticles in biological research has increased exponentially in the last five years. Unique physical, chemical, and optical characteristics have been identified at a nanoscale. As a result, novel synthetic methods for precisely controlling the size and shape of nanoparticles to tailor absorption and emission characteristics have been created. Concurrently, surface modification of nanoparticles, known as 'biofunctionalization,' has taken use of the high surface-to-volume ratio to allow multivalent ligand binding to target biomolecules. The molecular targeting of nanoparticle beacons is now enabling several scientific applications (Nune, *et al.,* 2009).

There is now a lot of interest in the creation of nanoparticle probes for bioimaging and diagnostics. The fundamental idea is that discrete molecules or bulk materials do not have the functional or structural qualities that nanometre-sized particles do. When combined with biomolecular affinity ligands such as small molecules, peptides, or antibodies, these nanoparticles have the potential to detect tumour cells and molecular biomarkers with high specificity and sensitivity. Nanoparticles also have vast surfaces that may be used to attach a variety of diagnostic and therapeutic agents. Biodegradable nanostructures for drug administration, iron oxide nanocrystals for magnetic resonance imaging, and luminous quantum dots (QDs) for multiplexed molecular diagnostics and *in vivo* imaging have all recently been developed (Kairdolf, *et al.,* 2013). A QD is a fluorescent nanoparticle that may be employed as a sensitive probe for screening cancer indicators in fluids, a particular label for categorizing tissue samples, and a contrast agent with high resolution for medical imaging able to detect and identify the tiniest malignancies (Chan & Nie, 1998). These particles have the unusual capacity to be detected sensitively across a wide variety of length scales, from macroscale viewing to atomic resolution utilizing electron microscopy. Most crucially for cancer detection, QDs have large multiplexing capabilities for concurrently detecting several cancer indicators, which holds enormous potential for unravelling the complicated gene expression patterns of malignancies and accurate clinical diagnosis (Smith, *et al.,* 2006).

### 1.4.Quantum dots Properties

Semiconductor QDs are a new type of nanoparticle probe for bioimaging and diagnostics that display optical and electronic features. The unique properties of QDs make them the best fluorophores for biomedical applications. QDs absorb and emit visible light at room temperature due to a quantum effect, known as the size-confinement of the exciton. When the particle's size is too small to be equivalent to the wavelength of the electron, the quantum confinement effect is noticed. If the QD is smaller than the Bohr radius, confinement occurs, resulting in a change from continuous to discrete energy levels (Singh, 2015). QDs have distinctive optical and electrical features brought about by the quantum confinement phenomenon, which gives them several benefits over the present fluorophores. Their absorbance and emission wavelengths are affected by the diameter of the nanocrystal. Some of an electron's energy is lost to atomic vibrations once it is energized. Typically, this energy is transformed into heat. Because of the energy loss, when an electron decays into the ground state, it emits light at a larger wavelength - this is known as normal band-edge emission. The fluorescence spectrum red-shifted in comparison to the absorbance spectrum due to thermal energy loss (Stokes shift). The nanoparticles may also produce a distinct form of fluorescence as a result of an electron being trapped at the crystal surface. When a defect becomes entrapped in a crystal, it brings a potential energy state into the band gap. In this condition, electrons are trapped. Trap-state emission occurs when an electron emits from this state and decays to the ground state. Because the corresponding fluorescence band is wider than the band-edge emission and positioned at a longer wavelength at the same time, QDs have a broad absorption characteristic with continuous and controllable narrow-emission spectra (Yordanov & Dushkin, 2011).

The ability to simultaneously view and track several molecular targets using multicolour QD probes is another benefit of QDs. Given that cancer and many other illnesses include a huge number of genes and proteins, this is undoubtedly one of the most potent qualities of QDs for medicinal applications. Narrow emission bands combined with wide absorption bands make it possible to multiplex QD signals. Multiple QDs may be activated by a single short-wavelength light source thanks to broad absorption bands, which simplifies sensor design, speeds up detection, and lowers cost. In the visible spectrum, QD emission bands can be as small as 20 nm, making it possible to concurrently detect several signals. Contrarily, organic dyes and fluorescent proteins have very large emission bands and narrow absorption bands, which makes it much more difficult to identify signals from different fluorophores that are significantly

separated from one another (Smith, *et al.*, 2006). The emission spectra of QDs are narrow, which can be readily manipulated by altering the core size and composition, as well as the surface coatings. Furthermore, the QDs are exceptionally resistant to photobleaching and can stay luminous for hours when exposed to UV radiation. Finally, QDs have a long fluorescence lifespan after excitation, which is useful in time-gated imaging (Jamieson, *et al.*, 2007). The most obvious benefit of QDs over organic fluorophores is their greater photostability, which has been established in various studies. This might be used in circumstances where long-term monitoring of tagged compounds is necessary, and it is an area where QDs could be useful (Yordanov & Dushkin, 2011).

### 1.5.Synthesis of Quantum dots

Several strategies have been utilized to synthesize QDs, but in general, top-down processing methods and bottom-up procedures are used (Valizadeh, *et al.*, 2012). The top-down technique is focused on broad materials with critical nanoscale specifics. The bottom-up method, by comparison, assembles microscopic materials such as molecules and atoms to form larger structures. Examples of these procedures are shown in Figure 1.5 (Liu, *et al.*, 2011). However, the production of nanoparticles can have a negative influence on their capacity to perform successfully in real-world applications. These drawbacks include, but are not limited to, instability in harsh conditions, toxicity, bioaccumulation, and the difficulty of recycling, reusing, and regeneration. Additionally, the toxicity of these nanoparticles would be a problem due to their use in medical therapeutics as well as their use in the degradation and oxidation of toxic pollutants and waste. These particles would need to be produced more sustainably to prevent toxicity that could negatively affect all lives. With an increasing awareness of how unsustainable materials and procedures have harmed the Earth, as well as the accumulation of these materials that are not easily degradable, more sustainable ways that generate less harmful waste is important (Khan, 2021, Singh, *et al.*, 2018).

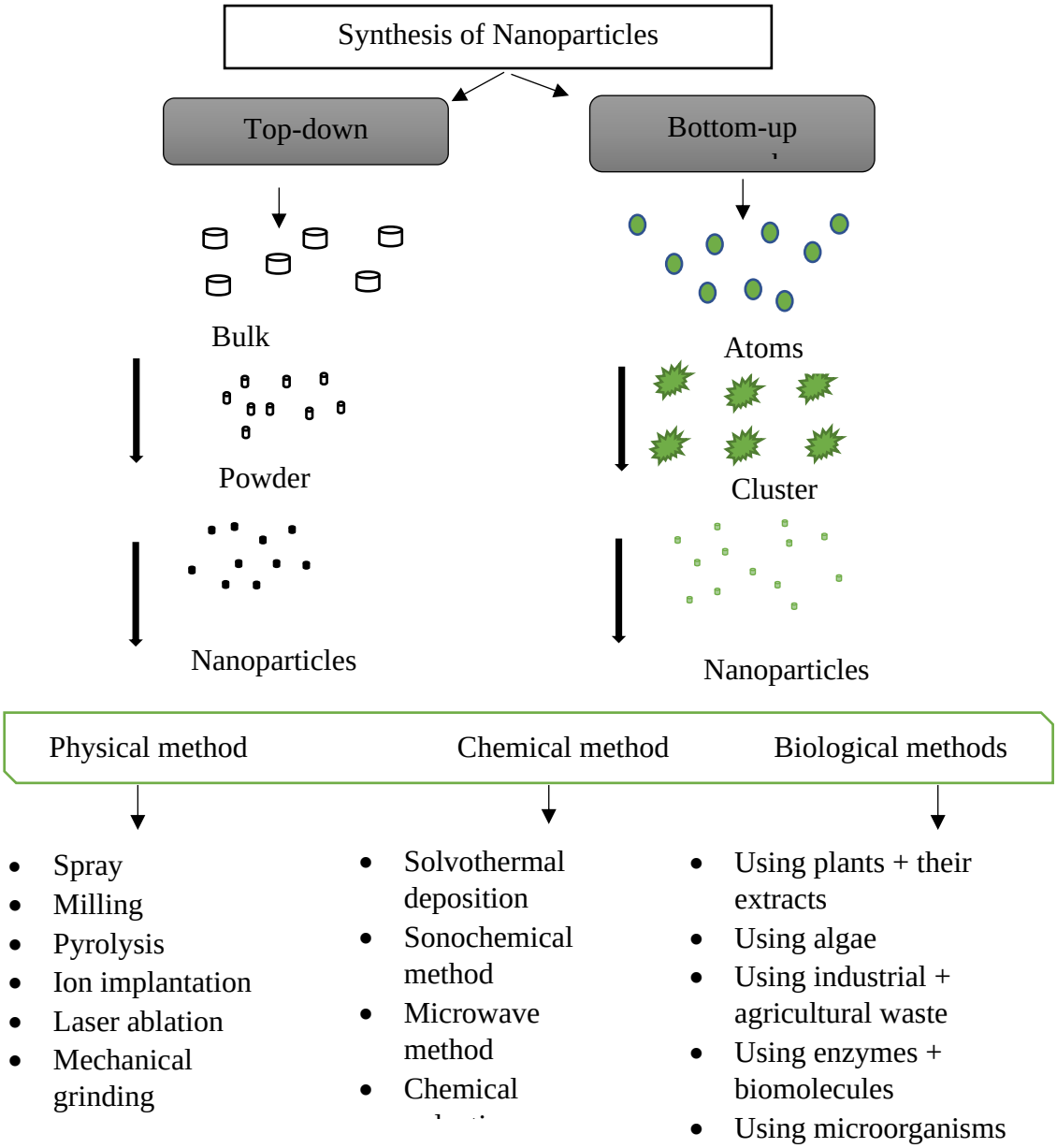


**Figure 1.5:** Bottom-up and top-down synthesis methods of nanoparticles (Rajasekhar & Kanchi, 2018).

The pursuit of environmentally friendly and sustainable methods for the synthesis of nanomaterials is a major topic in green synthesis (Biju, *et al.*, 2010). It is also critical to use green methods to meet sustainable development goals (SDGs) by 2023. The Sustainable Development Goals' 12th target is responsible consumption and production. One of the objectives of this goal is to achieve environmentally sound management of chemicals and all waste throughout the life cycle by 2020, by accepted international frameworks, and to drastically reduce their release to air, water, and soil to minimize their detrimental effects on

human health and the environment. By 2030, to substantially reduce waste generation through prevention, reduction, recycling, and reuse (United Nations, 2021). In QD-based applications, the synthesis of nanomaterials with highly monodispersed, crystallinity, shape control, and limited size distribution is crucial. Figure 1.6 shows two commonly used green synthetic methods for the preparation of QDs. The first green synthetic process is organometallic colloidal synthesis (OCS). An experimental condition for this procedure is that it be performed in an inert environment, along with a hot injection of metallic precursors. Recent discussions on the impact of hot injection in OCS have indicated that QDs created using hot injection have greater quantum yield but worse sensing properties compared to QDs synthesized at room temperature (RT) (Mir, *et al.*, 2016). Despite the outstanding performances of QDs generated by OCS, these processes demand nongreen settings, dangerous chemicals, and a lot of energy. Furthermore, the most environmentally friendly approach to OCS comprises using environmentally renewable raw materials solvents and coordinating agents, such as oleic acids. These coordinating agents are used to eliminate the usage of air-sensitive, hazardous, and costly compounds like tri-octyl phosphine (TOP), tri-octyl phosphine oxide (TOPO), and hexadecyl amine (HDA) (Biju, *et al.*, 2010).

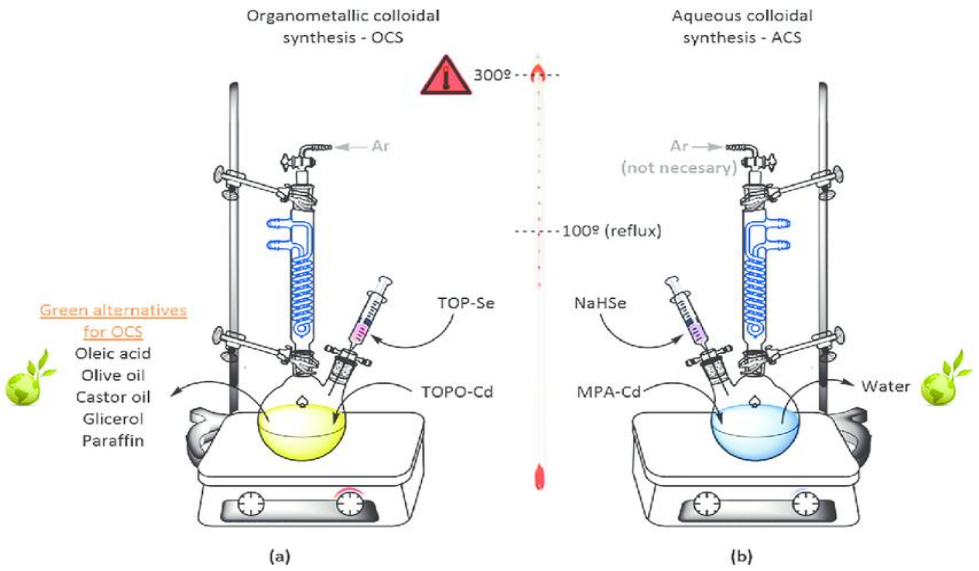


**Figure 1.6:** Green synthetic experimental methods of QDs (Bonilla & Kouznetsov, 2016).

The second method is aqueous colloidal synthesis (ACS). ACS emerges in response to the requirement for TOPO/TOP-QDs solubilization in biological applications. Typically, the hydrophobic layer in TOPO/TOP-QDs is substituted by hydrophilic molecules in the liquid phase, such as amines, polyhydroxy alcohols, and notably thiols. The photoluminescence of

QDs can be significantly reduced as a result of this surface alteration. To address this issue, the least toxic and most biocompatible solvent, water, is used in ACS to directly synthesize QDs. In a typical ACS, hydrophilic agents such as thioglycolic acid (TGA), mercaptosuccinic acid (MPA), or glutathione coordinate the easy dissolution of heavy metal precursors in water (Bonilla & Kouznetsov, 2016). Furthermore, when compared to organic-based synthesis, ACS is preferred as the primary procedure for QD preparation in biological studies because it is more reproducible, has lower toxicity, is less expensive, and is more environmentally friendly, resembling many of the goals pursued by green nanotechnology (Biju, *et al.,* 2010).

### 1.6.Characterization of Quantum dots

When the term "characterization" is used in science, it refers to the comprehensive and all-encompassing process of analysing and measuring a material's structure and characteristics to better understand and regulate the nanoparticles for specific applications (Zhang, *et al.,* 2009). Upon synthesis, QDs are characterized using different characterization techniques before they can be used in any type of application. Microscopy and spectroscopy are the two sub-branches in characterization. A class of characterization methods known as microscopy explores and maps the surface and sub-surface structure of a material. These methods collect information on the structure of a material over a wide variety of length scales using photons, electrons, ions, or physical cantilever probes. Microscopic characterization techniques include an electron microscope called a scanning electron microscope (SEM), an optical microscope often called a light microscope, and transmission electron microscopy (TEM) amongst others. A family of characterization methods known as spectroscopy uses many concepts to reveal a material's chemical composition, crystal structure, composition variation, and photoelectric properties. Examples include but are not limited to UV- Vis spectroscopy, Fourier-transform infrared spectroscopy (FTIR), Photoluminescence (PL), Energy-dispersive X-ray spectroscopy (EDS, EDX, EDXS, or XEDS), and Dynamic light scattering (DLS) (Drbohlavova, *et al.*, 2009).

For the quick, non-destructive, and contactless optical evaluation of QDs, UV-Vis, and photoluminescence spectroscope is frequently used. The optical characteristics of QDs may be fine-tuned by the size of the QDs, which is a critical parameter that influences the spectrum location and purity of photoluminescence (Drbohlavova, *et al.,* 2009). The size of QDs is often determined using traditional methods such as SEM, TEM, and DLS. Several characterization techniques, including TEM, atomic force microscopy (AFM), or, more preferably, scanning tunnelling microscopy (STM), are often used to monitor the size of epitaxially produced QDs.

The surface chemistry of QDs is also highly essential since it adds to the ultimate hydrodynamic diameter of QDs, hence a technique providing qualitative information on this parameter is required. Several approaches, including X-ray photoelectron spectroscopy, nuclear magnetic resonance spectroscopy, and Rutherford backscattering, have been used to analyse QD surface chemistry to date (Drbohlavova, *et al.*, 2009).

### 1.7.Functionalization of Quantum dots

Synthesized QDs can be in different forms such as bare/ uncoated QDs (such as CdSe, InP, CdTe, etc), also called core QDs or, can be core-shelled QDs (such as CdSe/ZnS where CdSe is the core and ZnS is the shell), others can be core/shell/shell, for example, CdSe/ZnSe/ZnO and core/multi-shells (Vasudevan, *et al.*, 2015, Yordanov & Dushkin, 2011). Biological applications cannot be achieved with bare uncoated QDs, despite their excellent photostability, tunable fluorescence under single-wavelength light, and longer lifespan than conventional fluorophores. Uncoated QDs' fluorescence characteristics can be diminished by surface restriction caused by the high surface energy of crystalline nanoparticles. Furthermore, long-term exposure of uncoated QDs in biomedical applications to ionic fluid or cellular media can induce photochemical degradation, surface oxidation, and metal ion leaching from the QDs core, resulting in metal ion toxicity. To remove surface defects and excessive reactivity, QD surfaces must be capped with stable chemicals. Surface changes are necessary for QDs to be used in biological applications (Karakoti, *et al.*, 2015). Figure 1.7 shows an example of a core or bare uncoated QD and a core/shell QDs where the CdSe core is coated with a ZnS shell.

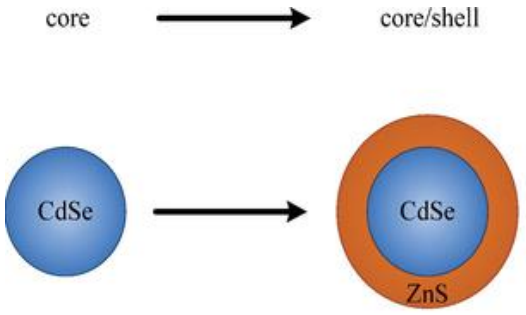


**Figure 1.7:** Classes of quantum dots (AbouElhamd, et al., 2019).

The core QDs can be capped with ligands such as ZnS, ZnTe, CdO, etc, shells in a single synthesis step to achieve core-shell morphology. Although capping QDs in an outer shell boosts their stability and manufacturing, it does not affect their water solubility. Core/shell QDs cannot be employed in bio-applications because they are hydrophobic. They are further functionalized with water-soluble biodegradable green polymers or molecules such as

mercaptocarbonic acids that provide carboxy groups to make them hydrophilic. Functionalization is the process of adding new functions, features, capabilities, or characteristics of a material by altering its surface chemistry. These polymers must be biocompatible and have reactive functional groups to bind to biomolecules for the bioconjugation process (Tan & Zhang, 2005). There are three basic approaches for replacing or coating QDs with hydrophilic ligands (green polymers): Surface salinization, amphiphilic combination, and ligand exchange. Ligand exchange is a popular strategy (Karakoti, *et al.,* 2015).

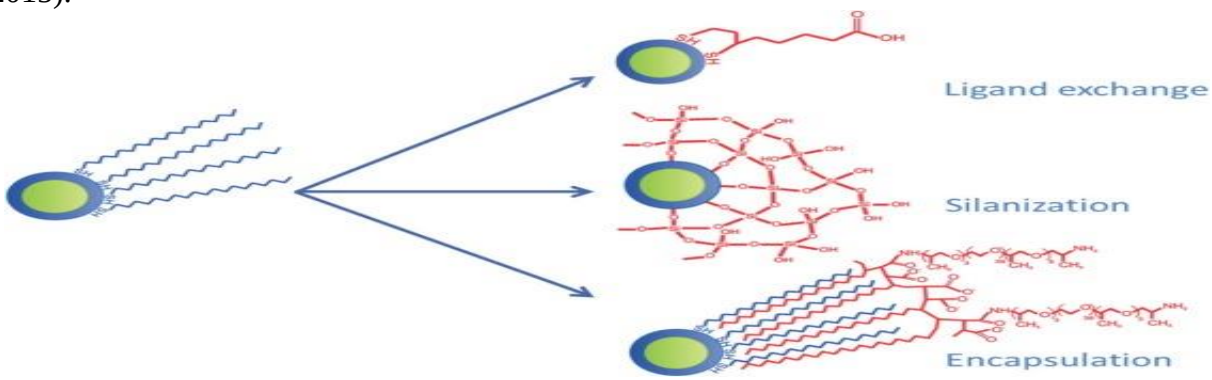


**Figure 1.8:** The three major approaches for replacing or overcoating QDs with hydrophilic ligands (Foubert, *et al.,* 2016).

Figure 1.8 shows an image of the three strategies whereby the ligand exchange technique involves replacing an existing non-functional ligand with a mono- or bi-functional ligand, which confers new properties on QDs such as solubility, motility, and targeting. Ligand exchange can occur with hydroxyl-giving compounds such as mercaptocarbonic acids, mercaptopropionic acid, mercaptoacetic acid, and mercaptodecanoic acid (Tan & Zhang, 2005, Karakoti, *et al.,* 2015). Silanization is the process of covering nanoparticle surfaces with amorphous silica. The coating of QDs with amphiphilic molecules to limit polymer molecule desorption is known as the amphiphilic combination (Karakoti, *et al.,* 2015). Ligand exchange is the most common approach. Although just a few examples have been reported, biodegradable polymers have shown promise for developing new, complex, and efficient drug delivery systems capable of delivering a wide spectrum of bioactive chemicals. QD functionalization also enables future conjugation to biomolecules such as proteins, immunoglobulins, aptamers, oligonucleotides, and others (Foubert, *et al.,* 2016).

## 1.8.Bioconjugation of Quantum dots

Core/shell QDs are made hydrophilic by coating polymers for them to be used for bio applications. But these water-soluble QDs must be linked to functional biomolecules such as proteins, antibodies, enzymes, and nucleic acids to be employed in bioimaging, detection, and other applications such as drug delivery (Karakoti, *et al.,* 2015). Bioconjugation is a chemical process that results in the development of a stable covalent connection between two molecules, one of which must be a biomolecule. Bioconjugation combines the unique properties and utility of both materials, such as plasmonic particles' optical capabilities and biomolecules' ability to attach to particular targets via molecular recognition. Bioconjugation mechanisms are critical in protein modification. Proteins may be modified to fulfil a variety of functions, including cellular monitoring, imaging biomarkers, and medicine administration (Karakoti, *et al.,* 2015). QDs functionalized with biocompatible polymers allow for bioconjugation with biomolecules. There are two ways to bind these biomolecules to the surface of QDs: non-covalent and covalent connection (Foubert, *et al.*, 2016) and Figure 1.9 shows the methods for both covalent and non-covalent.

Covalent linkage and non-covalent binding, which involves connecting directly to the QD surface or coating the QD with a surface ligand, are the two primary techniques for immobilizing biomolecules on the QD surface (Pandey & Bodas, 2020). Covalent bonds between QDs and molecules or other particles can be made using a variety of coupling agents. Cross-linkers can be divided into three categories: zero-length, homobifunctional, and heterobifunctional. The contact between two functional groups is facilitated by the zero-length coupling agents, leading to the creation of a new bond without the introduction of any more atoms. Homobifunctional agents have two identical reactive sites, one at either end of a spacer arm, which allows them to conjugate two identical functional groups (typically an alkyl chain). In heterobifunctional cross-linkers, two reactive sites can form covalent bonds with two distinct functional groups. In both homobifunctional and heterobifunctional coupling agents, a spacer arm will be added during the connecting process between the reactive sites (Hermanson, 2013). The functional groups present on the surface of QDs or in the molecule must be considered while selecting a coupling reagent (Pereira, *et al.,* 2019, Bilan, *et al.,* 2015).

.

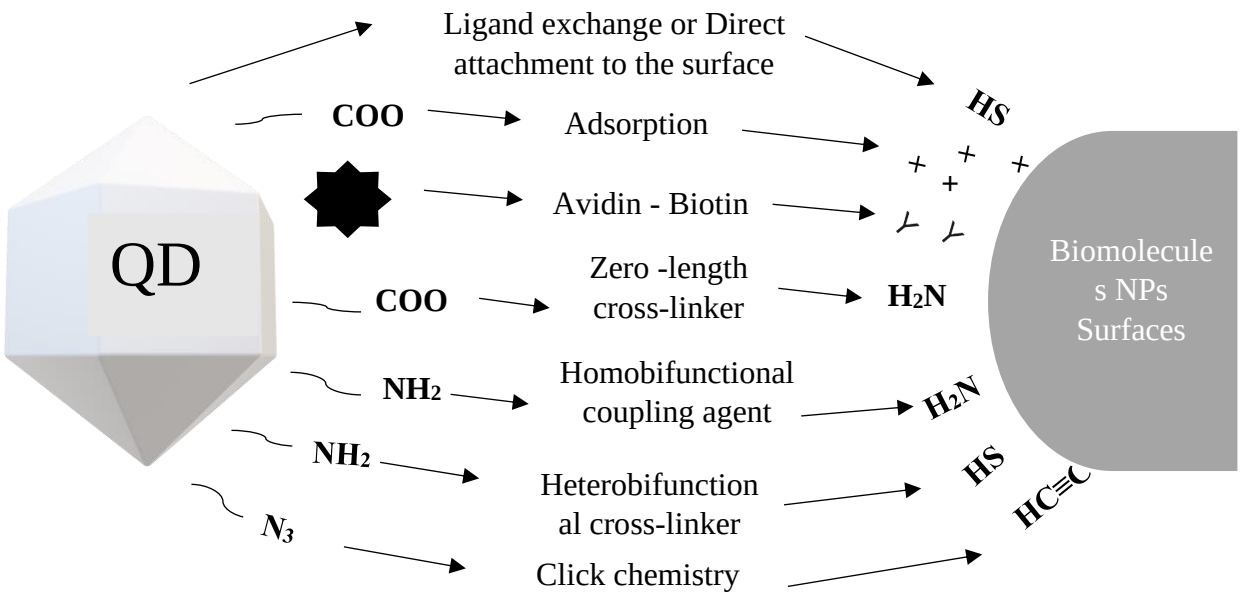


**Figure 1.9:** Currently used methodologies for conjugating QDs to (bio)molecules, nanoparticles (NPs), and surfaces (Pereira, et al., 2019 ).

Non-covalent interactions between biomolecules and the QD surface determine non-covalent binding; a covalent connection is created via different bioconjugation techniques using activated functional groups on the QD surface (Pandey & Bodas, 2020). Non-covalent binding between nanocrystals and biomolecules can be accomplished by a variety of mechanisms, including adsorption, direct attachment to the surface of QDs, and (strept)avidin-biotin affinity (Pereira, *et al.*, 2019). The ability to conjugate QDs to biomolecules was established by Bruchez and Chan in 1998, and it has subsequently been widely employed in imaging, immunoassays, and DNA sequencing processes (Karakoti, *et al.*, 2015). Even though quantum dots have several unique and valuable features, their use is currently limited. The main limitation that prevents these semiconductor nanocrystals from being employed in bio-applications is toxicity. (Pandey & Bodas, 2020).

### 1.9.Toxicity of Quantum dots

The long-term toxicity of QDs is a serious problem in biological applications and one of the most difficult challenges to overcome in clinical translation. The toxicity is caused mostly by a factor such as:

- Size and Concentration of the nanocrystals

- The effect of the outer functional group
- Frequently utilized heavy metals for particle cores
- substances that may cause poisonous substances to be released from the surface (particularly for Cd, Se, and Hg coatings)
- any reactive or free radicals produced as a result of excitement
- interactions between tissues and nano-colloids in biological settings (e.g., small particle size, positive surface charge, chemical composition)

There have been numerous reports of heavy metal toxicity in the literature, especially in light of the metals' exceptionally long biological half-lives and capacity to cross the blood-brain barrier. Despite the fact that surface coatings can be used to reduce the release of harmful substances from the QDs surface, it has recently been discovered that the coating itself may, in some circumstances, be much more toxic. The release of $Cd^{2+}$ ions from the nanoparticles poses the biggest danger of harmful impact, which can be mitigated slightly by encapsulating the QDs in a passivating ZnS shell or crosslinked polymer covering (Wagner, *et al.,* 2019). QDs enter the organism by breathing, skin contact, intake, intravenous injection, and other pathways during the process of manufacture, application, or environmental exposure. Drug therapy and biological monitoring are two other things that might expose one to QDs. Different QDs are absorbed, transferred, accumulated, degraded, and excluded by organisms in observable ways. These variations are mostly caused by QDs' physical and chemical characteristics, such as their particle size, surface charge, chemical properties on the surface, etc (Li, *et al.,* 2020).

Surface modifications with thiol-containing molecules or the use of a non-heavy metal barrier shell have been used to reduce their toxicity. Recently, biocompatible polymers were combined with QDs, resulting in hybrid materials with better hydrophilicity, stability, functionalization, and biocompatibility, making them effective for biological imaging and sensing (Shen, 2011). Polymer inclusion improves QD colloidal stability in an aqueous biological environment. Also, the use of non-cadmium-based QDs has had a tremendous interest in reducing toxicity, as a result, indium-based QDs are being researched (Bharali, *et al.,* 2005). To make additional progress in decreasing QD toxicity, it is suggested that semiconductor nanoparticles be manufactured with optimum colloidal stability under physiological settings, that QD size is controlled, and that surface characteristic be improved for better cellular absorption. QDs can also be passivated or bioconjugated with antibodies, polymers like polyethylene glycol (PEG), or nanoparticles like micelles (Wagner, *et al.,* 2019).

## 1.10. Problem Statement

The research on early-stage diagnosis and detection of medical disorders has been sparked by the increase in life expectancy. In addition to early prediction of the efficacy of a treatment regimen, disease treatment now requires ongoing monitoring and localized drug administration. It is not recommended to expose the entire body to medicine or radiation for the treatment of a localized issue at a particular place of an organ. Additionally, as many biologists are concentrating on the significance of examining how genes operate and interact with one another and with the proteins that these genes produce in cells, organs, and organisms, there is a need for techniques that can simultaneously identify several genes and proteins. As a result, multiplexed biological imaging can be used to make early diagnoses, effective treatments, and wise therapeutic decisions (Byers & Tholouli, 2017). For years, intra- and extracellular imaging as well as *in-vitro* test detection have been accomplished using fluorescent labelling by dye molecules. However, the fixed and wide emission and limited absorption patterns of the organic/bioorganic fluorophores and dye molecules place limitations on their physicochemical qualities. The limited photo-stability of these fluorophores also prevents long-term monitoring, imaging, and multiplexing without the employment of sophisticated equipment or extensive post-processing and analysis. Semiconductor nanocrystals and quantum dots (QDs) are therefore investigated to replace or conjugate organic fluorophores (Cotta, 2020).

The use of QDs has increased for a variety of biological applications over the past 20 years, including but not limited to: a) *In-vitro* and *in-vivo* imaging probes b) Pathogen and toxin detections Genomics and profiling c) fluorescence resonance energy transfer (FRET). Compared to the traditional organic fluorescent probes, semiconductor QDs are a versatile tool for numerous imaging applications in *in-vitro* and *in-vivo* imaging because of their size-dependent fluorescence, among other special qualities (Cotta, 2020). QDs are used to label cells in early *in vitro* imaging studies. The usage of these materials, however, has raised severe questions concerning toxicity and safety, particularly because the most well-known and extensively researched QDs include cadmium, such as cadmium selenide (CdSe), cadmium telluride (CdTe), and cadmium sulphide (CdS) (Eren, *et al.*, 2021). For biological systems, cadmium (Cd) is recognized to be very poisonous and carcinogenic. Several investigations of Cd-based QDs have quantified the toxicity of these materials in cell cultures (Eren, *et al.*, 2021). As a result, the focus has shifted in recent years to the production of non-cadmium-based QDs for biological applications.

Indium phosphide (InP), which emits light in the visible spectrum (450–700 nm), has become a viable alternative to Cd-based QDs (Lee & McLaurin, 2018). Tris (trimethylsilyl)phosphine $(TMS)_3P$ was first used as a phosphorus precursor in the 1995 initial synthesis of InP-based QDs. But $(TMS)_3P$ is a costly, extremely pyrophoric substance. In addition, when phosphine comes into contact with damp air, it releases a very poisonous gas. As a result, recent studies have looked into substituting the $(TMS)_3P$ precursor with other affordable and "greener" precursors, such as PCl3, P4, and tris(dialkylamino)phosphines. Amino phosphines, in particular, have become safer and more affordable starting materials to create InP-based QDs with features similar to those produced by $(TMS)_3P$ standard methods (Lignos, *et al.*, 2021).

### 1.11. Rationale

Quantum dots (QDs) are one of the most promising new fluorescents used as labels for cellular imaging. Researchers have chosen to do research on unconventional bioimaging over conventional organic dyes due to the stunning colours emitted by QDs. Due to their reduced tendency to photo bleach, QDs are interesting fluorescence probes for a variety of labelling studies (Kumar, *et al.*, 2018). Over the last few years, the use of QDs as luminescence probes in a variety of biological and biomedical applications has gotten a lot of attention. The use of QD as luminescence probes in cell imaging has captivated the curiosity of many researchers since the first instances from Bruchez and Nie's groups in 1998. Fluorescent QDs are used as bioimaging probes primarily because of their optical and chemical properties, which include high photochemical stability, excellent resistance to chemical and photochemical degradation, tunable photoluminescence that spans the entire visible spectrum, and good fluorescence quantum yield. The capacity to direct QDs to particular organelles, receptors, or cell types, similar to how organic fluorophores are directed, is a crucial aspect of using QDs for bioimaging (Pandey & Bodas, 2020). QDs made of elements such as cadmium, lead, and mercury have been reported to be toxic when applied in biomedical applications. Numerous methods have been developed to lessen or eliminate toxicity. Indium-based QDs have been researched as promising nanocrystals to replace toxic ones. These metal-based core QDs are passivated with polymeric shell coatings, which can actually prevent heavy metal ions from leaching from inside and increase stability, to further lessen their toxicity. In addition to using polymer coatings, harmful QDs can be bioconjugated using surface modifications with suitable water-soluble ligands or biomolecules, such as amine, carboxylic acid, biotin, peptide, antibodies, and DNA. Traditional QDs are viable for biological applications due to heavy metal

surface modifications and the use of heavy metal-free QDs, but in actuality, it is crucial to create QD materials that are safer and more environmentally friendly (Zhua, *et al.*, 2019).

Indium phosphide QDs, for example, is particularly promising in this regard because they are not only cadmium-free but also structurally more durable due to the presence of covalent bonds in their matrix. This structural resilience is due to the non-erosion of component ions in biological systems, which provides greater optical stability and, most importantly, lower toxicity (Yong, *et al.,* 2009). To reduce toxicity effects on indium phosphide QDs, they are further functionalized with capping agents such as zinc sulphide (ZnS), zinc-telluride (ZnTe), or zinc selenide (ZnSe). For solubility, they are made soluble through the ligand exchange process with molecules such as mercaptocarbonic acids or with polymers that possess reactive functional groups for further attachment with biomolecules (Tan & Zhang, 2005).

## 1.12. References


AbouElhamd, A. R., Al-Sallal, K. A. & Hassan, A., 2019. Review of Core/Shell Quantum Dots Technology Integrated into Building's Glazing. *Energies* , 12(16).

Allied Market Research, 2022. *Medical/Diagnostic Imaging Market By Product Type (CT Scanners, X ray Imaging Systems, MRI Systems, Ultrasound Imaging Systems, Nuclear Imaging Systems, Mammography Systems), By Application (Obstetrics and Gynecology Health, Orthopedics and Musculoskeleta,* Canada : Allied Market Research.

Anon., 1995. Clinical applications: MRI, SPECT, and PET. *Magn Reson Imaging,* pp. 1119-1124.

Beloglazova, N. V. *et al.,* 2017. Fluorescently labelled multiplex lateral flow immunoassay based on cadmium-free quantum dots. *Methods,* pp. 141-148.

Bharali, D. J. *et al.,* 2005. Folate-Receptor-Mediated Delivery of InP Quantum Dots for Bioimaging Using Confocal and Two-Photon Microscopy.. *Journal of the American Chemical Society,,* 127(32), pp. 11364-11371.

Biju, V., Itoh, T. & Ishikawa, M., 2010. Delivering quantum dots to cells: bioconjugated quantum dots for targeted and nonspecific extracellular and intracellular imaging. *Chem.Soc. Rev,* p. 3031–3056.

Bilan, R., Fleury, F., Nabiev, I. & Sukhanova, A., 2015. Quantum Dot Surface Chemistry and Functionalization for Cell Targeting and Imaging. *Bioconjugate Chem,* p. 609–624.

Bonilla, C. A. M. & Kouznetsov, V. V., 2016. "Green" Quantum Dots: Basics, Green Synthesis, and Nanotechnological Applications. In: *Green Nanotechnology.* London: IntechOpen, pp. 173-192.

Byers, R. & Tholouli, E., 2017. Multiplexed Bioimaging Using Quantum Dots. In: *Biofunctionalization of Nanomaterials.* s.l.:J. Mater. Chem. B, pp. 115-146.

Chan, W. C. W. & Nie, S., 1998. Quantum Dot Bioconjugates for Ultrasensitive Nonisotopic Detection. *Science* , pp. 2016-2018.

Cotta, M. A., 2020. Quantum Dots and Their Applications: What Lies Ahead?. *ACS Appl. Nano Mater,* pp. 4920-4924.

Dios, A. S. & ElenaDíaz-García, M., 2010. Multifunctional nanoparticles: Analytical prospects. *Analytica Chimica Acta,* pp. 1-22.

Drbohlavova, J., Adam, V., Kizek, R. & Hubalek, J., 2009. Quantum Dots — Characterization, Preparation and Usage in Biological Systems. *Int J Mol Sci,* p. 656–673.

Eren, G. O. *et al.,* 2021. Cadmium-Free and Efficient Type-II InP/ZnO/ZnS Quantum Dots and Their Application for LEDs. *ACS Appl. Mater. Interfaces* , Volume V, p. 32022−32030.

Fleisher, T. A. & Oliveira, J. B., 2019. 92 - Flow Cytometry. *Clinical Immunology (Fifth Edition),* pp. 1239-1259.

Foubert, A. *et al.,* 2016. Bioconjugation of quantum dots: Review & impact on. *Trends in Analytical Chemistry,* Volume 83, pp. 31-48.

Frangioni, J. V., 2008. New Technologies for Human Cancer Imaging. *Journal of Clinical Oncology* , pp. 4012-4021..

Georgia Tech, 2022. *BioImaging | Bioengineering.* [Online] Available at: https://bioengineering.gatech.edu/bioimaging

Gil, H. M. *et al.,* 2021. NIR-quantum dots in biomedical imaging and their future. *iScience.*

Grumezescu, A. M., 2016. *Nanobiomaterials in Medical Imaging: Applications of Nanobiomaterials.* Romania: William Andrew.

Hermanson, G. T., 2013. *Bioconjugate Techniques.* London: Academic press.

Jamieson, T. *et al.,* 2007. Biological applications of quantum dots. *Biomaterials,* pp. 4717-4732.

Kairdolf, B. A. *et al.,* 2013. Semiconductor Quantum Dots for Bioimaging and Biodiagnostic Applications. *Annu Rev Anal Chem (Palo Alto Calif),* p. 143–162.

Kang, H., Kang, M.-W., Kashiwagi, S. & Choi, H. S., 2022. NIR fluorescence imaging and treatment for cancer immunotherapy. *Journal for ImmunoTherapy of Cancer,* 10(7), pp. 1-12.

Karakoti, A. S., Shukla, R., Shanker, R. & Singh, S., 2015. Surface functionalization of quantum dots for biological applications. *Advances in Colloid and Interface Science,* pp. 28-45.

Khan, M., 2021. *What is Green Synthesis of Nanoparticles?,* s.l.: AZoNetwork.

Kumar, S., Aziz, S. T., Girshevitz, O. & D.Nessim, G., 2018. One-Step Synthesis of N-Doped Graphene Quantum Dots from Chitosan as a Sole Precursor Using Chemical Vapor Deposition. *J.Phys.Chem.C,* pp. 2343-2349.

Lee, S. K. & McLaurin, E. J., 2018. However, (TMS)3P is a highly pyrophoric and expensive compound. Moreover, a highly toxic gas, phosphine, is released upon contact with moist air.20,22 Consequently, recent studies have explored replacing the (TMS)3P precursor with other economic and “gree. *Current Opinion in Green and Sustainable Chemistry,* Volume 12, pp. 76-82.

Lignos, I. *et al.,* 2021. A high-temperature continuous stirred-tank reactor cascade for the multistep synthesis of InP/ZnS quantum dots. *React. Chem. Eng,* Volume 6, p. 459–464.

Li, L. *et al.,* 2020. Nephrotoxicity Evaluation of Indium Phosphide Quantum Dots with Different Surface Modifications in BALB/c Mice. *Int J Mol Sci.*

Liu, Y. *et al.,* 2011. Differences between top-down and bottom-up approaches in mineralizing thick, partially-demineralized collagen scaffolds. *Acta Biomate,* 24 April.pp. 1742-1751.

Luc, M. B., John, L. .., Gikas, S. M. & Lawrence, N., 2010. Imaging in Radiation Oncology. *Leibel and Phillips Textbook of Radiation Oncology (Third Edition),* pp. 120-154.

Malik, N., Arfin, T. & U.Khan, A., 2019. Graphene nanomaterials: chemistry and pharmaceutical perspectives. *Nanomaterials for Drug Delivery and Therapy,* pp. 373-402.

Mir, I. A., Das, K., Rawat, K. & Bohidar, H. B., 2016. Hot Injection versus Room Temperature Synthesis of CdSe Quantum Dots: A Differential Spectroscopic and Bioanalyte Sensing Efficacy Evaluation. *Colloids and Surfaces A Physicochemical and Engineering Aspects.*

National Cancer Institute, 2019. [Online] Available at: https://www.cancer.gov/about-cancer/causes-prevention/risk/radiation#:~:text=Radiation%20of%20certain%20wavelengths%2C%20called,forms%20of%20high%2Denergy%20radiation.

National Institute of Biomedical Imaging and Bioengineering, 2020. *Optical Imaging,* Bethesda: National Institute of Biomedical Imaging and Bioengineering.

Nature Journal, 2021. Fluorescent probes. *Nature Journal.*

Nune, S. K. *et al.,* 2009. Nanoparticles for biomedical imaging. *Expert Opin Drug Deliv.,* p. 1175–1194.

Offenhäusser, A. & Rinaldi, R., 2009. Cell-Based Nanobioelectronics. *Nanobioelectronics - for Electronics, Biology, and Medicine,* pp. 255-257.

Pandey, S. & Bodas, D., 2020. High-quality quantum dots for multiplexed bioimaging: A critical review. *Advances in Colloid and Interface Science,* pp. 1-16.

Pereira, G. *et al.,* 2019. (Bio)conjugation Strategies Applied to Fluorescent Semiconductor Quantum Dots. *J. Braz. Chem. Soc,* pp. 2536-2560.

Prasad, P. N., 2003. Bioimaging: Principles and Techniques. In: *Introduction to Biophotonics* . s.l.:s.n., p. 203–254.

Rajasekhar, C. & Kanchi, S., 2018. Green Nanomaterials for Clean Environment. *Handbook of Ecomaterials,* pp. 1-18.

Serrao, E. M., Thakor, A. S., Goh, V. & Gallagher, F. A., 2021. Functional and Molecular Imaging for Personalized Medicine in Oncology. *Grainger & Allison's Diagnostic Radiology,* pp. 1752-1765.

Shen, L., 2011. Biocompatible Polymer/Quantum Dots Hybrid Materials: Current Status and Future Developments. *J Funct Biomater.,* 2(4), pp. 355-372.

Singh, D. P., 2015. *What is Quantum confinement effect?.* [Online].

Singh, J. *et al.,* 2018. Green' synthesis of metals and their oxide nanoparticles: applications for environmental remediation.. *Journal of Nanobiotechnology,* 16(84).

Smith, A. M. *et al.,* 2006. Multicolor quantum dots for molecular diagnostics of cancer. *Expert Rev. Mol. Diagn,* pp. 231-244.

Tan, W. B. & Zhang, Y., 2005. Surface modification of gold and quantum dot nanoparticles with chitosan for bioapplications. *Journal of Biomedical Materials Research Part A,* 75A(1), pp. 56-62.

Tetsuo, N., 2010. Development of fluorescent probes for bioimaging applications. *Proc Jpn Acad Ser B Phys Biol Sci,* 86(8), p. 837–847.

The Society of Nuclear Medicine, 2016. [Online] Available at: https://s3.amazonaws.com/rdcms-snmmi/files/production/public/FileDownloads/Patients/FactSheets/What%20is%20Optical%20imaging%202016.pdf

Thermo Fisher Scientific, 2021. *Fluorescent Probes*, Massachusetts: Thermo Fisher Scientific.

Ueno, S., 2020. *Bioimaging: Imaging by Light and Electromagnetics in Medicine and Biology.* Florida: CRC Press, 2020.

United Nations, 2021. *The 2023 agenda for sustainable development.* s.l.:United Nations.

Valizadeh, A. *et al.,* 2012. Quantum dots: synthesis, bioapplications, and toxicity. *Nanoscale research letters,* 7, (1)((480)).

Vasudevan, D., Gaddamb, R. R., Trinchic, A. & Cole, I., 2015. Core–shell quantum dots: Properties and applications. *Journal of Alloys and Compounds*, pp. 395-404.

Wagner, A. M., Knipe, J. M., Orive, G. & Peppas, N. A., 2019. Quantum dots in biomedical applications. *Acta Biomaterialia,* pp. 44-63.

Yong, K.-T. *et al.,* 2009. Imaging Pancreatic Cancer Using Bioconjugated InP Quantum Dots. *ACS Nano,* pp. 502-510.

Yordanov, G. G. & Dushkin, C. D., 2011. Quantum Dots For Bioimaging Applications: Presents Status and Prospects. *ANNUAIRE DE L'UNIVERSITÉ DE SOFIA "ST. KLIMENT OHRIDSKI",* pp. 81-306.

Zhang, S., Li, L. & Kumar, A., 2009. *Materials characterization techniques.* s.l.: CRC Press.

Zhang, Z. *et al.,* 2015. Dual Emissive Cu:InP/ZnS/InP/ZnS Nanocrystals: Single-Source "Greener" Emitters with Flexibly Tunable Emission from Visible to Near-Infrared and Their Application in White Light-Emitting Diodes. *Chem. Mater,* Volume 27, p. 1405–1411.

Zhua, C. *et al.,* 2019. Recent advances in non-toxic quantum dots and their biomedicalapplications. *Progress in Natural Science: Materials International.*

# 2. Literature Review

## 2.1.Introduction of Quantum dots

Semiconductor quantum dots (QDs) are inorganic compounds made up of elements from groups II-VI or III-V that have distinct optical properties (Karakoti, *et al.*, 2015). With nanometre-sized diameters, these semiconductor nanocrystals exhibit quantum size effects in their optical and electronic properties. Many QD materials systems now have tunable and efficient photoluminescence (PL) with narrow emission and photochemical stability, as well as core-shell structures. As a result, QDs have been used as active elements in a wide range of devices and applications (Cotta, 2020). These unique properties have attracted a lot of attention in the biomedical field in recent years because they enable real-time tissue imaging (bioimaging), diagnostics, single molecule probes, and drug delivery, among many other things. Quantum dots' optical properties can be tuned by size and composition, and their high brightness, photobleaching resistance, multiplexing capacity, and high surface-to-volume ratio make them excellent candidates for intracellular tracking, diagnostics, *in vivo* and *in vitro* imaging, and therapeutic delivery (Wagner, *et al.*, 2019). For these nanocrystals to be fully comparable in the biomedical field, their surface needs to be modified to enhance fluorescence quantum yield, stability, and biocompatibility (Yadav, *et al.*, 2019).

## 2.2.Surface modification of Quantum dots

Surface modification is the act of modifying a material's surface by introducing physical, chemical, or biological properties that differ from those found on the material's original surface. This modification is typically applied to solid materials, but examples of the modification to the surface of specific liquids can be found. Different methods can be used to modify a wide range of surface properties, including hydrophilicity, roughness, surface charge and energy, biocompatibility, and reactivity (London, *et al.*, 2013). The modification of QDs for biological applications is a growing research topic. Bare (core) QDs are unable to be used in biological studies due to the high toxicity posed by metal ion leach from the QD core. Core/shell QDs are created by capping bare QDs with stable compounds such as zinc sulphide (ZnS) sulphide surface defects and high reactivity. While capping the bare QDs with an outer shell such as ZnS helps improve their stability and yield, it has no effect on QD solubility in aqueous media. Coating these QDs with hydrophilic ligands, polymers, and molecules containing functional groups such as carboxylic acids, thiols, and alcohols results in water-soluble QDs (Karakoti, *et al.*, 2015, Tan & Zhang, 2005). Studies have been made whereby the surface of QDs is

modified to apply them in the biomedical field as they require high-quality *water-soluble quantum dots.*

Saikia, *et al.,* described the synthesis, characterization, and biological use of CdTe and CdTe/ZnS QDs capped with mercaptosuccinic acid (MSA). The QDs were created using a straightforward one-pot aqueous method and it was discovered that the synthesized CdTe/ZnS QDs showed excellent stability as compared with that of the CdTe QDs. The CdTe/ZnS had excellent stability up to 100 days after preparation as shown in Figure 2.2c. They also displayed a higher photoluminescence quantum yield (PLQY), which was about 50% higher than that of CdTe QDs, which was only around 12%. Saikia, *et al.,* expanded their research to include bioimaging of E. coli cells using the QD samples and discovered that CdTe/ZnS QDs performed better than uncoated CdTe QDs. The optical properties and stability of CdTe/ZnS QDs are controlled by the ZnS shell. The CdTe/ZnS was found to be superior to CdTe in terms of stability application as bioimaging agents, and the CdTe/ZnS core-shell was found to be superior to CdTe QDs. As a result, their work shed new light on the development of protocols for Core/Shell synthesis and their application to the ever-growing field of bioimaging agents (Saikia, *et al.,* 2017, Mansur, *et al.,* 2017).

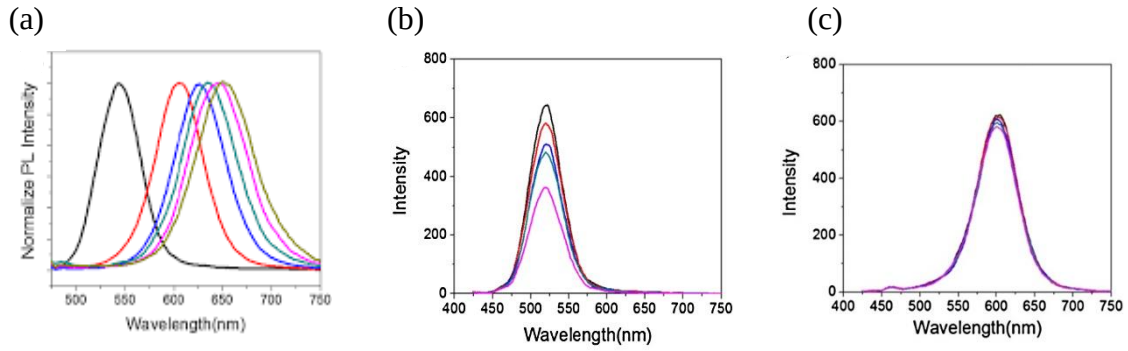


**Figure 2.2:** (a) PL spectra of CdTe QDs and CdTe/ZnS QDs synthesized at different time intervals, (b) PL spectra of CdTe QDs and (c) CdTe/ZnS QDs for different time intervals up to 100 days (Saikia, *et al.,* 2017).

Pandey, *et al.,* synthesized core cadmium telluride (CdTe) QDs that were made biocompatible and hydrophilic by coating them with polydimethylsiloxane (PDMS), an organic polymer. The PDMS-QDs were conjugated with organelle-specific antibodies or biomarkers for *in-vitro* imaging in NIH 3T3 cells. The effect of the QDs on cell viability was measured using the MTT assay. Figure 2.3 shows the results of the reduced viability of NIH 3T3 cells treated with various concentrations of PDMS-QDs and uncoated CdTe QDs. The results showed that

PDMS-QDs were less toxic at 6.25 g/mL concentrations, whereas bare QDs were toxic at all concretions due to $cd^{2+}$ ion leaching (Pandey, *et al.*, 2021).

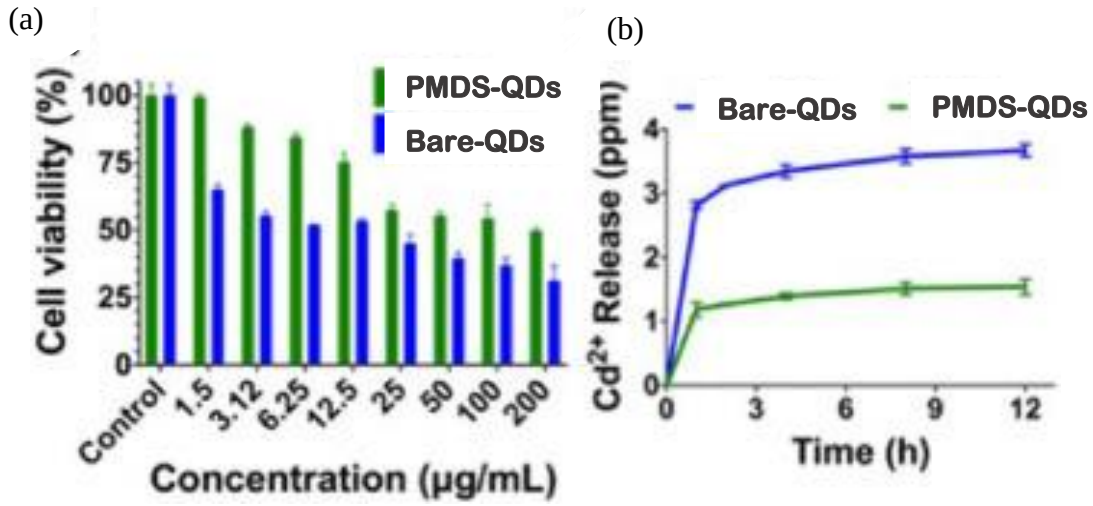


**Figure 2.3:** (a) Cytotoxicity testing on PMDS-QDS and bare-QDs with NIH 3T3 cells, (b) Time-dependent ion leaching studies show that PMDS-QDs release less $Cd^{2+}$ than bare counterparts. (Pandey, *et al.*, 2021).

The core/shell nanocrystals are less susceptible to environmental changes, surface chemistry, and photo-oxidation because the shell creates a physical barrier between the optically active core and the surrounding medium. Additionally, the shell effectively passivates the surface trap states, which results in a significantly increased fluorescence quantum yield. The usage of nanocrystals in applications like biological labelling and light-emitting devices, which depend on their emission qualities, requires this phenomenon as a key precondition. (Reiss, *et al.*, 2009).

When QDs are synthesized, their outer layer is normally composed of hydrophobic molecules such as trioctylphosphine (TOP) or trioctylphosphine oxide (TOPO). To render them water soluble they are normally capped with mercaptocarbonic acids with carboxyl groups such as mercaptoacetic acid, mercaptopropionic acid, or mercaptodecanoic acid to obtain a hydrophilic surface, or with biodegradable polymers. When QDs are capped with mercaptocarbonic acids they are normally kept in buffer solutions or deionized water. However, when QDs are dialyzed against these solvents for an extended period, the thiol-QD bonds formed are far less stable, and QDs begin to precipitate. Furthermore, most QDs are not biocompatible and are somewhat toxic when used in biological applications without any prior surface modification.

Encapsulating QDs within a polymeric sphere is another method for stabilizing them in aqueous solutions. This polymeric material should ideally be biocompatible and have reactive functional groups for further biomolecule attachment. Polymers such as gelatin, chitosan, polyethylene glycol (PEG) and polyacrylic acids (PAG) are often used.

Tan and Zhang reported that CdSe/ZnS QDs, which have been widely used in many fields, were capped with 3MPA and then encapsulated with chitosan, a natural polymer, to improve their biocompatibility. Cell culture studies with HT29 human colon carcinoma and NIH 3T3 mouse fibroblast cells were used to assess the biocompatibility of both types of nanoparticles. The MTT and trypan blue exclusion assays revealed that chitosan-encapsulated QDs were more biocompatible than their bare, non-encapsulated counterparts. As a result, the study well demonstrated that chitosan could be used to encapsulate QDs to improve their biocompatibility (Tan & Zhang, 2005). Figure 2.4 shows the UV -Vis spectra of the chitosan-capped QDs.

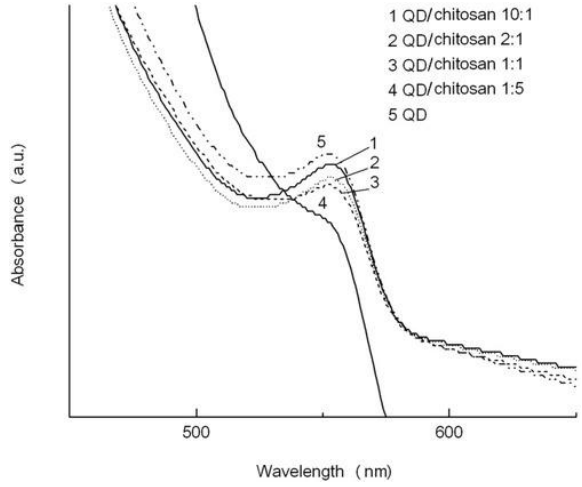


**Figure 2.4:** UV- Vis spectra of chitosan-encapsulated QDs (Tan & Zhang, 2005).

The effects of functionalized, core-shell CdSe/CdS QDs capped with 3MPA and PEG on the brain microenvironment, including QD colloidal stability, toxicity, and cellular uptake *in vitro*, *ex vivo*, and *in vivo*, were thoroughly evaluated by Zhang et al. Importantly, QDs' stability, toxicity, and absorption by cells were all interdependent. They discovered that surface chemistry had a significant impact on brain QD behaviour. PEG coatings resulted in steady, diffuse cellular uptake, reduced cytotoxicity in brain slices, and increased QD stability in complicated neurophysiologically relevant fluids (Figure 2.5). However, when exposed to brain-relevant fluids, non-PEGylated QDs quickly destabilized, preventing penetration into brain tissue. Additionally, they discovered that the delivery of functionalized QDs to brain slices can cause toxicity in a dose-dependent manner (Zhang, *et al.*, 2019).

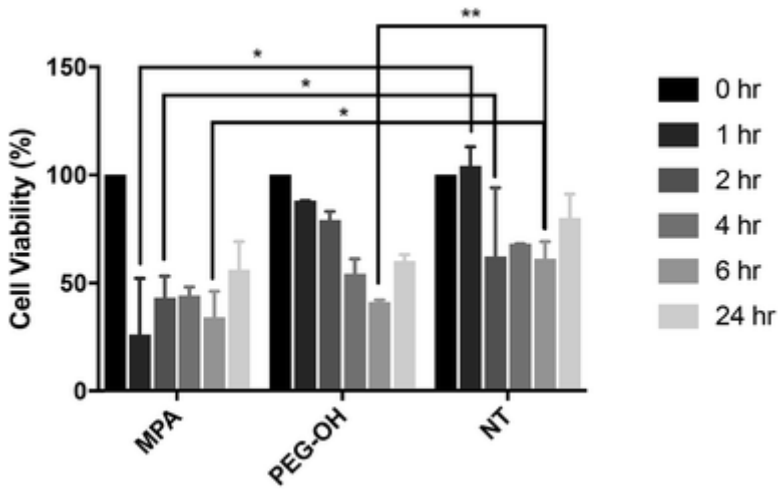


**Figure 2.5:** Toxicity of QDs on *in vitro* BV-2 cells (Zhang, *et al.,* 2019).

For QDs to be fully applied in biological applications, they must be conjugated with targeting ligands such as antibodies, proteins or peptides that are highly effective in detecting antigens or receptors for further biological applications such as disease diagnosis (Liang, *et al.*, 2021). Vo *el at.* presented some results from the conjugation of an E. coli antibody to a highly luminescent core/shell structure CdSe/ZnS. The CdSe core was successfully synthesized using a chemical "green" method. Before the antibody attachment step, the capping surfactant TOPO was replaced with MPA to obtain water-soluble and biological compatibility. Finally, the E. coli antibody was linked to CdSe/ZnS QDs. Bioconjugation of CdSe/ZnS QDs with Antibody E. coli O157:H7: 40 L sulfo-NHS and 40 L 1-ethyl-3-(3-dimethyl aminopropyl) carbodiimide H7 (EDC) [EDC/NHS] coupling chemistry is frequently used to modify the surface chemistry of nanoparticles (NPs) with biological molecules to reduce their toxicity as shown in Figure 2.6. A cross-linker called EDC creates amide bonds between amine and carboxyl groups (Vo, *et al.,* 2015).

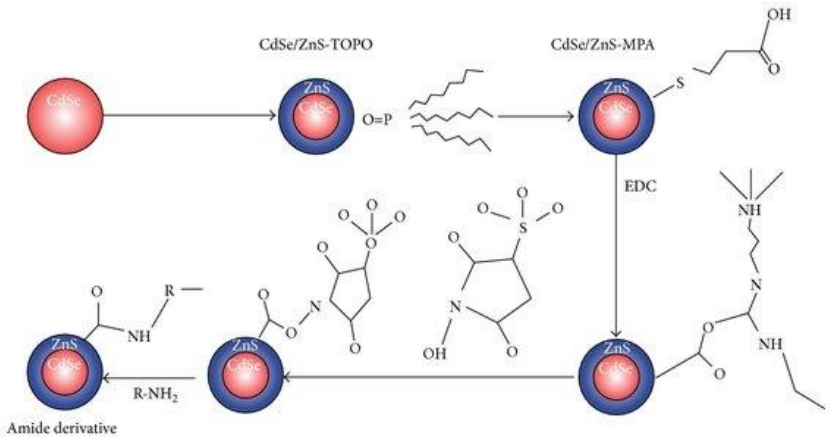

**Figure 2.6:** The bioconjugation procedure of CdSe/ZnS quantum dots (Vo, *et al.*, 2015).

Using NIR QDs functionalized with extra-branched NT4 peptides, Brunetti et al. reported tumour targeting and imaging *in vitro* and *in vivo*. First, a thiol-reactive QD that was attached to the NT4 peptides was created by conjugating the QDs-NH2 with sulfo-SMCC as shown in Figure 2.7. By reacting with a terminal cysteine contained in the peptide sequence, which has a thiol group, the covalent link was created. Nuclear magnetic resonance spectroscopy (NMR), transmission electron microscopy (TEM), dynamic light scattering (DLS) studies, and absorbance/emission spectroscopies were used to characterize these conjugates. When QDs-NT4 was incubated with the human colon cancer cell line (HT29), flow cytometry analysis revealed unique labelling (Brunetti, *et al.*, 2018) (Pereira, *et al.*, 2019).

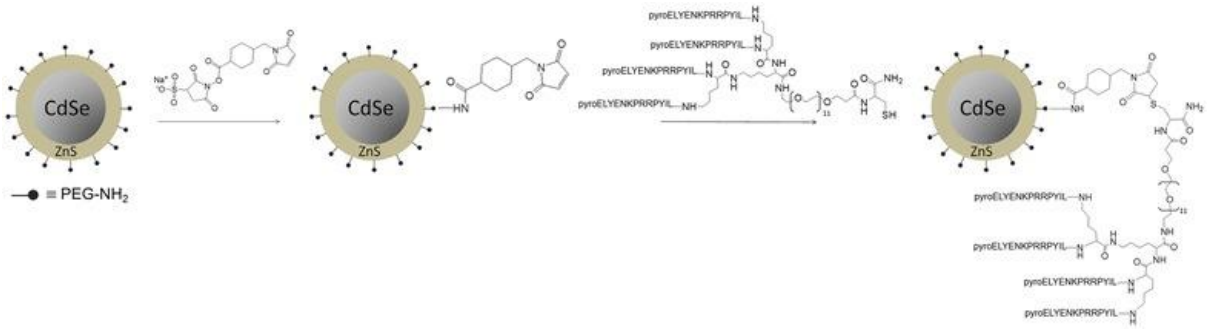


**Figure 2.7:** The synthesis of NT4-QDs (Brunetti, *et al.*, 2018).

Ruan and colleagues used CdSe/ZnS QDs as fluorescent labelling probes to target the phosphatidylserine exposed in the plasma membrane as a result of drug-induced apoptosis. A phospholipid-binding protein known as annexin AV kept an eye on this bioprocess (AV). BS3 was employed as the coupling reagent in the conjugation of amino-QDs with AV. Electrophoresis and fluorescence correlation spectroscopy (FCS) was used to characterize the conjugates. The QD-AV conjugate was treated with both healthy and apoptotic PANC-1 cells, and the results were analysed using flow cytometry and fluorescent microscopy. The outcomes demonstrated the effectiveness of QD-AV conjugates for apoptosis detection (Ruan, *et al.*, 2018) .

### 2.3.Biomedical applications of Quantum dots

Quantum dots (QDs), a more popular name for semiconductor nanoparticles, have distinct, shape- and size-dependent optoelectronic capabilities. Due to the numerous applications they enable, including real-time tissue bioimaging, diagnostics, single-molecule probes, and medication administration, these unique properties have recently attracted a lot of attention in

the biomedical community. The optical properties of QDs can be tailored based on their size and composition, high brightness, immunity to photobleaching, and multiplexing ability. They are good candidates for intracellular tracking, diagnostics, *in vivo* imaging, and therapeutic administration due to their high surface-to-volume ratio (Wagner, *et al.,* 2019). For several bioanalytical applications, including the detection of proteins, DNA, and other biomolecules, cellular labelling, and binding assays, QDs have been utilized effectively as fluorescent labels to probe for target events utilizing fluorescence resonant energy transfer. Biomedical fluorescence imaging continues to be the most alluring and sophisticated QDs application (V.G.Reshma & P.V.Mohanan, 2019). Alivisatos's and Nie provided the first report on the use of QDs as labels in biological research, they were also the first to conjugate biomolecules with QDs in 1998. Ever since the first report on the use of QDs for bio applications, they have been employed more often in biological research for fluorescent applications (Bruchez, et al., 1998, Chan & Nie, 1998).

Highly luminous semiconductor ZnS/CdSe QDs were produced by Chan & Nie and covalently attached to biomolecules, transferrin, and immunomolecules for ultrasensitive biological detection. Figure 2.8 shows ZnS-capped CdSe QD (CdSe/ZnS) that is covalently coupled to a protein by mercaptoacetic acid. In comparison to organic dyes, this class of luminous labels has 20 times the brightness, 100 times the photobleaching stability, and one-third of the spectral linewidth. These conjugates, which are nanometre-sized, are water-soluble and biocompatible. In cultured HeLa cells, transferrin-labelled quantum dots underwent receptor-mediated endocytosis, and immune-molecule-labelled quantum dots recognised particular antibodies or antigens. Chan & Nie also deduced that the biomolecules had covalent bonds with the semiconductor QDs for single-dot level ultrasensitive detection. They hypothesised that the enhanced photostability might enable in-cell molecular trafficking and ligand-receptor interactions to be observed in real-time. Additionally, the current combinatorial labelling method with conventional organic dyes can only detect 25 DNA sequences at once (Speicher, *et al.,* 1996). Further synthetic efforts may produce sufficiently monodispersed QDs *(Peng, et al.,* 1998), which should be important for developing multiplexed detection schemes. The use of QD probes should create new opportunities for the detection of single native biomolecules like cytokines and viral RNA when combined with sandwich immunoassay or nucleic acid hybridization (Chan & Nie, 1998).

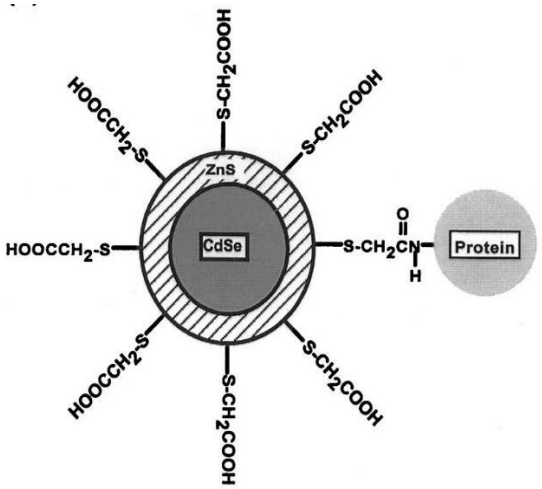


**Figure 2.8:** Schematic CdSe/ZnS QDs that are covalently coupled to a protein by mercaptoacetic acid (Chan & Nie, 1998).

Bruchez, Moronne, Gin, Weiss, & Alivisatos evaluated the cytotoxicity of hydrophobic polysilane capped CdS/CdSe QDs on the human embryonic kidney (HEK-293) and breast cancer (MCF-7) cells as well as enrichment ascites cells (EAC) using the MTT assay. For the core-shell QDs, biotoxicity of about 65 percent was seen in the MCF-7cell line. They conjugated QDs to biotin, to label F-actin cell filaments using a biotin-streptavidin strategy. They concluded that these QDs may work well in other optoelectronic devices. The generated QDs had excellent optical qualities. The particle size was determined to be between 3 and 4 nm, with a cubic crystal structure and a spherical shape (Bruchez, *et al.,* 1998).

Cadmium-based and Tellurium-based QDs such as CdSe, CdTe, and CdS QDs have been used most frequently in biology and medical research to date, frequently with additional protective shells such as ZnS, CdSe, HgS, etc. These Cd-based QDs are quite popular because they are simple to make using commonly accessible precursors and basic solution phase synthesis techniques. These QD preparation and application procedures have been relatively standardized. Additionally, they are easily accessible commercially in configurations designed for certain biological experiments and uses (Kirchner, *et al.,* 2005, Xu, *et al.,* 2016). Furthermore, these QDs include hazardous heavy metal components and their toxicity in *in vivo* and *in vitro* which has sparked widespread negative interest (Li, *et al.*, 2020).

QDs have been shown to influence cell development, change gene expression, cause DNA damage, and induce cell death in human cells, mice, zebrafish, and even microbes. (Liang & Tang, 2019, Fan, *et al.,* 2016). Nguyen and co-workers investigated the effects of cadmium telluride quantum dots (CdTe-QDs) on mitochondria in HepG2 cells from human

hepatocellular carcinoma. The CdTe-QD treatment caused mitochondrial enlargement, which was observed using transmission electron microscopy (TEM) and confocal microscopy. Because of their inherent fluorescence, the CdTe-QDs appeared to associate with isolated mitochondria. The CdTe-QD caused mitochondrial membrane potential disruption, increased intracellular calcium levels, impaired cellular respiration, and decreased adenosine triphosphate (ATP) synthesis, according to additional research. The effects of CdTe-QDs on mitochondrial oxidative phosphorylation were demonstrated by changes in the levels and activities of electron transport chain enzymes. The increase in peroxisome proliferator-activated receptor-coactivator levels after CdTe-QD treatment suggested that CdTe-QDs affected mitochondrial biogenesis. Their findings also revealed that the toxic effects of CdTe-QDs were comparable to or greater than those of cadmium chloride at equivalent cadmium concentrations, implying that the toxic effects of CdTe-QDs were not solely due to cadmium released from the NPs. Overall, the study found that CdTe-QDs caused multifaceted toxicity by altering mitochondrial morphology and structure, impairing mitochondrial function, and stimulating mitochondrial biogenesis (Liang & Tang, 2019, Nguyen, *et al.*, 2015).

Chen *et al.*, discovered that CdTe QDs may cluster in human hepatocellular carcinoma cells (HepG2), human kidney cells 2 (HK-2), and Madin-Darby canine kidney (MDCK) cells and produced considerable toxicity in all three cell lines (Chen, *et al.*, 2016). According to several earlier research, the release of harmful ions such as cadmium ions from the core is primarily responsible for the biological toxicity of heavy metal based QDs. While bulk cadmium selenide's (CdSe) cytotoxicity is widely known, some studies have found that CdSe QDs are not harmful, at least not to some immortalized cell lines. Derfus, Chan, and Bhatia discovered that CdSe-core QDs were acutely hazardous under specific circumstances using primary hepatocytes as a liver model. They discovered that surface coatings, UV light exposure, and synthesis processing conditions might all affect how lethal QDs are. Their findings further suggested that the degradation of the CdSe lattice coincides with the release of free $Cd^{2+}$ ions, which correlates with cytotoxicity. The CdSe-core QDs may be made harmless and utilized to monitor cell movement and re-organization *in vitro* when they are properly coated *(Derfus, et al.*, 2004). On the other hand, even without considering the possible effects of Cd-QDs on the environment, the inherent toxicity of Cd-based QDs has very little promise for real-life bioimaging and diagnostics *in vivo*. Due to this, eco-friendly QDs have been developed and have garnered a lot of attention during the past 10 years, which one set is described below (Li, *et al.*, 2020).

## 2.4.Indium Phosphide Quantum dots

Colloidal quantum dots (QDs) made of indium phosphide (InP) have drawn a lot of interest over the past two decades as a possible less toxic substitute for QDs made of cadmium. Their innovations in colloidal synthesis techniques have made it possible to synthesise a variety of materials, heterojunctions, dopants, and ligands, enabling spectral tuning from the blue to the near-infrared, narrow emission line widths, and perfect quantum yields close to unity. They also have better optical stability than cadmium chalcogenides due to their higher covalency. Modern InP QDs have excelled in many applications, including light-emitting diodes, luminescent solar concentrators (LSCs), and commercially viable solar cells, thanks to their attractive optical and electronic properties (Jalali, *et al.,* 2022). Among semiconductor QDs, InP has one of the highest levels of colloidal synthesis evolution (Kim, *et al.,* 2018).

### 2.4.1. Synthesis of Indium Phosphide Quantum dots

In 1989, Healy et al. created InP for the first time through an organometallic reaction involving $InCl_3$ and tris(trimethylsilyl) phosphine $(TMS)_3P$ (Healy, et al., 1989). Then, in 1995, Wells et al. successfully produced nanocrystalline InP by thermally decomposing and annealing intermediate powders resulting from silyl cleavage reactions, then removing $Me_3SiCl$ one step at a time (Wells, *et al.,* 1995). Wells' method featured a number of thermal processes that, at high temperatures, led to precipitation and irreversible particle aggregation. Additionally, compared to CdSe QDs, these processes resulted in InP QDs with weaker quantum confinement and worse emission properties. The reaction times for these processes ranged from 3 to 7 days (Murray, *et al.,* 1993). Hot-injection, heat-up, and seeded growth techniques for the synthesis of InP QDs were created to address these problems. The majority of reported QDs are typically synthesised using the first two techniques (Jalali, *et al.,* 2022).

- Hot injection

The hot-injection method involves rapidly injecting precursor A into a hot reaction medium containing precursor B or rapidly injecting both precursor A and precursor B into a hot medium (Murray, *et al.,* 1993, Wang, *et al.,* 2016). The rapid injection causes monomer formation and a burst of nucleation, which is followed by the growth stage. Murray et al. used hot injection for the first time to synthesize Cd-based QDs (Tamang, *et al.,* 2016). Inspired by the classic synthesis of CdSe QDs, Battaglia et al. introduced a novel synthesis method for InP QDs in 2002 that was faster (3-4 h), less expensive, and "greener" than previous studies. By quickly injecting $(TMS)_3P$ precursors to indium acetate in 1-octadecene (ODE) and fatty acids while

closely monitoring the reaction parameters and the crucial degassing procedure, they were able to create InP QDs. This process became "greener" and more affordable when 1-ODE took the place of the organophosphine oxide solvent (Battaglia & Peng, 2002). They were able to produce InP QDs by rapidly introducing (TMS)3P precursors to indium acetate in 1-octadecene (ODE) and fatty acids while meticulously monitoring the reaction parameters and the essential degassing procedure. When 1-ODE replaced the organophosphine oxide solvent, the procedure became "greener" and more affordable (Chen, *et al.*, 2020), (Jalali, *et al.*, 2022). The reaction setup is shown in Figure 2.9.

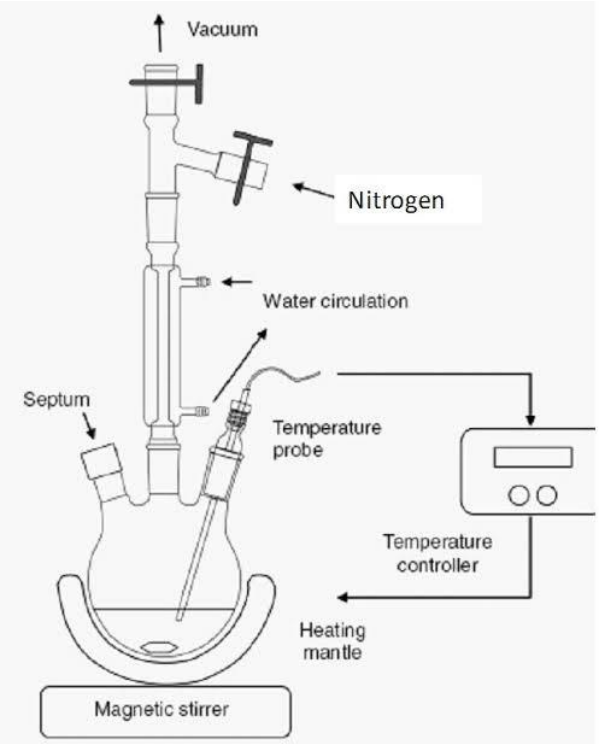


**Figure 2.9:** Diagram showing a typical hot injection method (Jasim, 2015).

- Heat-up method

The heat-up method is a non-injection technique that involves gradually heating the precursors in the presence of the ligand. The heat-up method is generally regarded as a more efficient method of preparing nanocrystals because it allows them to be prepared in a single pot without the need for injection. Because nucleation events are spread over a significant period, the majority of heat-up synthesis methods produce polydisperse particle size distribution.

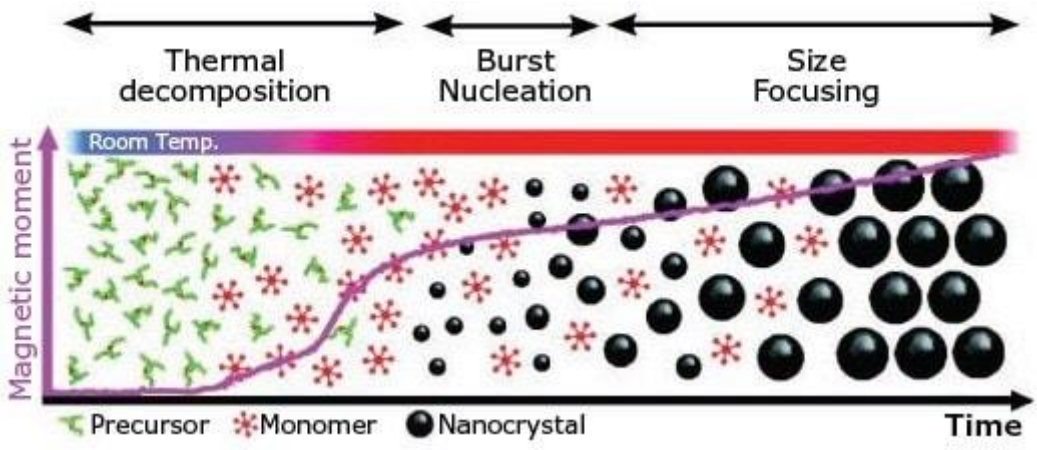


**Figure 2.10:** The heat-up method is depicted schematically (Sinatra, *et al.,* 2017).

- Hazards of the phosphorus precursor: $(TMS)_3P$

One of the major challenges in the hot-injection method of synthesis of InP is the use of $(TMS)_3P$ as a phosphorus precursor due to its excessive cost. Li et al. devised a novel synthesis route based on in situ generated gaseous $PH_3$ from calcium phosphide to address this issue. However, the toxicity of $PH_3$ limited the method's further development. Amino phosphines were recently proposed as an alternative to $(TMS)_3P$ by researchers. Tessier et al. demonstrated new chemistry for the formation of InP QDs by using phosphine as both a precursor and a reducing agent (Jalali, *et al.,* 2022, Tessier, *et al.,* 2016).

Ellis and co-workers prepared InP/ZnS QDs using tris (dimethyl amino) phosphine as a phosphorus precursor via a hot-injection method. Poly (maleic anhydride -*alt*-1-1octadecene) was used as an amphiphilic polymer to make the QDs water soluble. The toxicity of these synthesized QDs was tested on N2a cells using a trypan blue toxicity assay. Their results concluded that InP/ZnS QDs are suitable for cellular investigation processes and biomedical applications as alternatives to Cd-based QDs (Ellis, *et al.,* 2016).

Dobhal et al. showed how to label and detect exosomes from the THP-1 cell line (monocyte cell line) using InP/ZnS (using tris (diethyl amino) phosphine as a phosphorus precursor). By employing a CD63 antibody, they focused on a protein (CD63) that is known to be present on the exosome surface. A ligand-exchange technique was used to initially make the quantum dots water-soluble before the antibody was added. This illustrates the potential for targeting nanoscale biomarkers that might then be used for the detection of various diseases using a non-toxic compound. In addition, Dobhal et al. concluded that using InP/ZnS QDs instead of

cadmium offered a more reliable and secure substitute. They are sufficiently small to be able to pinpoint their location precisely. These nanomaterials could be employed in vitro for deep tissue imaging with minimal background fluorescence interferences because of the tailoring of their near-infrared fluorescence during manufacture (Dobhal, *et al.*, 2018).

### 2.5.Biocompatibility of Indium Phosphide Quantum dots

The cytotoxicity of InP as an alternative to Cd-based QDs has been investigated by different groups. Of these, the InP QDs coated with ZnS shell forming InP/ZnS is the most reported type of QDs for bio applications. According to several types of research, InP/ZnS QDs exhibit less biological toxicity than Cd-based QDs (Liu, *et al.*, 2015, Riviere, *et al.*, 2018). Brunetti *et al.*, showed that water-soluble InP/ZnS core/shell QDs using $(TMS)_3P$, as a safer alternative to CdSe/ZnS core/shell QDs for biological applications by comparing their toxicity *in vitro* and *in vivo*. By quickly adding (TMS)3P precursors to indium acetate in 1-octadecene (ODE) and fatty acids while meticulously monitoring the reaction parameters and the crucial degassing procedure, they were able to make InP QDs. The procedure was made "greener" and more affordable when 1-ODE took the place of the solvent, organophosphine oxide. After 24 hours of incubation at 1 nM concentration, the toxic effect of Cd-containing QDs was observed (Fig. 2.11A and B). For CdSe/ZnS QD concentrations as low as 10 pM, a detectable reduction in cell viability was observed after 48 hours of exposure. The neuronal cell line had the highest toxicity, with a 27% viability loss after 24 hours that increased to 46% after 48 hours (Fig. 2.11B, red bars) with 5 nM CdSe/ZnS QDs. The epithelial cell line appeared to be more resistant under these conditions, with a loss of viability of 33% after 48 h (Fig. 2.11A, red bars) with 5 nM CdSe/ZnS. In contrast, incubation for 48 h with 5 nM InP/ZnS QDs produced only a statistically insignificant reduction in cell viability (Brunetti, *et al.*, 2013).

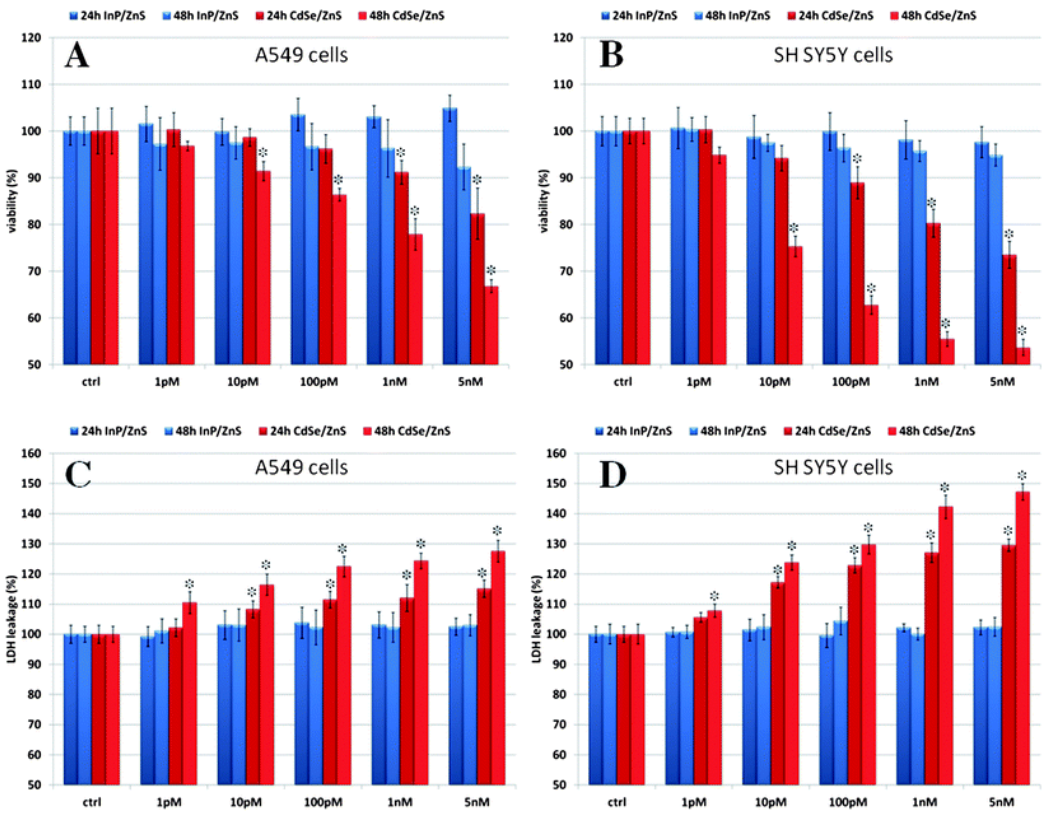


**Figure 2.11:** (A and B) WST-8 proliferation assay and (C and D) LDH assay on A549 and SH SY5Y cells incubated with increasing concentrations of InP/ZnS and CdSe/ZnS QDs at different times (24 and 48 h) (Brunetti, *et al.*, 2013).

Highly monodispersed hydrophilic InP/ZnS nanocrystals were synthesized, and Bharali and associates described how to employ them as luminescence probes for live cell imaging. These QDs were enclosed in mercaptoacetic acid (MAA), which made it simple for folic acid to conjugate with them. They were subsequently investigated in A549 cells, a human lung cancer cell line lacking the folic acid receptor, and KB cells, a human nasopharyngeal epidermal carcinoma cell line overexpressing the surface receptor for folic acid as a positive control (Bharali, *et al.*, 2005).

(Yong, *et al.*, 2009) revealed the successful use of quantum dots (QDs) made without cadmium as extremely effective and non-toxic optical sensors for observing live pancreatic cancer cells. Hot colloidal synthesis was used to create indium phosphide (core)-zinc sulphide (shell) quantum dots, or InP/ZnS, with high quality and brilliant luminescence in non-aqueous mediums. Mercaptosuccinic acid was subsequently used to functionalize the surfaces of these QDs, making them highly dispersible in aqueous solutions. Pancreatic cancer cell lines could be specifically targeted in vitro by adding pancreatic cancer-specific monoclonal antibodies to the functionalized InP/ZnS QDs, such as anti-claudin 4 and anti-prostate stem cell antigen

(anti-PSCA) (both immortalized and low passage ones). The observation of poor in vitro targeting in non-pancreatic cancer-based cell lines that are negative for the claudin-4- receptor further supported the receptor-mediated transport of the bioconjugates. These findings point to the enormous potential of InP/ZnS QDs as non-cadmium-based optical imaging nanoprobes for diagnostic imaging, notably for the early identification of cancer.

### 2.6.Bioimaging with Indium Phosphide Quantum dots

Alivisatos and Nie's groups pioneered the use of QDs for luminescent probes due to their high photochemical stability, tunable PL, and good PLQY. However, due to the toxicity of Cd-based QDs, researchers have been looking for Cd-free QDs for bioimaging (Jalali, *et al.,* 2022). Over the last two decades, indium phosphide (InP) colloidal quantum dots (QDs) have received considerable attention as a potentially less toxic alternative to cadmium based QDs. Their innovations in colloidal synthesis techniques have made it possible to synthesise a variety of materials, heterojunctions, dopants, and ligands, enabling spectral tuning from the blue to the near-infrared, narrow emission line widths, and perfect quantum yields close to unity. Additionally, compared to cadmium chalcogenides, it has a higher covalency, which results in improved optical stability (Jalali, *et al.,* 2022). The main attraction of these semiconductors is the strength of the covalent link in the group III-V semiconductor matrix, as opposed to the ionic bond in the group II-VI semiconductors. The existence of the covalent bond has two advantages: it improves the optical stability of QD systems and reduces toxicity *(Mushonga, et al.,* 2012). InP QDs, like CdSe QDs, have a photoluminescence (PL) wavelength that can be adjusted from blue to near-infrared (NIR) by changing the particle size. By coating an InP core in a ZnS shell, the PL quantum yield of InP/ZnS core/shell QDs can be greatly increased. This can passivate surface flaws, limit excitons, stop core oxidation, and passivate the material's surface chemistry (Brown, *et al.,* 2018, Xie, *et al.,* 2007). Because of their high sensitivity and low toxicity, high-performance InP QDs have been used as fluorescent probes for cell imaging, cell diagnostics, and also antibiotic potentiators.

Nanocrystals with narrow emission spectra and low toxicity are required for biomedical applications. The ability to synthesize quantum dots (QDs) in large quantities while retaining desirable optical properties has been a major challenge in biomedical research. Before 2016, no report on the use of InP/ZnSe QDs for bio application was carried out. Kiplagat *et al.,* synthesized InP/ZnSe using (TMS)3P and carried out cytotoxicity studies using two different types of non-cancerous human cell lines, namely KMST6 and MCF-12A, which clearly

showed that the nanocrystals have low toxicity and are suitable for biological applications as shown in Figure 2.12 (Kiplagat, *et al.*, 2016).

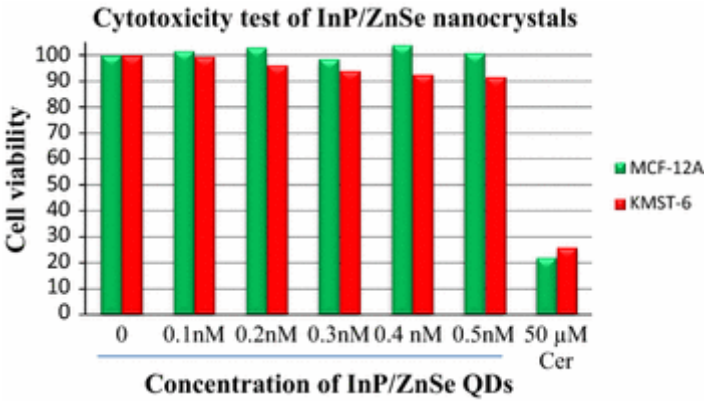


**Figure 2.12:** The cytotoxicity studies of InP/ZnSe nanocrystals tested using MCF-12A and KMST-6 non-cancerous cell lines (Kiplagat, *et al.*, 2016).

The successful synthesis of cadmium-free QDs and indium phosphide QDs has demonstrated their utility as fluorescent labels and makes them suitable for use in rapid fluorescent multiplex tests (Beloglazova, *et al.*, 2017). QDs' massive multiplexing capabilities enable the simultaneous detection of multiple disease indicators. QDs have enormous potential in multiplexed bioimaging for deciphering the complicated gene expression patterns of malignancies and for precise clinical diagnosis. (Smith, Dave, Nie, True, & Gao, 2006) Due to their decreased toxicity and capacity to tune their emission from the visible to near-infrared ranges, indium phosphide QDs are a desirable option (Ramasamy, *et al.*, 2017).

### 2.7.Multiplexed Bioimaging

The primary focus of biological and biomedical research is on how genes and the protein products they produce function and interact in individual cells, organ systems, and organisms. Therefore, a method is required that can simultaneously detect multiple genes or proteins and also provide good spatial and cellular resolution at the morphological level. The aforementioned strategy, for instance, has led to global gene expression profiling studies in the field of cancer that have identified a number of gene signatures as markers, either of tutor categories with distinct behaviours or predictive of disease progression and therapeutic response. The application of such signatures to individual patients in a clinical setting has the potential to greatly improve diagnosis, guide tailored molecular therapy, and make informed therapeutic decisions. As a result, there is a clear need for a generic method for the simultaneous

visualization of multiple genes, which will allow researchers to investigate the spatial localization of microarray gene signatures (Byers & Tholouli, 2017).

Panagiotopoulou et al. reported the use of molecularly imprinted polymer (MIP) coated QDs for multiplexed bioimaging. They coupled InP/ZnS QDs with glucuronic acid (GlcA) with green QDs and N-acetylneuraminic acid (NANA) with red QDs for multiplexed labelling of human keratinocytes. They demonstrated MIP-QD-based multiplexed imaging with a single excitation wavelength. Green and red QDs were stimulated at 365 nm and released fluorescent light at 550 nm and 660 nm, respectively (Panagiotopoulou, *et al.,* 2016) . Their research shows for the first time that molecularly imprinted polymers can be used as a versatile multiplexed imaging tool when conjugated to quantum dots of different emission colours.

For the first time, a sensitive method based on the use of non-cadmium quantum dots (QDs) was given by Beloglazova et al. for the simultaneous qualitative detection of two mycotoxins. They created luminous nanostructures based on InP QDs that are water-soluble. They were made up of InP/ZnS QDs with a core and a shell that was encased in a silica shell to allow for water solubility. A new silica shell-encapsulated fluorescent was then used in immunoassays for quick multiplexed screening. Zearalenone and deoxynivalenol, two mycotoxins, were found in maize and wheat at the same time because the two QD@SiO2 tagged conjugates emit at two distinct, independently identifiable wavelengths. Zearalenone and deoxynivalenol, which are found in both maize and wheat, have cut-off values of 50 and 500 g $kg^{-1}$ in the simultaneous determination, respectively. The outcome was verified using LC-MS/MS, a combination of liquid chromatography and tandem mass spectrometry. (Beloglazova, *et al.,* 2017, Kairdolf, *et al.*, 2013).

This literature review showed vast research on bare cadmium and core/shell cadmium-based QDs for biological applications. The high toxicity associated with these nanocrystals has opened a field of research on indium-based QDs amongst other QDs. Indium-phosphide-based were researched and synthesized using $(TMS)_3P$ as the phosphorus precursor, due to their hazardous nature, tris (dialkyl amino) phosphines are being researched. Amongst core/shell indium-based QDs that exist, the majority of the literature reports InP/ZnS for bio applications. In conclusion, this study will report the green synthesis of indium-phosphide -based core/shell QDs for multiplexed bioimaging. InP/ZnS and InP/ZnSe will be synthesized using dialkylamino phosphines (tris (diethyl amino) phosphine and tris (dimethyl amino) phosphine) as safer alternatives to $(TMS)_3P$. This study is the first to report a ligand exchange of InP/ZnS

and InP/ZnSe with 3-mercaptopropionic acids (3MPA), followed by capping a chitosan polymer. Chitosan will be used as a polymer for ligand exchange to make the QDs stable and less toxic. Chitosan contains functional groups that will allow further bioconjugation with biomolecules. The synthesized QDs will be further characterized with characterization techniques such as PL, UV-Vis, FTIR, HRTEM, XRD, and DLS. These techniques will be used for the determination of different parameters such as particle size, and shape.

### 2.8.Aim and Objectives

This research aims to achieve simultaneous visualization of multiple genes.

1. To synthesize indium-based core/shell quantum dots: InP/A, A= ZnS; ZnSe; core/shell QDs.
2. To bioconjugate the synthesized core/shell quantum dots with 3-mercaptopropionic acid and chitosan.
3. To characterize all the synthesized quantum dots with different analytical techniques such as UV-Vis, PL, FTIR and HRTEM.
4. To carry out toxicity studies in live cells, namely KMST- 6, Caco-2, and H9C2.

## 2.9.References


Allocca, M *et al.,*. 2019. An Integrated Multilevel Analysis Profiling Biosafety and Toxicity Induced by Indium- and Cadmium-Based Quantum Dots in Vivo. *Environ. Sci. Technol*, p. 3938–3947.

Ankireddy, S. R. & Kim, J., 2015. Dopamine-functionalized InP/ZnS quantum dots as fluorescence probes for the detection of adenosine in microfluidic chip. *Int. J. Nanomed*, p. 121–128.

Battaglia, D. & Peng, X., 2002. Formation of High Quality InP and InAs Nanocrystals in a Noncoordinating Solvent. *Nano Letters*, p. 1027–1030..

Beloglazova, N. V. *et al.,* 2017. Fluorescently labelled multiplex lateral flow immunoassay based on cadmium-free quantum dots. *Methods*, pp. 141-148.

Brown, R. P., Gallagher, M. J., Fairbrother, H. & Rosenzweig, Z., 2018. Synthesis and Degradation of Cadmium-Free InP and InPZn/ZnS Quantum Dots in Solution. *Langmuir*, p. 13924–13934.

Bruchez, J. M. *et al.,* 1998. Semiconductor Nanocrystals as Fluorescent Biological Labels. *Science,,* 281(5385), pp. 2013-2016.

Brunetti, V. *et al.,* 2013. InP/ZnS as a safer alternative to CdSe/ZnS core/shell quantum dots: in vitro and in vivo toxicity assessment. *Nanoscale,,* Volume 5, pp. 307-317.

Byers, R. & Tholouli, E., 2017. Multiplexed Bioimaging Using Quantum Dots. In: *Biofunctionalization of Nanomaterials.* s.l.:J. Mater. Chem. B, pp. 115-146.

Chan, W. C. W. & Nie, S., 1998. Quantum Dot Bioconjugates for Ultrasensitive Nonisotopic Detection. *Science* , pp. 2016-2018.

Chen, B., Li, D. & Wang, F., 2020. InP Quantum Dots: Synthesis and Lighting Applications. *Small.*

Chen, M. *et al.,* 2016. ABC transporters affect the elimination and toxicity of CdTe quantum dots in liver and kidney cells. *Toxicology and Applied Pharmacology,* pp. 11-20.

Derfus, A. M., Chan, W. C. W. & Bhatia, S. N., 2004. Probing the Cytotoxicity of Semiconductor Quantum Dots. *Nano Letters* , pp. 11-18.

Fan, J. *et al.,* 2016. Inhibition of autophagy overcomes the nanotoxicity elicited by cadmium-based quantum dots. *Biomaterials*, pp. 102-114.

Healy, M. D., Laibinis, P. E., Stupik, P. D. & Barron, A. R., 1989. The reaction of indium(III) chloride with tris(trimethylsilyl)phosphine: a novel route to indium phosphide. *J. Chem. Soc., Chem. Commun*, p. 359–360.

Huang, S. *et al.,* 2016. Systematical investigation of in vitro interaction of InP/ZnS quantum dots with human serum albumin by multispectroscopic approach. *Colloids Surfaces B*, p. 165–172..

Jalali, H. B. *et al.,* 2022. Past, present and future of indium phosphide quantum dots. *Nano Research*, pp. 1-22.

Janus, Ł. *et al.*, 2019. Chitosan-Based Carbon Quantum Dots for Biomedical Applications: Synthesis and Characterization. *Nanomaterials*, 9(274), pp. 1-13.

Jiang, W., Choi, Y. & Chae, H., 2021. Efficient green indium phosphide quantum dots with tris(dimethylamino)-phosphine phosphorus precursor for electroluminescent devices. *Journal of Materials Science: Materials in Electronics* , p. 4686–4694.

Kairdolf, B. A. *et al.*, 2013. Semiconductor Quantum Dots for Bioimaging and Biodiagnostic Applications. *Annu Rev Anal Chem (Palo Alto Calif)*, p. 143–162.

Karakoti, A. S., Shukla, R., Shanker, R. & Singh, S., 2015. Surface functionalization of quantum dots for biological applications. *Advances in Colloid and Interface Science*, Volume 215, pp. 28-45.

Kim, T. -G. *et al.*, 2018. Trap Passivation in Indium-Based Quantum Dots through Surface Fluorination: Mechanism and Applications. *ACS Nano*, p. 11529–11540..

Kiplagat, A. *et al.*, 2016. The cytotoxicity studies of water-soluble InP/ZnSe quantum dots. *J Nanopart Res*, pp. 1-12.

Kirchner, C. *et al.*, 2005. Cytotoxicity of colloidal CdSe and CdSe/ZnS nanoparticles. *Nano Lett*, pp. 331-338.

Kumari, A., Sharma, A., Malairaman, U. & RajSingh, R., 2018. Proficient surface modification of CdSe quantum dots for highly luminescent and biocompatible probes for bioimaging: A comparative experimental investigation. *Journal of Luminescence*, pp. 174-182.

Levy, M. *et al.*, 2019. Near-Infrared-Light-Triggered Antimicrobial Indium Phosphide Quantum Dots. *Angew. Chem. Int. Ed*, pp. 11414-22528.

Liang, X. & Tang, M., 2019. Research Advances on Cytotoxicity of Cadmium-Containing Quantum Dots.. *J. Nanosci. Nanotechnol*, p. 5375–5387.

Liang, Z., Khawar, M. B., Liang, J. & Sun, H., 2021. Bio-Conjugated Quantum Dots for Cancer Research: Detection and Imaging. *Front Oncol.*

Li, L. *et al.*, 2020. Nephrotoxicity Evaluation of Indium Phosphide Quantum Dots with Different Surface Modifications in BALB/c Mice. *Int J Mol Sci.*

Liu, J. *et al.*, 2015. Cytotoxicity assessment of functionalized CdSe, CdTe and InP quantum dots in two human cancer cell models. *Materials Science and Engineering*, pp. 222-231.

Mahajan, S., Rani, M., Dubey, R. B. & Mahajan, J., 2013. SYNTHESIS OF CdSe CRYSTAL USING HOT INJECTION METHOD. *International Journal of Latest Research in Science and Technology* , pp. 518-521.

Mansur, A. A. P. *et al.*, 2017. Carboxymethylcellulose/ZnCdS fluorescent quantum dot nanoconjugates for cancer cell bioimaging. *International Journal of Biological Macromolecules*, pp. 675-686 .

Muralidhara, S., Malu, K., Gaines, P. & M.Budhlall, B., 2019. Quantum dot encapsulated nanocolloidal bioconjugates function as bioprobes for in vitro intracellular imaging. *Colloids and Surfaces B: Biointerfaces.*

Murray, C. B., Norris, D. J. & Bawendi, M. G., 1993. Synthesis and characterization of nearly monodisperse CdE (E = S, Se, Te) semiconductor nanocrystallites. *J. Am. Chem. Soc.*, p. 8706–8715.

Mushonga, P., 2013. Fabrication of type I indium-based near-infrared emitting quantum dots for biological imaging applications. *University of the Western Cape Library Services,* pp. 3-4.

Mushonga, P., Onani, M. O., Madiehe, A. M. & Meyer, M., 2012. Indium Phosphide-Based Semiconductor Nanocrystals and Their Applications. *Journal of Nanomaterials* .

Muxika, A. *et al.,* 2017. Chitosan as a bioactive polymer: processing, properties and. *International Journal of Biological Macromolecules,* pp. 1-49.

Nguyen, K. C., Rippstein, P., Tayabali, A. F. & Willmore, W. G., 2015. Mitochondrial Toxicity of Cadmium Telluride Quantum Dot Nanoparticles in Mammalian Hepatocytes. *Toxicol Sci,* pp. 31-42.

Panagiotopoulou, M. *et al.,* 2016. Molecularly Imprinted Polymer Coated Quantum Dots for Multiplexed Cell Targeting and Imaging. *Angewandte Chemie International Edition,* pp. 8244-8248.

Pandey, S. *et al.,* 2021. Multiplexed bio-imaging using cadmium telluride quantum dots synthesized by mathematically derived process parameters in a continuous flow active microreactor. *Materials Today Bio.*

Peng, X., Wickham, J. & Alivisatos, A. P., 1998. Kinetics of II-VI and III-V Colloidal Semiconductor Nanocrystal Growth: "Focusing" of Size Distributions. *J Am. Chem.*, p. 5343–5344.

Peuschel, H. *et al.,* 2016. Penetration of CdSe/ZnS quantum dots into differentiated vs undifferentiated Caco-2 cells. *Journal of Nanobiotechnology.*

Peynshaert, K. *et al.,* 2017. Coating of Quantum Dots strongly defines their effect on lysosomal health and autophagy. *Acta Biomaterialia,* pp. 195-205.

Ramasamy, P. *et al.,* 2017. Tunable, Bright, and Narrow-Band Luminescence from Colloidal Indium Phosphide Quantum Dots. *Chem. Mater.* , Volume 29, p. 6893−6899.

Riviere, J. E. *et al.,* 2018. Modeling gold nanoparticle biodistribution after arterial infusion into perfused tissue: effects of surface coating, size and protein corona. *Nanotoxicology,* p. 1093–1112.

Saikia, D. *et al.,* 2017. Aqueous synthesis of highly stable CdTe/ZnS Core/Shell quantum dots for bioimaging. *Luminescence,* pp. 401-408.

Smith, A. M. *et al.,* 2006. Multicolor quantum dots for molecular diagnostics of cancer. *Expert Rev. Mol. Diagn,* pp. 231-244.

Speicher, M. R., Ballard, S. G. & Ward, D. C., 1996. Karyotyping human chromosomes by combinatorial multi-fluor FISH. *Nat Genet.*

Tamang, S. *et al.,* 2016. Chemistry of InP Nanocrystal Syntheses. *Chem. Mater,* p. 2491–2506.

Tan, W. B. & Zhang, Y., 2005. Surface modification of gold and quantum dot nanoparticles with chitosan for bioapplications. *Journal of Biomedical Materials Research Part A,* 75A(1), pp. 56-62.

Tessier, M. D. *et al.,* 2016. Aminophosphines: A Double Role in the Synthesis of Colloidal Indium Phosphide Quantum Dots. *J. Am. Chem. Soc.,* pp. 5923-5929.

V.G.Reshma & P.V.Mohanan, 2019. Quantum dots: Applications and safety consequences. *Journal of Luminescence,* pp. 287-298.

Vinay, P., Ravi, K. A., Smita, Z. & Suresh, G., 2013. Bioinspired inimitable cadmium telluride quantum dots for bioimaging purposes. *Journal of Nanoscience and Nanotechnology,* pp. 3826-3831.

Vo, N. T. *et al.,* 2015. Conjugation of E. coli O157:H7 Antibody to CdSe/ZnSQuantum Dots. *Journal of Nanomaterials.*

Wagner, A. M., Knipe, J. M., Orive, G. & Peppas, N. A., 2019. Quantum dots in biomedical applications. *Acta Biomaterialia,* pp. 44-63.

Wang, A. *et al.,* 2016. Controlled Synthesis of Lead-Free and Stable Perovskite Derivative Cs2SnI6 Nanocrystals via a Facile Hot-Injection Process. *Chem. Mater.,* p. 8132–8140.

Wells, R. L. *et al.,* 1995. Synthesis of Nanocrystalline Indium Arsenide and Indium Phosphide from Indium(III) Halides and Tris(trimethylsilyl)pnicogens. Synthesis, Characterization, and Decomposition Behavior of I3In.cntdot.P(SiMe3)3. *Chem. Mater,* p. 793–800..

Xie, R., Battaglia, D. & Peng, X., 2007. Colloidal InP nanocrystals as efficient emitters covering blue to near-infrared. *J. Am. Chem,* p. 15432–15433..

Xing, Y. & Rao, J., 2008. Quantum dot bioconjugates for in vitro diagnostics & in vivo imaging. *Cancer Biomark,* pp. 307-319.

Xu, G. *et al.,* 2016. New Generation Cadmium-Free Quantum Dots for Biophotonics and Nanomedicine. *Chem. Rev. ,* p. 12234−12327.

Yong, K.-T.*et al.,* 2009. Imaging Pancreatic Cancer Using Bioconjugated InP Quantum Dots. *ACS Nano,* pp. 502-510.

Zhao, L., Zong, W., Zhang, H. & Liu, R., 2018. Kidney Toxicity and Response of Selenium Containing Protein-glutathione Peroxidase (Gpx3) to CdTe QDs on Different Levels. *Toxicological Sciences,* pp. 201-208.

# Chapter 3: Methods and Materials

## 3.1. Introduction

This chapter describes the experimental procedures and reagents used in the material synthesis. Synthetic procedures for nanocrystals, functionalization strategies, and nanocrystal characterization techniques are also described.

## 3.2. Experimental Reagents

**Table 3.2 A**: A list of the chemicals used in this research.

| Chemical Name | Frequent Name | Chemical formula | Company |
|---|---|---|---|
| **1-Octadecene** | ODE | $C_{18}H_{36}$ | Sigma Aldrich, St. |
| **3-(4,5-Dimethyl-2-thiazolyl)-2,5-diphenyl-2H-tetrazolium bromide** | MTT | $C_{18}H_{16}BrN_5S$ | Sigma Aldrich, St Louis, USA |
| **3-Mercaptopropionic acid** | 3MPA | $C_3H_6O_2S$ | Sigma Aldrich, St. Louis, USA |
| **Acetone** | - | $C_3H_6O$ | Kimix Chemical and Lab supplies, Cape Town, SA |
| **Boric acid** | - | $H_3BO_3$ | Sigma Aldrich, St. Louis, USA |
| **Butanol** | - | $C_4H_{10}O$ | Sigma Aldrich, St. Louis, USA |
| **Chitosan** | - | - | Sigma Aldrich, St. Louis, USA |
| **Deionized water** | d ($H_2O$) | $H_2O$ | - |
| **Dimethyl sulfoxide** | DMSO | C2H6OS | Sigma Aldrich, St Louis, USA |
| **Dulbecco Modified Eagle medium** | DMEM | - | Biochrom, Cambridge, UK |

| | | | |
|---|---|---|---|
| **Ethanol** | - | $C_2H_5OH$ | Kimix Chemical and Lab supplies, Cape Town, SA |
| **Foetal Bovine Serum** | FBS | - | Biochrom, Cambridge, UK |
| **Indium (III) chloride** | - | $InCl_3$ | Sigma Aldrich, St. Louis, USA |
| **Indium (III) iodide** | - | $InI_3$ | Sigma Aldrich, St. Louis, USA |
| **Oleylamine** | OAM | $C_{18}H_{37}N$ | Sigma Aldrich, St. Louis, USA |
| **Phosphate buffered saline** | PBS | - | Kimix Chemical and Lab supplies, Cape Town, SA |
| **Selenium** | - | Se | Sigma Aldrich, St. Louis, USA |
| **Sodium hydroxide** | - | NaOH | Sigma Aldrich, St. Louis, USA |
| **Sulfur** | - | S | Sigma Aldrich, St. Louis, USA |
| **Toluene** | - | $C_7H_8$ | Sigma Aldrich, St. Louis, USA |
| **Tris (diethyl amino) phosphine** | $(DEA)_3P$ | $P[N(C_2H_5)_2]_3$ | Sigma Aldrich, St. Louis, USA |
| **Tris (dimethyl amino) phosphine** | $(DMA)_3P$ | $P(Me_2N)_3$ | Sigma Aldrich, St. Louis, USA |
| **Tri-octyl-phosphine** | TOP | $[CH_3(CH_2)_7]_3P$ | Sigma Aldrich, St. Louis, USA |
| **Zinc bromide** | - | $ZnBr_2$ | Sigma Aldrich, St. Louis, USA |
| **Zinc chloride** | - | $ZnCl_2$ | Sigma Aldrich, St. Louis, USA |

| | | | |
|---|---|---|---|
| **Zinc stearate** | - | $Zn(C_{18}H_{35}O_2)_2$ | Sigma Aldrich, St. Louis, USA |

**Table 3.2 B**: Analytical tools used in this research.

| **Technique** | **Common Name** | **Machine** | **Supplier** | **Location** |
|---|---|---|---|---|
| **Ultraviolet-Visible Spectroscopy** | UV- Vis | POLARstar Omega Plate reader | BMG Labtech | Offenburg, Germany |
| **Fourier Transforms Infrared Spectroscopy** | FTIR | PerkinElmer Spectrometer | Anton Paar | Graz, Austria |
| **Photoluminescence Spectroscopy** | PL | Nanolog | Horiba Scientific | Edison, New Jersey, USA |
| **X-ray diffraction** | XRD | | | |
| **Centrifuge** | - | Eppendorf mini spin | Eppendorf | Hamburg, Germany |
| **High-resolution transmission electron microscopy** | HRTEM | F20 Tenai EDAX $G^2$ | FEI | Eindhoven, Netherlands |

**Table 3.2 C**: Cell types used in this research.

| **Cell line** | **Abbreviations** | **Cell type** | **Tissue of origin** | **Company and location** |
|---|---|---|---|---|
| **Colon Adenocarcinoma** | Caco-2 | Cancer | Colon carcinoma | ATCC, Manassas, USA |
| **Cardiomyocytes** | H9C2 | Normal | Heart | ATCC, Manassas, USA |

| | | | | |
|---|---|---|---|---|
| **Human Fibroblast** | KMST-6 | Normal | Skin (dermis) | ATCC, Manassas, USA |

### 3.3. Experimental Procedures

#### 3.3.1. Glassware Preparation

Before usage, all glassware was properly cleaned with soap and distilled water, followed by acetone rinses, and oven drying.

#### 3.3.2. Preparation of InP/ZnS nanocrystals

The synthesis of InP/ZnS QDs follows a procedure reported by Beloglazova, et al. with some modifications. In a round bottom flask, 0.1014 g of indium chloride ($InCl_3$), 0.2012 g of zinc chloride ($ZnCl_2$), 0.1700 g of zinc bromide ($ZnBr_2$), and 5 mL of oleylamine were mixed. The flask was subjected to a Schlenk line and degassed for 30 minutes at 120 °C before being raised to 170 °C under nitrogen gas. After reaching 170 °C, 0.45 ml of tris (diethylamino) phosphine $(DEA)_3P$ was injected. The synthesis of InP nanocrystals took 50 minutes. After 50 minutes, 1.7 mL (2.2 M) of TOP-S was injected into the reaction mixture. The temperature was then raised to 220 °C for 30 minutes. Finally, 1.5001 g of $Zn(stearate)_2$ dissolved in 6 mL ODE was injected. The temperature was then raised to 280 °C for 30 minutes. The InP/ZnS QDs were precipitated in ethanol at 4000 rpm for 10 minutes before being suspended in toluene. The QDs were then placed in glass poly top vials and foil-wrapped (Beloglazova, *et al.,* 2017).

### 3.3. Preparation of InP/ZnSe nanocrystals

The synthesis of InP/ZnSe QDs follows a procedure reported by Liu, et al. with some modifications. In this procedure, a three-neck flask was used to mix 0.0520 g of indium iodide ($InI_3$), 0.3400 g of zinc bromide ($ZnBr_2$), and 5 mL of oleylamine. First, these mixtures were degassed for 20 minutes at 120 °C. Then, under the gas of nitrogen, the mixture was heated to 200 °C. Immediately after the mixture above reached 200 °C, 0.45 mL of tris (dimethyl amino) phosphine $(DMA)_3P$ was injected. InP nanocrystal synthesis took 40 min to complete. 1.2 mmol (2.2 M) TOP(Se) and 12 mL of zinc precursor solution (3g of zinc stearate dissolved in 12 mL of 1-octadecene) were added to the above-mentioned core solution after 40 minutes. The temperature was then raised to 260 °C, where the reaction was maintained for 120 minutes. The InP/ZnSe QDs were precipitated in ethanol (4000 rpm, 5 min) and suspended in toluene. The QDs were then stored in glass poly top vials and covered with foil (Liu, *et al.*, 2021).

The same synthesis was repeated with a change in the phosphorus precursor using tris (diethyl amino) $(DEA)_3P$ phosphine instead. Therefore, let InP/ZnSe QDs synthesized with $(DMA)_3P$ be InP/ZnSe1 and QDs synthesized with $(DEA)_3P$ be InP/ZnSe2.

### 3.4. Surface modification of Indium Phosphide Quantum dots

The quantum dots were transferred into the aqueous environment by adding 1 mL borate buffer (pH 9), 0.8 mL butanol, and 10 µL 3-mercaptopropanoic acid to 0.5 µL of InP/ZnS. For 15 minutes, the mixture was heated to 50 °C and vigorously stirred. After separating the aqueous layer containing the quantum dots, 1000 µL of borate buffer and 800 µL of butanol were added. For another 15 minutes, the mixture was vigorously stirred. The quantum dots were recovered through ethanol precipitation and dispersion in a 50 mM borate buffer. To clean the quantum dots, the precipitation with ethanol and dispersion in 50 mM borate buffer process was repeated twice. Finally, the product was dispersed in phosphate buffer saline (PBS) (pH 7.4) and stored at 4 °C for later use. UV - Vis, PL, and FTIR analyses were performed to determine which of the two methods was more effective in introducing the carboxyl group (-COOH) to the quantum dots. Figure 3.4 shows how the quantum dots suspended in an organic solvent were successfully transferred to the aqueous layer (Brunetti, *et al.,* 2013). This process was repeated for InP/ZnSe1 and InP/ZnSe2.

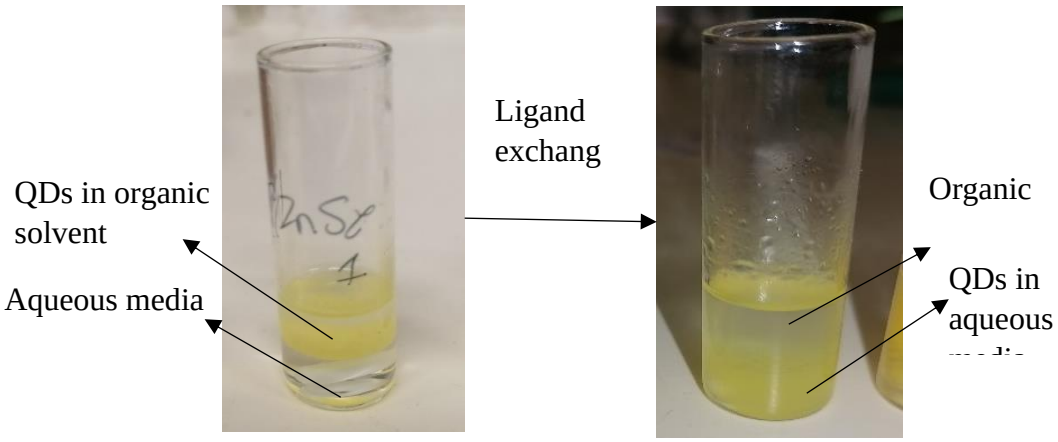


**Figure 3.4:** Diagram illustrating the effective transfer of quantum dots from the organic layer to aqueous layers.

To make a chitosan stock solution, 1 g of chitosan was first dissolved in 100 mL of a 1.5 v/v % acetic acid solution. Chitosan was completely dissolved by sonicating the stock solution for 4 hours. After that, the stock solution was diluted to a concentration of 0.005 w/v %. As

previously reported, InP nanocrystals were first created, and after that, ZnS and ZnSe shells were added. Next, 3MPA was combined with these QDs to create water-soluble InP/ZnS-3MPA, InP/ ZnSe1-3MPA, and InP/ ZnSe2-3MPA QDs. To create a QD/chitosan, water-soluble QDs were mixed with 0.005 w/v % chitosan in five mL under vigorous stirring at 1000 rpm. The resulting solution was then centrifuged at a speed of 13,000 rpm, and the leftover material was cleaned with deionized water. The leftover chitosan-encapsulated nanocrystals were centrifuged, vortexed, and then stored in 5 mL of deionized water (Ayabei, 2016) (Tan, *et al.,* 2007).

### 3.5. Characterization of Quantum dots

#### 3.5.1. Ultraviolet-visible (UV-Vis) spectroscopy

Uv-vis is a spectroscopic technique used to measure the extinction of electromagnetic radiation when it is passed through a sample. This extinction is quantified by summing up the amount of light absorbed and scattered by the material in question (nanoComposix , n.d.). The emitted radiation is from the ultraviolet (UV) and visible (Vis) regions of the electromagnetic spectrum (Weckhuysen, 2004). To obtain absorption spectra, the sample is placed in the middle of a radiation source and a photodetector, then the intensity of the beam of ultraviolet-visible radiation is measured before and after going through the sample, which is used to illustrate this phenomenon (nanoComposix , n.d.). This technique is very helpful and valid for the early characterization of nanomaterials as it can be used to study their synthesis and stability (Xi-Feng, *et al.,* 2016). Quantum dots have special optical properties that are dependent on factors such as concentration, aggregation level, shape, and size making Uv-Vis spectroscopy a suitable technique for characterizing, identifying, and studying these nanocrystals. Furthermore, this technique is inexpensive, straightforward, and quick and it takes a very short amount of time to complete a single measurement (Xi-Feng, *et al.,* 2016). In the present study, the absorption spectra of all the prepared QDs were obtained using UV-Vis Spectroscopy through a POLAR star Omega plate reader at the Life sciences building, University of the Western Cape (UWC). The samples were added to a 96 non-sterile well plate, which was inserted into the plate reader and the absorbance measurements were made over the wavelength range of 300-600 nm at 100 μL of each sample. UV-Vis spectroscopy is very helpful and valid for the early characterization of nanomaterials as it can be used to monitor and confirm their synthesis and stability (Zhang *et al.,* 2016). QDS has special optical properties that are dependent on factors such as concentration, aggregation level, shape, size, and the refractive index close to the surface of the nanoparticles. All this makes UV-Vis spectroscopy a suitable

technique for characterizing, identifying, and studying QDS (Prakash *et al.*, 2013, Khorrami *et al.*, 2018).

(a)

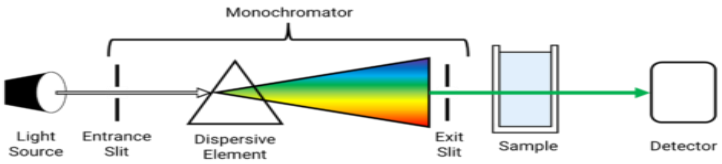


(b)

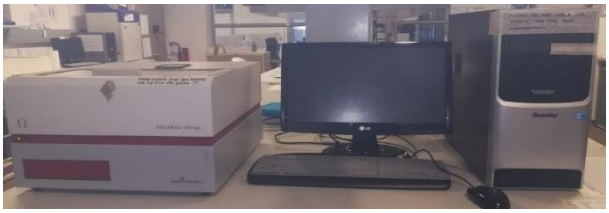

**Figure 3.5.1:** Typical UV-Vis single beam spectrometer (JASCO, n.d.), (b) POLAR star Omega.

### 3.5.2 Photoluminescence Spectroscopy

PL, also known as photoluminescence spectroscopy, is the study of how light energy, or photons, stimulates the emission of a photon from any substance. This technique for probing materials is non-contact and non-destructive (HORIBA Scientific , n.d.). Figure 3.5.2 shows a schematic of an emission experiment. One monochromator chooses an excitation wavelength, and the luminescence is seen through a second monochromator that is typically angled at 90 degrees to the incident light to reduce the amount of scattered light that reaches the detector. If the excitation wavelength is fixed and the emitted radiation is scanned, an emission spectrum is produced (Ye & Barron, 2019). The emission spectra of all the synthesized QDs were obtained using photoluminescence spectroscopy through a Nanolog machine at the Sensor lab, Chemical science building, University of the Western Cape (UWC). For analysis 10 µL sample and 900 µL of solvent were mixed in a high-precision cell made of high-performance quartz glass. The emission measurements were made depending on the excitation wavelength of each sample.

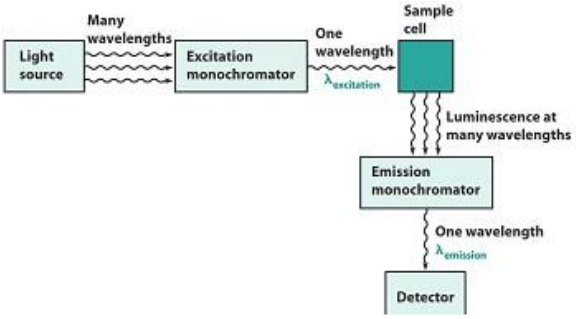


**Figure 3.5.2:** (a) Schematic diagram of Photoluminescence spectroscopy (Ye & Barron, 2019).

### 3.5.3 Fourier Transform Infrared Spectroscopy

Fourier-transform infrared (FTIR) spectroscopy is a well-established analytical technique used for the determination and structural identification of materials. The functional groups and chemical bonds present in the samples are identified through the peaks found in the IR spectra since each peak represents the excitation of vibrational modes of the molecules present in each sample. As a result, the IR spectrum of a compound is an important feature of its physical properties and can be thought of as a "fingerprint" because no two different compounds can have the same spectra in the fingerprint region (600 to 1400 $cm^{-1}$) (Sedman, *et al.*, 1997) (Amir, *et al.*, 2013). It regulates the wavelength from a broadband infrared source through an interferometer. The intensity of the light that is either transmitted or reflected by the sample is measured by a photodetector as a function of its wavelength. The resulting signal is then recorded as an interferogram which needs to be converted to a single-beam infrared spectrum using a computer with Fourier transforms (Munajad, *et al.*, 2018). Figure 3.5.3 shows a basic scheme of an FTIR spectrometer. In this work, the structural composition of the core/shell QDs, core/shell-3MPA, and core/shell-chitosan QDs was evaluated by FTIR spectroscopy through the identification of functional groups present in each sample by observing the vibrational spectra of molecules between 4000-600 cm-1. The FTIR spectra were recorded on the PerkinElmer spectrometer at UWC, chemistry department. The analysis was performed by adding potassium bromide (KBr) into dry QD samples and mixing using a mortar and pestle. A pellet was made using a hand-press pellet maker. The mortar and pestle and KBr pellets were thoroughly cleaned with acetone and wiped dried with a tissue after each measurement.

(a) (b)

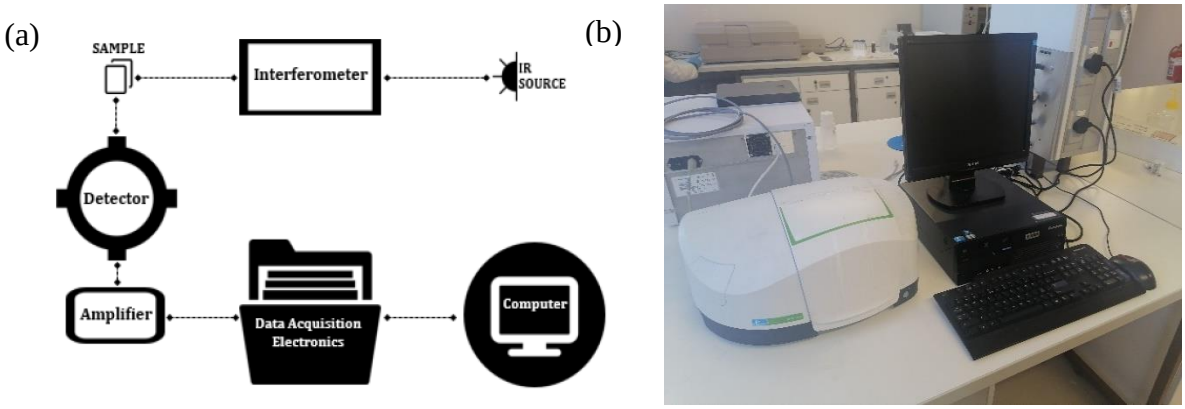


**Figure 3.5.3:** (a) Schematic diagram of Fourier transform infrared (FTIR) spectrometer (Munajad, *et al.,* 2018). (b) PerkinElmer FTIR spectrometer.

### 3.5.4 High-Resolutionlution Transmittance Electron Microscope

HR-TEM is a very well-established and powerful analytical technique commonly used for characterizing nanomaterials by providing their crystallographic, surface morphology, particle sizes, and size distribution information (Xi-Feng, *et al.,* 2016). During HR-TEM analysis, the sample is bombarded with a focused beam of electrons under high vacuum and increasing voltage so that all the sample's information can be collected in a short amount of time through high magnification and resolution imaging at the nanoscale range (Anjum & Sougrat, 2016). Sizes and surface morphologies of the core/shell QDs, core/shell-3MPA, and core/shell-chitosan QDs were probed using HR-TEM with a resolution of ~0.2 nm at 200 keV on an F20 TECNAI EDAX G2 microscope by drop coating ~ 2 mL of each sample on ultrathin carbon-film-coated copper grids. HR-TEM was used in conjunction with ImageJ software to determine the diameter of the particles. HR-TEM analysis was performed at the electron microscope unit at UWC. It is feasible to obtain direct knowledge about the crystallographic structure of materials from photographs because the HRTEM directly images the atomic structure of the samples. The TEM data were also used to obtain EDS and SAED data. The SAED was used to analyse the electron diffraction pattern produced by the electron beam's interaction with the sample atoms to determine the sample's crystallinity, lattice parameters, crystal structure, and orientation. To identify the chemical elements contained in a sample and estimate their relative abundance, EDS was used (Goldstein, *et al.*, 2003).


**Figure 3.5.4:** Image of an HR-TEM setup system.

### 3.5.5 X-ray Diffraction

The primary function of X-ray powder diffraction (XRD), a quick analytical method that can reveal information about unit cell dimensions, is to identify the phase of crystalline materials. Before calculating the average bulk composition, the sample being studied is finely powdered and homogenized (Dutrow & Clark, n.d.). The foundation of X-ray diffraction is constructive interference between monochromatic X-rays and a crystalline sample. The X-rays are generated by a cathode ray tube, which is then filtered to produce monochromatic radiation, focused by collimation, and directed at the sample. When the circumstances are in accordance with Bragg's Law ($n\lambda=2d \sin \theta$), the interaction of the incident rays with the sample results in constructive interference (and a diffracted ray). This law establishes a relationship between the wavelength of electromagnetic radiation and the lattice spacing and diffraction angle in a crystalline sample. These diffracted X-rays are then located, investigated, and counted. Due to the random orientation of the powdered material, it is necessary to scan the sample through a variety of $2\theta$ angles in order to obtain all possible lattice diffraction directions. The identification of the mineral is made possible by converting the diffraction peaks to d-spacings because each mineral has a unique set of d-spacings. This is frequently done by making comparisons between the d-spacings and recognised reference patterns. X-ray diffraction was used to determine the crystallinity of the indium phosphide-based nanocrystals. The X-ray diffraction experiments were carried out at Themba Labs, Cape Town using a Bruker AXS D8 Advanced Diffractometer equipped with a CuK$\alpha$ ($\lambda$ = 1.5418 Å) X-ray source. X-ray

diffraction is premised on the fact that the diffraction patterns are characteristic of both the crystal form and spacing of the chemical compounds and not their constituent elements or chemical groups. Therefore, when a beam of monochromatic X-rays strikes the planes of atoms in a given crystal, interference occurs, and the X-ray beams are diffracted from the crystal in specific directions

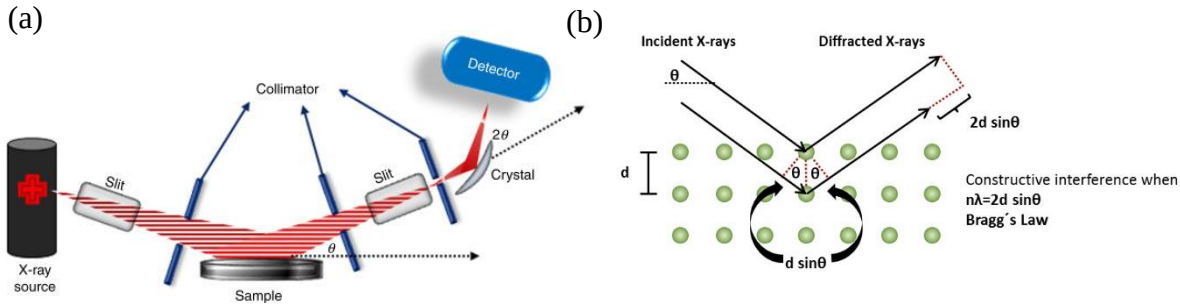


**Figure 3.5.5:** (a) Schematic diagram of XRD (Gumustas, *et al.*, 2017). (b) Schematic representation of Bragg's equation (Anton Paar, n.d.).

### 3.6.Effects of Quantum dots on cell viability

The cell viability of the QDs was assessed in accordance with biosafety level 2 guidelines at the Biolabels Node research labs (Department of Biotechnology, UWC). The laboratory's disposal protocol, which is outlined in their standard operating procedure, was followed when disposing of the biological waste.

The experiments were carried out on our behalf by Miss Miche Desline Meyer, a PhD student in Biotechnology department.

#### 3.6.1. Cell Culture

The experiments were carried out using Caco-2, H9C2 and KMST-6 cell lines, these cells were purchased from American Type Culture Collection (Manassas, VA, USA). All cells were cultured in Dulbecco's Modified Eagle Medium (DMEM; Gibco, Rockville, MD, USA) supplemented with 1% pen-strep (Lonza, Basel, Switzerland) and 10% Foetal Bovine Serum (FBS), in T25 cell culture flask. The cells were cultured at 37 °C in a humidified atmosphere of 5% CO2, in a (Illinois, Lake Forest, USA), the media was changed every three days until the cells reached ~80% confluency before subculturing.

### 3.6.2. Trypsinization of cells

Trypsinization was used to detach the adherent cells from T25 cell culture flasks when the cells reached 70-80% confluency. The media was removed from the flasks and the flasks were washed with 2 mL of phosphate buffered saline (PBS). The PBS was replaced with 3 mL of trypsin (Lonza) was added to the flasks and incubated at 37 °C for 5-10 minutes, until the cells appeared detached. The cells were observed using an EVOS XL Core inverted microscope (Invitrogen Corporation, San Diego, CA, USA) to check if the cells were detached. Once detached, 2 mL of media was added to the cell suspension. The cells were then transferred into 15 mL greiner tubes, and spun down in an ALLEGRA X-12R centrifuge (Beckman Coulter, Indianapolis, IN, USA) for 5min at 3000 rpm. The supernatant was removed and the pellet were resuspended in 2 mL of media.

### 3.6.3. Cell count: Trypan Blue Exclusion assay

After trypsinization, the cells were resuspended in 2mL of DMEM, then 20µl of the cell suspension was mixed with 20µl of trypan blue dye (Invitrogen). A volume of 20µl of the mixture was transferred into a Countess cell count slide and cell count was performed on a Countess™automated cell counter (Invitrogen). Once read, the cells were resuspended diluted in complete to media to have a desired concentration for the cytotoxicity studies.

### 3.6.4. Cytotoxicity studies: MTT Assay

This was evaluated using the MTT reduction assay as previously described (Gurunathan, *et al.,* 2013). Briefly, KMST-6, H9C2, and Caco-2 cells were seeded in individual 96 well in DMEM at 1 x $10^5$ cells/mL, 100 µL per well and incubated for 24 hours. After 24 hours, the culture media in all plates was discarded and replaced with fresh media consisting of various QDs, InP/ZnS-3MPA, InP/ZnS-CHT, InP/ZnSe1-3MPA, InP/ZnSe1-CHT, InP/ZnSe2-3MPA, InP/ZnSe2-CHT at 0.5mg/ml; 6% of Dimethyl sulfoxide (DMSO) was used as a positive control, and fresh media was used for negative control. The cells were treated for 24 hours. After each treatment the media was replaced with fresh media containing 10 % 5mg/mL of MTT (MTT prepared in dH2O) dye reagent (Sigma, St. Louis, MO, USA) by adding 100 µL to each well, and the plates were incubated for a further 3 hours at 37 °C. After that, the MTT containing media was removed and the resulting formazan was solubilized by adding 100 $\mu$L of DMSO in each cell with gentle shaking for another 10 minutes. The optical density was measured at 570 and 700 nm in the POLARstar Omega plate reader (BMG Labtech, Offenberg,

Germany). Percentage viability was calculated as absorbance of the treated cells divided by the absorbance of the untreated controls * multiplied by 100%.

### 3.7. References


Amir, R. M. *et al.,* 2013. Application of Fourier transform infrared (FTIR) spectroscopy for the identification of wheat varieties. *Journal of Food Science and Technology,* p. 1018–1023.

Anjum, D. H. & Sougrat, R., 2016. Transmission electron microscopy of mercury metal. *J Microsc.*

Ayabei, K., 2016. Fabrication of luminescent nanocomposites for diagnosis of breast cancer. *UWC Library,* pp. 1-218.

Beloglazova, N. V. *et al.,* 2017. Fluorescently labelled multiplex lateral flow immunoassay based on cadmium-free quantum dots. *Methods,* pp. 141-148.

Brunetti, V. *et al.,* 2013. InP/ZnS as a safer alternative to CdSe/ZnS core/shell quantum dots: in vitro and in vivo toxicity assessment. *Nanoscale,,* Volume 5, pp. 307-317.

Dutrow, B. L. & Clark, C. M., n.d. *X-ray Powder Diffraction (XRD).* [Online].

Goldstein, J. *et al.,* 2003. *Scanning Electron Microscopy and X-Ray Microanalysis: Third Edition.* s.l.:Springer US.

Gurunathan, S. *et al.,* 2013. Cytotoxicity of biologically synthesized silver nanoparticles in MDA-MB-231 human breast cancer cells. *Biomed Res Int.*

HORIBA Scientific , n.d. [Online] Available at: https://www.horiba.com/ind/scientific/technologies/photoluminescence-pl/photoluminescence-pl-electroluminescence-el/#:~:text=Photoluminescence%20spectroscopy%2C%20often%20referred%20to,nondestructive%20method%20of%20probing%20materials.

JASCO, n.d. *Instrumentation of UV Vis Spectrophotometer.* [Online].

Liu, P. *et al.,* 2021. Green InP/ZnSeS/ZnS Core Multi-Shelled Quantum Dots Synthesized with Aminophosphine for Effective Display Applications. *Adv. Funct. Mate,* pp. 1-7.

Munajad, A., Subroto, C. & Suwarno, 2018. Fourier Transform Infrared (FTIR) Spectroscopy Analysis of Transformer Paper in Mineral Oil-Paper Composite Insulation under Accelerated Thermal Aging. *Energies.*

nanoComposix , n.d. [Online] Available at: https://nanocomposix.com/pages/nanoparticle-characterization-techniques

Sedman, J., Voort, F. v. d. & Ismail McGill, A., 1997. Upgrading the AOCS Infrared trans Methodfor Analysis of Neat Fats and Oilsby Fourier Transform Infrared Spectroscopy. In: *Journal of the American Oil Chemists' Society.* s.l.:s.n., pp. 907-914.

Tan, W. B., Ning, Huang & Zhang, Y., 2007. Ultrafine biocompatible chitosan nanoparticles encapsulating multi-coloured quantum dots for bioapplications. *Journal of Colloid and Interface Science,* pp. 464-470.

Xi-Feng, Z., Liu, Z.-G., Wei, S. & Gurunathan, S., 2016. Silver Nanoparticles: Synthesis, Characterization, Properties, Applications, and Therapeutic Approaches. *Int J Mol Sci.*

Ye, R. & Barron, A. R., 2019. Photoluminescence Spectroscopy and its Applications. In: *Physical Methods in Chemistry and Nano Science.* s.l.:Pavan M. V. RajaAndrew R. Barron.

# Chapter 4: Results and Discussion

## 4.1.Indium phosphide Precursor

InP nanocrystals with a reasonable size dispersion were first synthesized in 1995 (Micic, *et al.,* 1995). Tris (trimethylsilyl)phosphine $(TMS)_3P$, the most used phosphorus precursor for the creation of InP QDs, was used in this synthesis (Woo-Seuk, *et al.,* 2013) (Tessier, *et al.,* 2015). To date, $(TMS)_3P$ has synthesized the bulk of InP QDs, including those of the highest grade ever reported. The $(TMS)_3P$, however, is an extraordinarily expensive pyrophoric material that, when exposed to air, emits the highly poisonous phosphine gas ($PH_3$). As a result, its use conflicts with economical and environmentally friendly chemistry and should be avoided in the future. Due to this, the synthesis of InP QDs has also been tried using several alternative P precursors to $(TMS)_3P$, such as phosphorus trichloride ($PCl_3$), tetra phosphorus tetramer ($P_4$), and amino phosphines. Among these, tris(dialkylamino)phosphines, a particular type of amino phosphine, might be thought of as a potential precursor that enables the creation of high-quality InP QDs (Gary, *et al.,* 2014 ) (Allen, *et al.,* 2010) (Chandrasiri, *et al.,* 2020) (Jo, *et al.,* 2020).

In the synthesis of InP QDs for various sizes, effective procedures based on amino phosphines have recently been developed (Woo-Seuk, *et al.,* 2013) (Tessier, *et al.,* 2015). An amino phosphine precursor has been shown to produce InP QDs of equivalent quality compared to the best samples obtained with $(TMS)_3P$, is less expensive than $(TMS)_3P$, and is safe to use in ambient conditions (Tessier, *et al.,* 2016) (Li, *et al.,* 2019, Allen, *et al.,* 2010, Woo-Seuk, *et al.,* 2013). Tris(dialkylamino)phosphines were discovered to form nanoparticles comparable to those of $(TMS)_3P$; however, their lower reactivity may allow for less demanding reaction conditions (Laufersky, *et al.,* 2018). Tris (dimethyl amino) phosphine ($(DMA)_3P$) is the most reported tris(dialkylamino) phosphine used as phosphorus precursors. Due to its low cost and toxicity, $(DMA)_3P$ has gained increased interest in the synthesis of InP QDs. Typically, $(DMA)_3P$ can react with indium halide to produce InP QDs when aliphatic amines are present as a surface organic ligand (Woo-Seuk, *et al.,* 2013). The precursor's halogen element can be changed to readily control the emission of InP QDs (Tessier, *et al.,* 2016)0. To achieve high efficiency and stability of InP core/shell QDs, broad bandgap shell materials (such as ZnSe and ZnS) are also used for surface passivation of InP QDs (Tessier, *et al.,* 2016, Liu, *et al.,* 2021).

### 4.2.Synthesis of InP/ZnS QDs

The synthesis of InP/ZnS QDs was carried out following a one-pot green synthesis using the hot injection method. This technique had been reported by Beloglazova, *et al.*, where they developed core/shell InP/ZnS QDs enrobed in a silica shell that allowed the water solubility (QD@SiO2). They then applied the QD@SiO2 as a novel, silica shell-encapsulated fluorescent label in immunoassays for rapid multiplexed screening (Beloglazova, *et al.*, 2017). The first step is the formation of the InP core by reacting $InCl_3$, $ZnCl_2$, $ZnBr_2$, and $(DEA)_3P$ where $InCl_3$ was used as an indium precursor and $(DEA)_3P$ as a phosphine precursor (Tessier, et al., 2016) (Grigel, *et al.*, 2016). As the uncoated InP QDs are not fluorescent, a ZnS shell was added around using zinc precursor and sulfur precursor. The zinc precursor was created by dissolving zinc stearate in a non-coordinating solvent ODE, while the sulfur precursor was created by dissolving sulfur in TOP which provides a hydrophobic layer. The hydrophobic layer in TOP is normally substituted by hydrophilic molecules in the liquid phase, such as amines, polyhydroxy alcohols, and notably, thiols via a ligand exchange method to make the QDs hydrophilic (Biju, *et al.*, 2010, Beloglazova, *et al.*, 2017). To render them water soluble, the layer of the hydrophobic TOP was exchanged for 3-mercaptopropionic acid (3MPA) that contains both thiol (-SH) and hydrophilic carboxylic (-COOH) group followed by chitosan with -OH and $NH_2$ functional groups. Tan and coworkers reported a synthesis of CdSe/ZnS QDs that were made hydrophilic by exchanging tri octyl phosphine oxide (TOPO) with 3MPA. They then encapsulated these QDs with natural biopolymer chitosan-forming monodisperse chitosan nanoparticles that were used to test cytotoxicity on myoblast cells. These biocompatible chitosan nanoparticles showed promise in biological applications as the cytotoxicity of myoblast cells reduced after chitosan encapsulation (Tan, *et al.*, 2007).

### 4.3.Synthesis of InP/ZnSe QDs

Notably, the preparation of InP/ZnSe1 and InP/ZnSe2 QDs also followed a one-pot synthesis where the difference in the synthesis of these QDs was the phosphorus precursor. In one of the reactions, $ZnBr_2$, $InI_3$, and $(DMA)_3P$ were reacted for the formation of InP with $InI_3$ acting as an indium precursor while $(DMA)_3P$ was used as a phosphine precursor in the production of InP/ZnSe1. The $(DEA)_3P$ was used as a phosphine precursor for the preparation of InP/ZnSe2. ZnSe shell was added to these QDs to make them fluorescent. The ZnS shell was coated with zinc precursor and selenium precursor. The zinc precursor was created by dissolving zinc stearate in a non-coordinating solvent ODE, while the selenium precursor was created by

dissolving sulfur in TOP which provides a hydrophobic layer. Same as the InP/ZnS, the layer of hydrophobic TOP was exchanged for 3-mercaptopropionic acid (3MPA) followed by chitosan polymer (Tan, et al., 2007).

### 4.4.Ligand Exchange Process

Luminescent quantum dots are only appropriate for biomedical applications when the nanocrystals are compatible with aqueous media (Chan & Nie, 1998). Water-soluble quantum dots can be created by introducing bifunctional hydrophilic capping ligands via ligand exchange reactions. Solubilization of quantum dots allows for additional functionalization via conjugation to a variety of biological molecules (Sapsford, *et al.,* 2006). One of the simplest ways to create a hydrophilic surface is to substitute hydrophobic molecules of TOP surfactants with mercaptocarbonic acids having carboxyl groups, such as mercaptoacetic acid, mercaptopropionic acid, or mercaptodecanoic acid (Tan, *et al.,* 2007)**.** The 3-mercaptopropionic acid was used in this study as shown in Figure 4.4. The 3MPA ligand contains a thiol group that anchors the ligand to the nanocrystal surface (Chen, *et al.,* 2009) and a terminal carboxyl group that allows for hydrophilicity and bioconjugation with other biomolecules. However, the capping ligands' hydrolysis or oxidation can quickly destroy QDs capped with these tiny molecules (Ayabei, 2016) (Mocatta, *et al.,* 2011). Also, when QDs are dialyzed against pure buffer or water for an extended period, the thiol-QD bonds formed are far less stable, and QDs begin to precipitate (Aldana, *et al.,* 2001). Encapsulating QDs within a polymeric sphere is another method for stabilizing them in aqueous solutions. This polymeric substance should ideally have reactive functional groups for future biomolecule attachment and be biocompatible. Chitosan, a natural polymer with one amino group and two hydroxyl groups in the repeating hexosaminidase residue, is one such substance. Due to its hydrophilicity, biodegradability, biocompatibility, lack of antigenicity, lack of toxicity, and bifunctionality, it is one of the perfect polymers for biological applications. Furthermore, chitosan's effectiveness in delivering medicines and other biomolecules intracellularly has a long history of research (Calvo, *et al.,* 1998). Significantly, chitosan was chosen as an encapsulating medium because of its outstanding biocompatibility and successful delivery of medicines, proteins, and DNA when administered intravenously or orally. It is also reported that the amino and hydroxyl groups of chitosan can be further utilized for the attachment of biomolecules, making chitosan a very desirable material option for the QDs' capping (Tan, *et al.,* 2007).

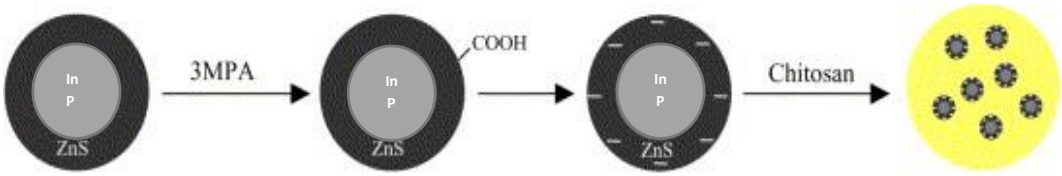


**Figure 4.4:** Description synthesis of InP/ZnS-MPA-Chitosan nanoparticles (Tan, *et al.*, 2007).

### 4.5.UV-Vis characterization of Quantum dots

#### 4.5.1. UV-Vis analysis of the core/shell QDs

The formation of indium-phosphide-based QDs synthesized using different phosphorus precursors was evaluated using UV-Vis spectroscopy. Figure 4.5.1 a, b, and c shows the UV-Vis spectra of synthesized core/shell QDs. The absorption peak of InP/ZnS QDs is located at ~ 448 nm, and InP/ZnSe1 and InP/ZnSe2 are located at ~ 453 nm and 474 nm respectively. These QDs emit absorption colours of blue-green, that is, they have similar colours as shown in Figure 4.5.1 d, e, and f, the QDs under a UV light. The InP/ZnSe synthesized QDs have a higher absorption wavelength compared to the InP/ZnS QD. Sulfur and selenium are both in group 16 in the periodic table with selenium below sulfur. Sulfur is more electronegative than selenium and electronegativity decreases down the periodic table group. The electron cloud changes slightly toward HOMO when electronegativity drops down the group. The electron is then driven to LUMO by low energy, increasing the wavelength (U.Jadhao & B.Naik, 2017). Selenium has smaller electronegativity and higher reactivity compared to sulfur hence it has higher absorption wavelengths compared to sulfur.

Jeong, *et al.,* synthesized InP/ZnS QDs using $(DEA)_3P$ with different reaction temperatures for InP core synthesis. The 30 minutes reaction temperature of 160 °C gave an absorption wavelength of ~ 535 nm and the reaction temperature of 180 °C gave an absorption wavelength of ~ 569 nm (Jeong, *et al.*, 2019). However, Drozd and co-workers also synthesized the same QDs using the same phosphorus precursor and the InP core was reacted at 320 °C for 10 minutes. The absorption of the InP/ZnS QDs was ~ 440 nm (Drozd, *et al.*, 2019). The InP/ZnS QDs synthesized in this report had an InP core prepared at 170 °C for 50 minutes and the syntheiszed InP/ZnS QDs gave an absorption peak of ~448 nm. These studies show the effect of temperature on the optical studies of the InP QDs, that low temperature values give high absorption peak values than high temperature values and low temperatures are much desired to accord to green synthesis requirements. The difference between Jeong, *et al.,* synthesis and the one reported in this report are the solvents used for the purification step and suspension of the

QDs. Jeong, *et al.,* purified their QDs using ethanol and chloroform and resuspended them in hexane, while in this report the QDs were purified using ethanol and resuspended in toluene. Chloroform is more polar than ethanol and polar solvents shift the wavelength absorption to red relative to non-polar solvents (Adeoye, *et al.,* 2009). Also, the number of masses and volumes of the materials used in Jeong, *et al.,* synthesis is double the amount of those used in this synthesis, hence the high absorption wavelengths (effects of doubling the ratio). Drozd and co-worker's synthesis, purification and suspension of the QDs is similar to the one reported in this report with InP temperature synthesis of 200 °C hence the difference in absorption wavelength is not that big compared to Jeong, et al.

Chandrasekaran, et al., synthesized InP/ZnSe QDs with $(DEA)_3P$ that has an absorption peak of 594 nm (Chandrasekaran, *et al.,* 2017). Meanwhile, Yu, et al., reported a synthesis of $InP/ZnSe_xS_{1-x}$ QDs with environmentally friendly phosphorus precursor $(DMA)_3P$. When x =1, $InP/ZnSe_xS_{1-x}$ becomes InP/ZnSe and had an absorption peak of 475 nm (Yu, *et al.,* 2022). These reports show that the synthesis of InP/ZnSe QDs with $(DEA)_3P$ as a phosphorus precursor gives absorption at higher wavelengths compared to those prepared using $(DMA)_3P$. These reports are in agreement with the findings of this research. The difference in these two precursors is the alkyl group whereby the $(DEA)_3P$ has ethyl ( $-C_2H_5$) and $(DMA)_3P$ has a methyl ( $-CH_3$) group. When compared to $-CH_3$ based molecules, heavier molecules like $-C_2H_5$ are projected to have slower mobility (kinetics), which will likely result in fewer reaction nucleation sites and higher absorption wavelengths of the QDs.

(a) (b) (c)

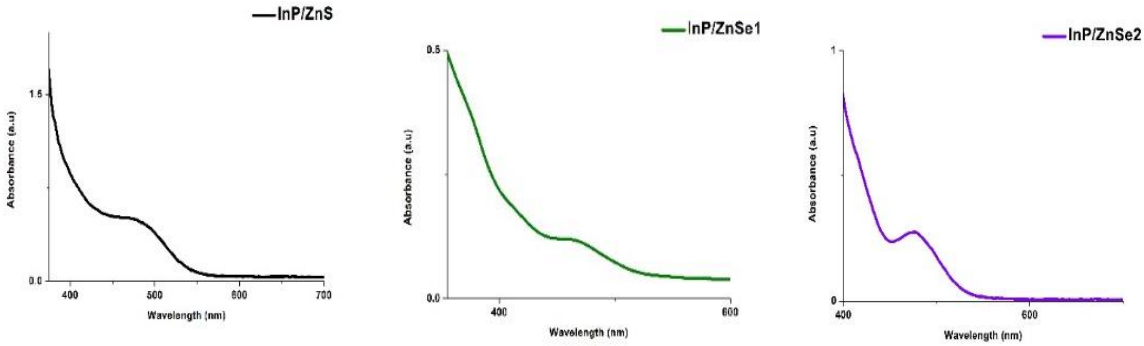


(d) (e) (f)

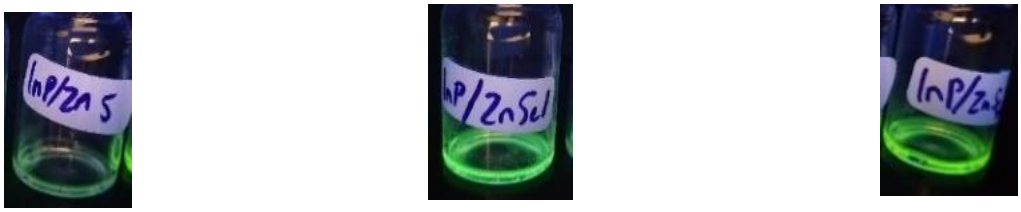

**Figure 4.5.1:** Overlay UV-Vis spectra of (a) InP/ZnS, (b) InP/ZnSe1, (c) InP/ZnSe2 QDs, and (d) InP/ZnS QDs under UV-Vis light, (e) InP/ZnSe1 QDs under UV-Vis light, (f) InP/ZnSe2 QDs under UV-Vis light.

### 4.5.2. UV-Vis analysis of 3MPA QDs

Figure 4.5.2 shows the UV-Vis of the water-soluble QDs. These QDs were made water-soluble by capping them with 3-mercaptopropionic acid (3MPA). The UV-Vis is expected to show a blue shift compared to the uncapped hydrophobic QDs. As the 3MPA is capped to the surface of the QDs, it is then firmly adsorbed onto the surface of the QDs and therefore quenching the QD's fluorescence resulting in low wavelengths. The InP/ZnS-3MPA showed an absorption peak at 330 nm, InP/ZnSe1-3MPA at 374 nm, and InP/ZnSe2-3MPA at 310 nm. When compared to the core/shell QDs, the 3MPA-capped QDs exhibit a blue shift as expected. The impact of "blueshift" in the confinement regime occurs as the number of emitted photons increases due to the addition of the 3MPA agent molecule, shortening the wavelength as it blocks some path of the QDs from the light (Nurul, *et al.*, 2018).

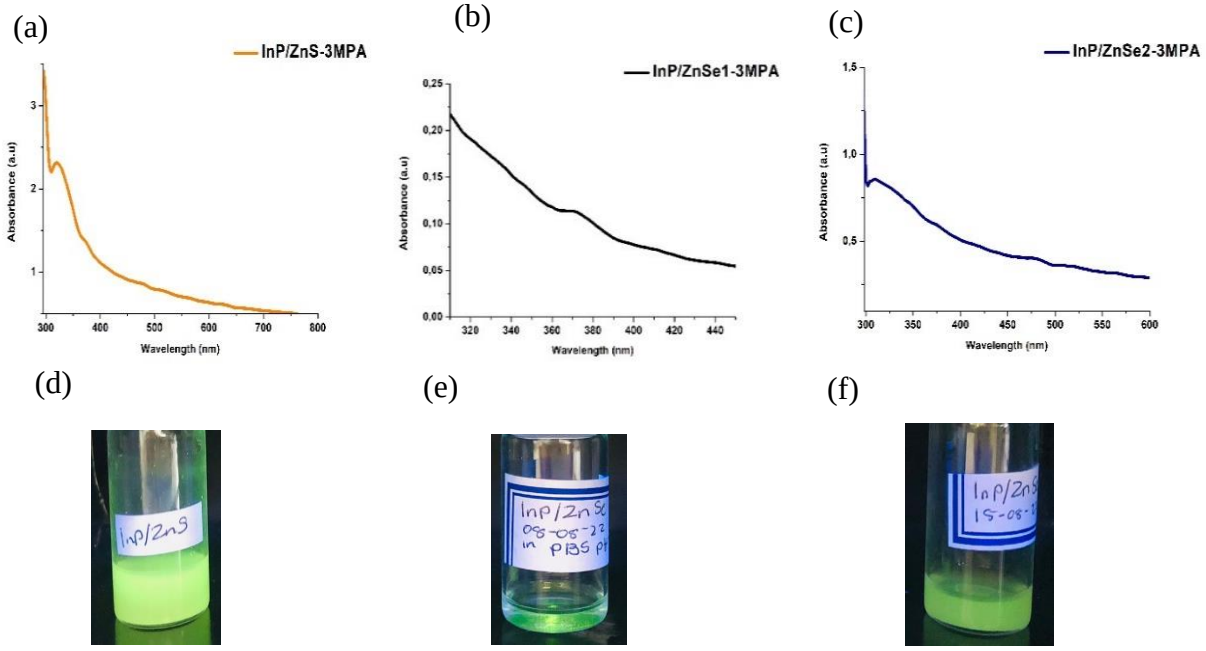


**Figure 4.5.2:** UV-Vis spectra of 3MPA capped nanocrystals of (a) InP/ZnS-3MPA, (b) InP/ZnSe1-3MPA, (c) InP/ZnSe2-3MPA, and (d) InP/ZnS-3MPA QDs-3MPA under UV-Vis light., (e) InP/ZnSe1-3MPA QDs-3MPA under UV-Vis light., (f) InP/ZnSe2-3MPA QDs-3MPA under UV-Vis light.

### 4.5.3. UV-Vis analysis of chitosan QDs

Figure 4.5.3 depicts a UV-Vis spectrum overlay of chitosan-capped QDs. The chitosan-encapsulated QDs are not expected to show any shift in the wavelength compared to the 3MPA-capped QDs. That is, the absorption wavelength of 3MPA-QDs and chitosan QDs is expected to be the same. As the 3MPA is adsorbed onto the surface of the QDs thus reducing their fluorescence, a chitosan molecule is added to the existing slots of 3MPA by substituting a functional group. Chitosan is not being attached to the surface of the QDs, thus being added onto 3MPA, therefore, it does not affect QDs fluorescence as it is not blocking anything. The absorbed UV-vis peaks for InP/ZnS-CHT, InP/ZnSe1-CHT, and InP/ZnSe2-CHT nanocrystals were 371 nm, 327 nm, and 300 nm respectively. The UV -Vis peak for InP/ZnS-CHT shows a red shift while the other two show a blue shift. Studies concerning QDs capped with 3MPA, and chitosan did not show any red/blue shift upon the addition of chitosan to 3MPA-QDs. Gupta and colleagues synthesized chitosan coated MPA- CdSe QDs that had a vertical shift in the absorbance without any change in absorbance maxima wavelength of chitosan-coated MPA-CdSe QDs and MPA-CdSe QDs (Gupta, *et al.*, 2022). R.Harish, *et al.*, synthesized CdS QDs and capped them with 3MPA and chitosan and also obtained the same results regarding their absorption wavelengths (R.Harish, *et al.*, 2020). The red and blue shift seen in this report cannot be due to the difference in selenium and sulfur precursors as R.Harish, *et al.*, and Gupta and colleagues have proven that regardless of what the QDs is composed of, the absorption of the 3MPA-QDs and chitosan capped 3MPA-QDs is the same. This shift can be attributed to the size reduction in QD size (shown in section 4.8).

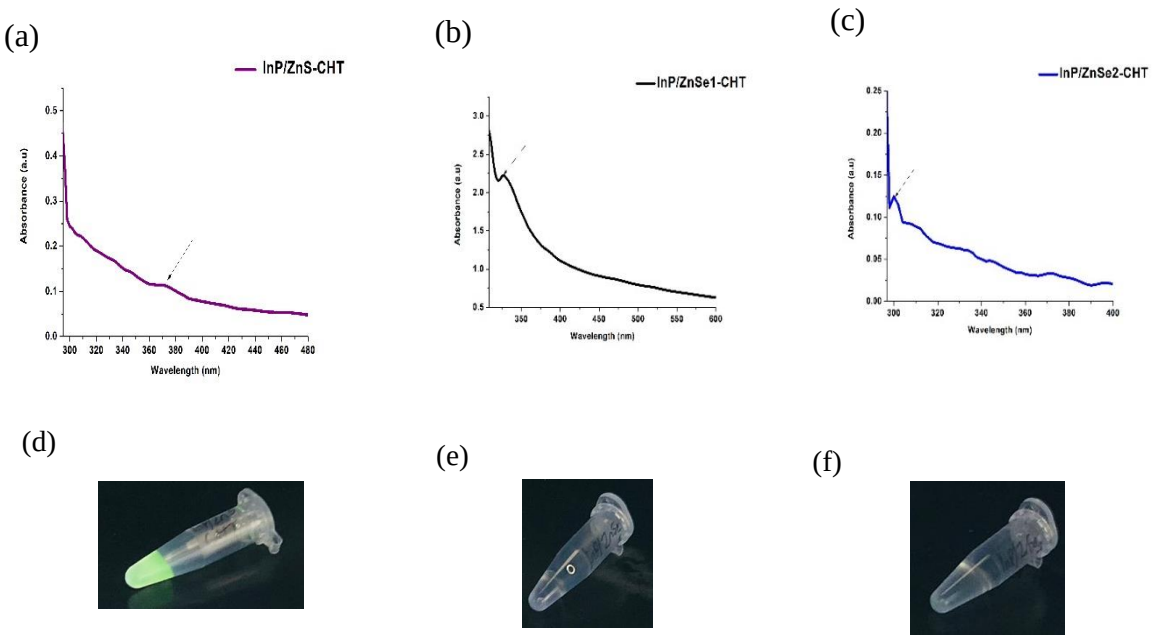

**Figure 4.5.3:** UV-Vis spectra of CHT capped nanocrystals (a) InP/ZnS-CHT, (b) InP/ZnSe1-CHT, (c) InP/ZnSe2-CHT nanocrystals, (d) InP/ZnS-CHT QDs under UV-Vis light, (e) InP/ZnSe1-CHT QDs under UV-Vis light, (f) InP/ZnSe2-CHT QDs under UV-Vis light

## 4.6. Photoluminescence Spectroscopy (PL) characterization of QDs

### 4.6.1. PL analysis of the core/shell QDs

The fluorescent properties of synthesized QDs were evaluated using photoluminescence spectroscopy. Figure 4.6.1 shows the photoluminescence emission spectra of the synthesized QDs. The excitation wavelength was set to 440 nm to test the emission profiles of these QDs, and the emission wavelengths were scanned from 400 nm to 800 nm in 1 nm increments. The PL spectra of InP/ZnS, InP/ZnSe1, and InP/ZnSe2 QDs had an emission peak of 501 nm, 505 nm, and 518 nm respectively. The emitted wavelengths are very close to each other; hence not suitable for the intended multiplex application, because the peaks overlap. Beloglazova, *et al.*, synthesized InP/ZnS QDs with $(DEA)_3P$ that had emission peaks at 609 nm and 560 nm (orange and yellow emitting) using different starting materials (Beloglazova, *et al.*, 2017)**.** Drozd and co-workers also synthesized the same QDs using the same phosphorus precursor and the fluorescence peak of the InP/ZnS QDs was ~ 480 nm (Drozd, *et al.*, 2019). Kim, *et al.*, reported a synthesis of InP/ZnS and InP/ZnSe with PL spectra at 505 nm and 532 nm respectively (Kim, *et al.*, 2019). Here, InP/ZnS QDs emission is still lower compared to InP/ZnSe, the results from this study agree with Kim, *et al.*, findings. The excitation wavelength was not specified for these reports, which renders the report inconclusive, however, would have been interesting.

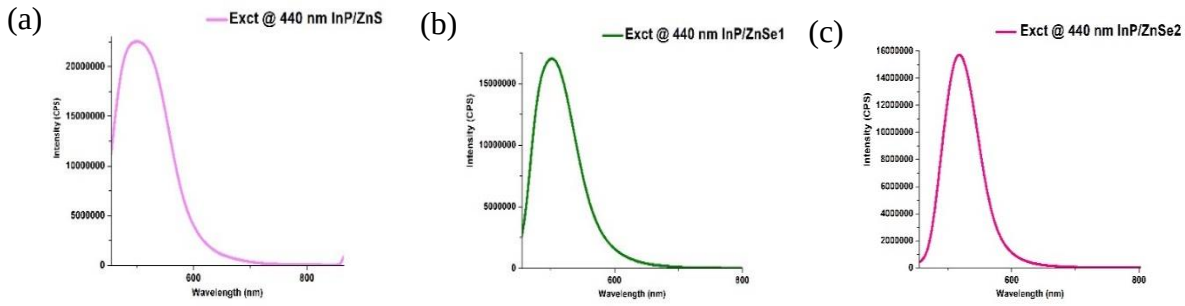


**Figure 4.6.1:** PL spectra of (a) InP/ZnS, (b) InP/ZnSe1, (c) InP/ZnSe2 nanocrystals**.**

### 4.6.2. PL analysis of the 3MPA core/shell QDs

Photoluminescence (PL) spectroscopy results of the QDs-3MPA are shown in Figure 4.6.2. The 3MPA-capped QDs were excited at different wavelengths to investigate emission profiles for possible multiplex applications. The excitation wavelength of 445 nm showed the best peaks for all three QDs as shown below. The emitting wavelengths are 523 nm, 519 nm, and 520 nm for InP/ZnS-3MPA, InP/ZnSe1-3MPA, and InP/ZnSe2-3MPA respectively. The increase in emission wavelength could be attributed to the increase in the excitation wavelength. However, the peaks are very close, which may cause overlap during the multiplex detection application.

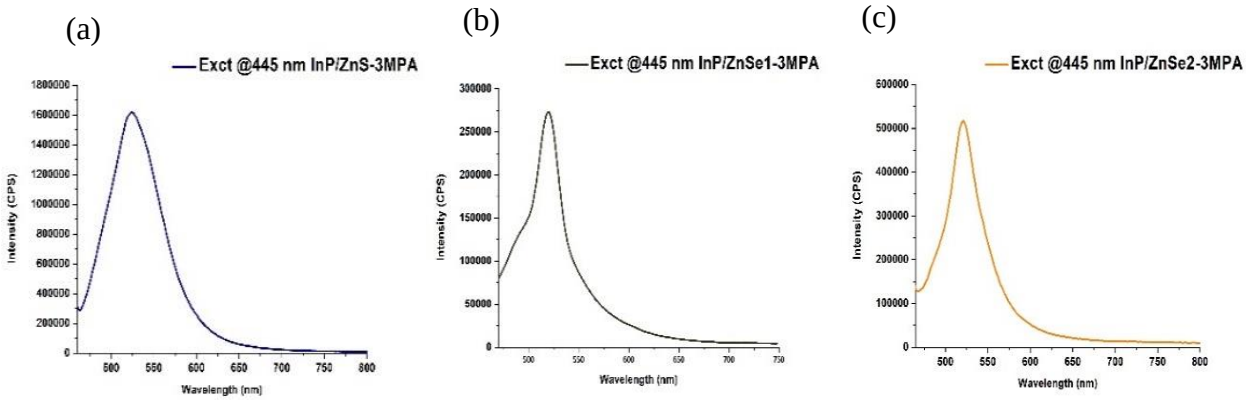


**Figure 4.6.2:** PL of 3MPA capped nanocrystals (a) InP/ZnS-3MPA, (b) InP/ZnSe1-3MPA, and (c) InP/ZnSe2-3MPA.

### 4.6.3. PL analysis of the chitosan core/shell QDs

The fluorescence properties of the QDs - chitosan nanocrystals at different excitation wavelengths were studied. Figure 4.6.3 shows photoluminescence spectroscopy spectra of InP/ZnS-CHT, InP/ZnSe1-CHT, and InP/ZnSe2-CHT excited at 430 nm, 440 nm, and 445 nm as shown in Table 4.6.3. The increase in the excitation wavelength of InP/ZnS-CHT had a slight decrease in the emission wavelength. Since InP/ZnSe1-CHT and InP/ZnSe2-CHT were synthesized using different phosphorus precursors, $(DMA)_3P$ and $(DEA)_3P$ respectively, it can be concluded these tris(dialkylamino) phosphines did not affect the photoluminescence of these QDs-CHT, as Table 3 shows that they had the same emissions at nearly all the excitation wavelengths. The emission wavelength of InP/ZnSe1-CHT and InP/ZnSe2-CHT excited at 445 nm is the same as the wavelength of InP/ZnSe1-3MPA and InP/ZnSe2-3MPA excited at this wavelength. This shows that the PL of 3MPA-capped QDs is the same as the PL of chitosan-

capped 3MPA-QDs. This then agrees with the studies done by R. Harish, *et al.*, and Gupta and colleagues discussed under the UV-Vis studies of chitosan-capped QDs. Therefore, this shows that the fluorescence properties of chitosan-coated 3MPA-QDs have not changed after surface modification with chitosan.

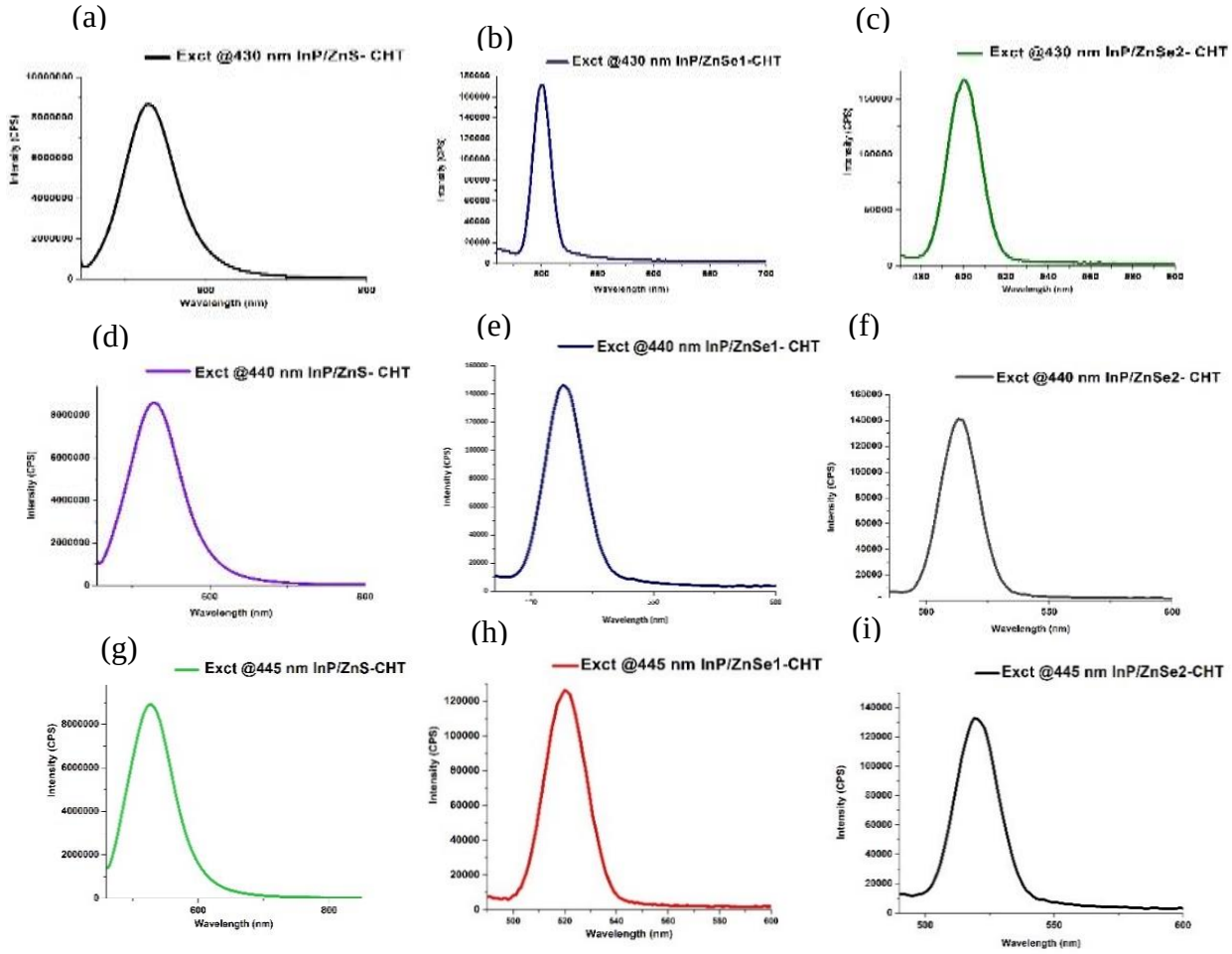


**Figure 4.6.3:** PL spectra of chitosan capped QDs with different excitation wavelengths (a), (b), and (c) InP/ZnS-CHT, InP/ZnSe1-CHT, and InP/ZnSe2-CHT nanocrystals with 430 nm excitation wavelength, (d), (e) and (f) InP/ZnS-CHT, InP/ZnSe1-CHT, and InP/ZnSe2-CHT nanocrystals with 440 nm excitation wavelength, (g), (h) and (i) InP/ZnS-CHT, InP/ZnSe1-CHT, and InP/ZnSe2-CHT nanocrystals with 445 nm excitation wavelength.

**Table 4.6.3:** Summary of chitosan-capped nanocrystal emission wavelengths.

| **QDs** | **Excitation Wavelength (nm)** | | |
|---|---|---|---|
| | 430 | 440 | 445 |
| | **Emission wavelength (nm)** | | |

| | | | |
|---|---|---|---|
| InP/ZnS-CHT | 529 | 528 | 527 |
| InP/ZnSe1-CHT | 500 | 513 | 519 |
| InP/ZnSe2-CHT | 500 | 513 | 520 |

## 4.7. Fourier transform infrared spectroscopy (FTIR) characterization of QDs.

### 4.7.1. FTIR analysis of core/shell and 3MPA core/shell QDs

The FTIR is used to analyse the chemical composition of a material by examining the chemical bonds and compositions presents, The FTIR analysis was used to identify functional groups present in each tested sample. Figure 4.7.1 b, c and d show the FTIR spectra of the QDs, the FTIR spectra of the 3MPA liquid sample used as a capping agent in the first ligand exchange phase, and the FTIR spectra of the 3MPA-capped QDs respectively. Figure 4.7.1 shows the QDs with functional groups after ligand exchange with 3MPA. The FTIR spectrum of InP/ZnS QDs (black curve) in Figure 4.7.1 b shows a peak at 720 cm−1, which is significant for Zn–S (metal sulphide) bond (Baruah, *et al.*, 2019). The characteristic bands at 1634 $cm^{-1}$ and the doublet at 2920 $cm^{-1}$ and 2884 cm -1 correspond to the C– H and the $CH_2$ stretching mode respectively. The N – H bending peak at 1454 $cm^{-1}$ suggests that amines are bound to the surface of the QDs. This strongly suggests that the surface of the QDs was primarily passivated by oleylamine (Fereshteh, *et al.*, 2012). After ligand exchange, these bands disappeared. The region between 3200 – 2700 $cm^{-1}$ shows no O - H peaks, clearly indicating that these QDs are not water-soluble. The 3MPA capped QDs show an O – H peak at 3477 cm-1, 3422 $cm^{-1}$, and 3473 $cm^{-1}$ for InP/ZnS-3MPA, InP/ZnSe1-3MPA, and InP/ZnSe1-3MPA respectively. The FTIR spectra of 3MPA-capped QDs are expected not to show the thiol group (2550 -2600 cm-1) (Hosseini & Pirouz, 2013), as shown in Figure 4.7.1 a, an example of ligand exchange of QDs with 3-mercaptopropionic acid (3MPA) indicating functional groups present in ligand exchange. This picture helps to see how the thiol (SH) functional group is not available after the ligand exchange and hence is not seen in the obtained FTIR spectra of 3MPA-capped QDs. The InP/ZnSe2-3MPA shows the C – H peak at 2929 $cm^{-1}$. The carbonyl group, C =O is present in all the spectra at 1623 $cm^{-1}$, 1627 $cm^{-1}$, and 1624 $cm^{-1}$ for InP/ZnS-3MPA, InP/ZnSe1-3MPA, and InP/ZnSe1-3MPA respectively. These observations confirm that 3MPA was successfully capped on the surface of indium phosphine QDs.

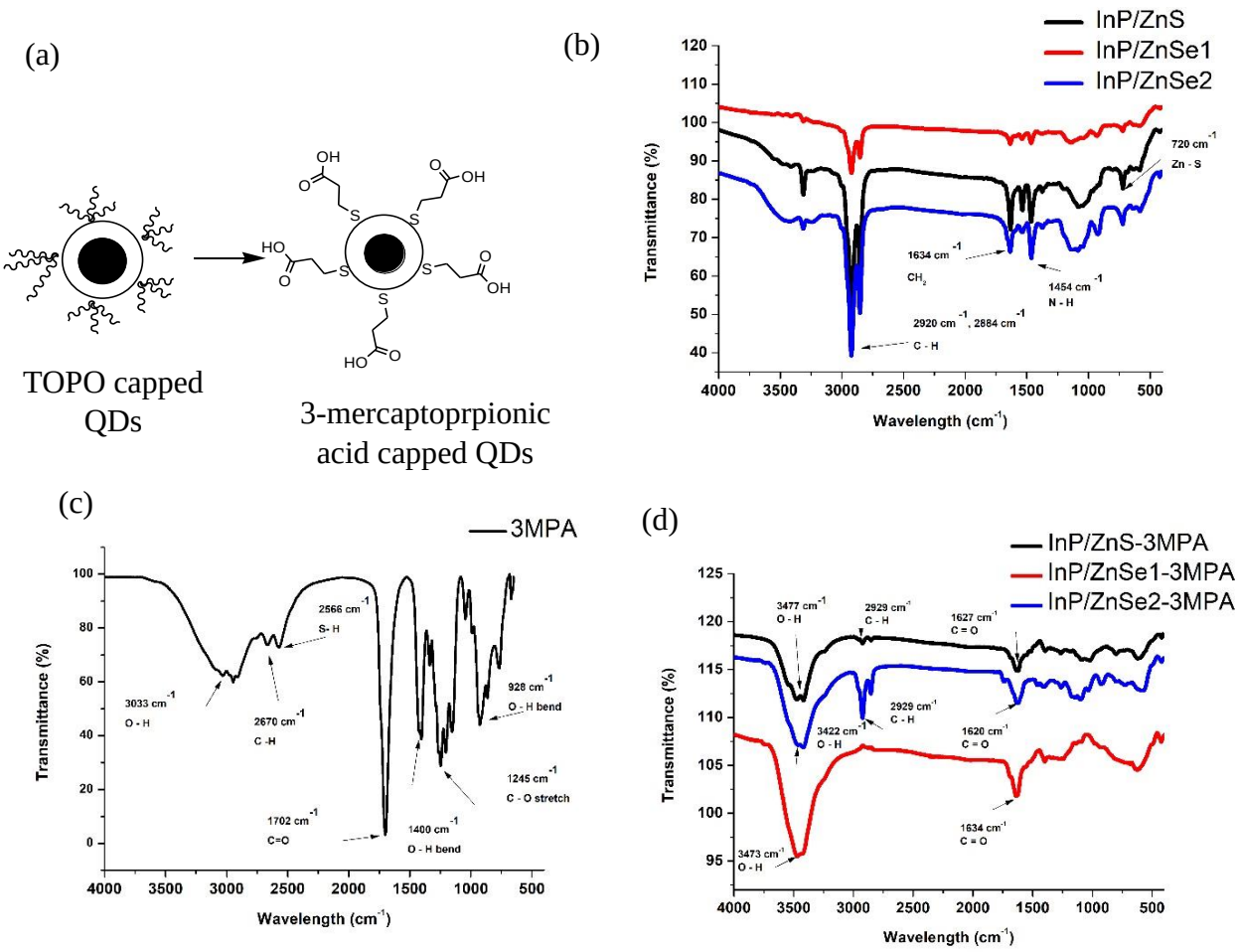


**Figure 4.7.1:** (a) Example ligand exchange of QDs with 3-mercaptopropionic acid (3MPA) (Mazumder, *et al.*, 2009), FTIR spectra of (b) synthesized QDs, (c) 3MPA, and (d) 3MPA capped quantum dots.

### 4.7.2. FTIR analysis of chitosan core/shell QDs

FTIR analysis of chitosan and chitosan/QDs nanocrystals was conducted, and results are given in Figure 4.7.2. Figure 4.7.2 show the attachment functional groups in each step of ligand exchange, from 3MPA to chitosan, giving a clear indication of the expected functional groups. Figure 4.7.2 b shows a comparison between chitosan and InP/ZnS-CHT FTIR spectrums. The band at 1652 $cm^{-1}$ corresponds to an amide group and the band at 1553 $cm^{-1}$ corresponds to an amino group. These bands appear at 1662 $cm^{-1}$ and 1556 $cm^{-1}$ for the amide and amino group respectively on the chitosan FTIR. These groups appeared at 1699 $cm^{-1}$ and 1651 $cm^{-1}$ for amide and amino when Tan *et al.*, prepared CdSe/ZnS-3MPA QDs and encapsulated them with chitosan (Tan, *et al.*, 2007). The alkane stretch is at 2858 $cm^{-1}$ and 2903 cm-1 for InP/ZnS-CHT and chitosan respectively. The hydroxyl stretch is at 3703 $cm^{-1}$ for InP/ZnS-CHT. The

functional groups present in the FTIR spectra of InP/ZnS-CHT prove that the chitosan was successfully capped to the surface of the InP/ZnS-CHT QDs. The black curve in Figure 4.7.2 c shows the FTIR spectra of the chitosan used in this research. phosphorus precursor. The spectra of InP/ZnSe1-CHT and InP/ZnSe2-CHT show peaks at 1630 $cm^{-1}$ and 1487 $cm^{-1}$ that corresponds to the amide and amino functional groups respectively. These peaks have small intensities compared to the chitosan sample due to the small concentration of chitosan in each sample. The hydroxy group at 3442 $cm^{-1}$ for both QD samples. The functional groups present in the FTIR spectra shown in Figure 4.7.2 prove that the chitosan was successfully capped to the synthesized QD. These amino groups may be used to further attach biomolecules to the chitosan nanocrystals (Tan, *et al.*, 2007).

(a)

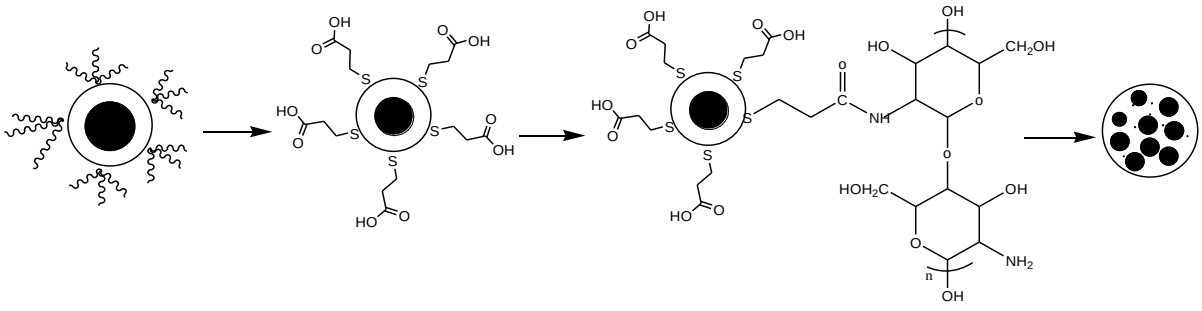

TOPO capped QDs | 3-mercaptoprpionic acid capped QDs | Amide bond formation between chitosan and QDs | Chitosan nanoparticles embedded with QDs

(b)

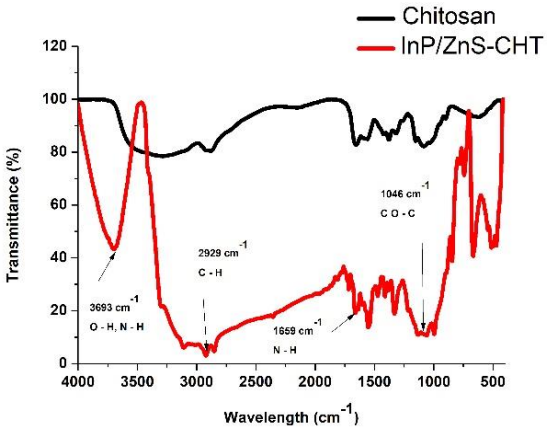


(c)

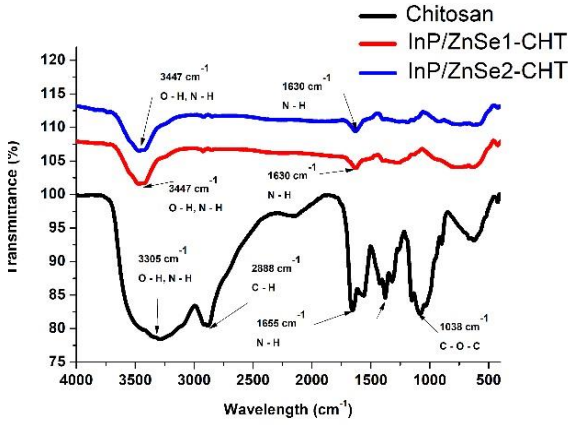


**Figure 4.7.2:** Ligand exchange of QDs with chitosan (Mazumder, *et al.*, 2009), FTIR spectra of (b) InP/ZnS-CHT, (c) InP/ZnSe1-CHT, and InP/ZnSe2-CHT

## 4.8. High-resolution transmission electron microscopy (HRTEM) of characterization of QDs

### 4.8.1. HRTEM analysis of the core/shell QDs

The direct visuals of the sample's atomic structure are provided by the HRTEM photographs. It aids in providing details about the characteristics of the surface, including shape, size, and structure. The average size of the produced QDs was calculated using the HRTEM micrograph and ImageJ software. Figure 4.8.1 shows the HRTEM micrograph and corresponding histogram showing the size distribution of the prepared InP/ZnS, InP/ZnSe1, and InP/ZnSe2 QDs. The size of the QDs was determined by selecting more than five particles at random from the HRTEM image. The InP/ZnS QDs had a size distribution ranging from 2.0 nm – 10.0 nm with an average size of 5.6 nm (Figure 4.8.1 b). The InP/ZnSe1 had a size distribution ranging from 3.5 nm – 7.5 nm with an average size of 5.39 nm (Figure 4.8.1 d) while InP/ZnSe2 QDs had a size distribution ranging from 2.6 nm – 6.0 nm with an average size of 3.60 nm (Figure 4.8.1 e). These are standard sizes found in the literature results. Reid *et al.,* reported a size of 14.1 nm of InP/ZnSe QDs synthesized with $(TMS)_3P$ (Reid, *et al.,* 2018) and Brodu, et al. had an average size of 10.2 ± 0.9 nm of InP/ZnSe QDs synthesized with $(DEA)_3P$ (Brodu, *et al.,* 2018). Brunetti, *et al.,* reported a size of InP/ZnS QDs of 13.4 ± 0.7 nm (Brunetti, *et al.,* 2013), while Massadeh, Xu, & Nann reported a size of 20 nm (Massadeh, *et al.,* 2009). It can be seen that our synthesized nanocrystals are smaller in size compared to those reported by Brodu, *et al.,* Reid *et al.,* and other literature papers which place our nanoparticles above the item. In biological applications, the larger nanocrystals introduce molecular-labelling biases due to steric hindrance and nonspecific binding. Larger QDs may therefore inhibit target labelling in molecularly packed microenvironments like a neural synapse and the cytoplasm, possibly resulting in nonspecific labelling that is not targeted. Physically, smaller probes are desired to increase labelling specificity while reducing bias. Up to now, efforts to reduce the QD hydrodynamic size have mostly concentrated on reducing the size of the organic surface coatings made of ligands and polymers (Le, *et al.,* 2020), therefore our QDs tend to address this from the core.

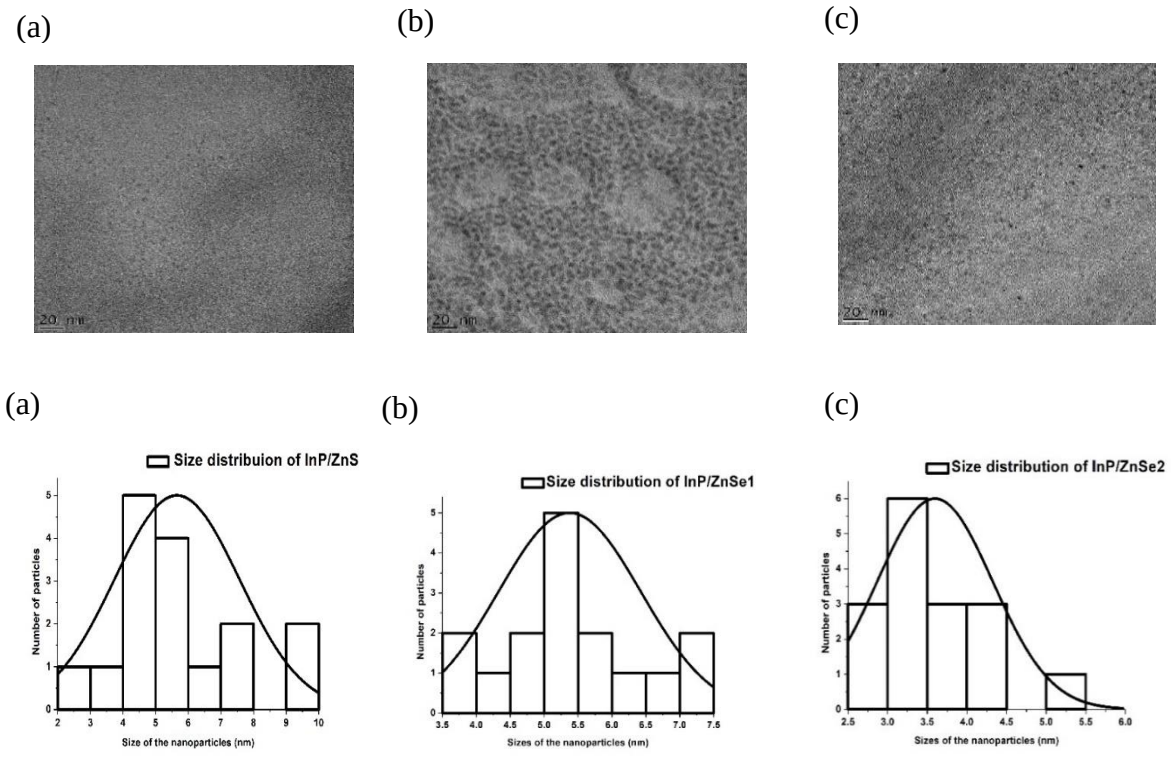


**Figure 4.8.1:** HRTEM micrographs of (a) InP/ZnS, (b) InP/ZnSe1, (c) InP/ZnSe2 QDs and their corresponding size distribution curves (a), (b), and (c).

### 4.8.2. HRTEM analysis of the 3MPA core/shell QDs

The HRTEM micrographs together with ImageJ software were used to estimate the size of the MPA-capped QDs. Figure 4.8.2 shows the HRTEM and size distribution curve of the MPA-capped QDs. Using the size distribution curve, the InP/ZnS-3MPA had a size distribution ranging between 2 - 8 nm with an average size of 4.7 nm. The InP/ZnSe1-3MPA had a size distribution ranging between 1.0 – 4.0 nm with an average size of 2.1 nm, while the InP/ZnSe2-3MPA had a size distribution ranging between 1.0 – 3.5 nm with an average size of 2.3 nm. It can be noticed that the size of these QDs decreased compared to the uncapped QDs. The decrease in the particle size of the 3MPA-capped QDs is due to the quenching of the QDs as the 3MPA is adsorbed onto the surface of these nanocrystals. Light's energy and wavelength are inversely proportional. As a result, the proportionate energy decreases as the wavelength of the emitted colour increases. When it comes to nanoparticle size, as the particle size increases, less energy is released. The decrease in size of these particles can also be attributed to a change in a solvent. The 3MPA QDs were dispersed in a phosphate buffer saline (PBS) solvent of pH 7.4. Acidification of nanoparticles leads to smaller particles (Gorji, *et al.*, 2015). Literature studies reporting 3MPA capped QDs did not include characterization of capped and

uncapped QDs to further discuss the effect of these changes, they only reported the capped QDs leaving room for discussion between capped and uncapped QDs.

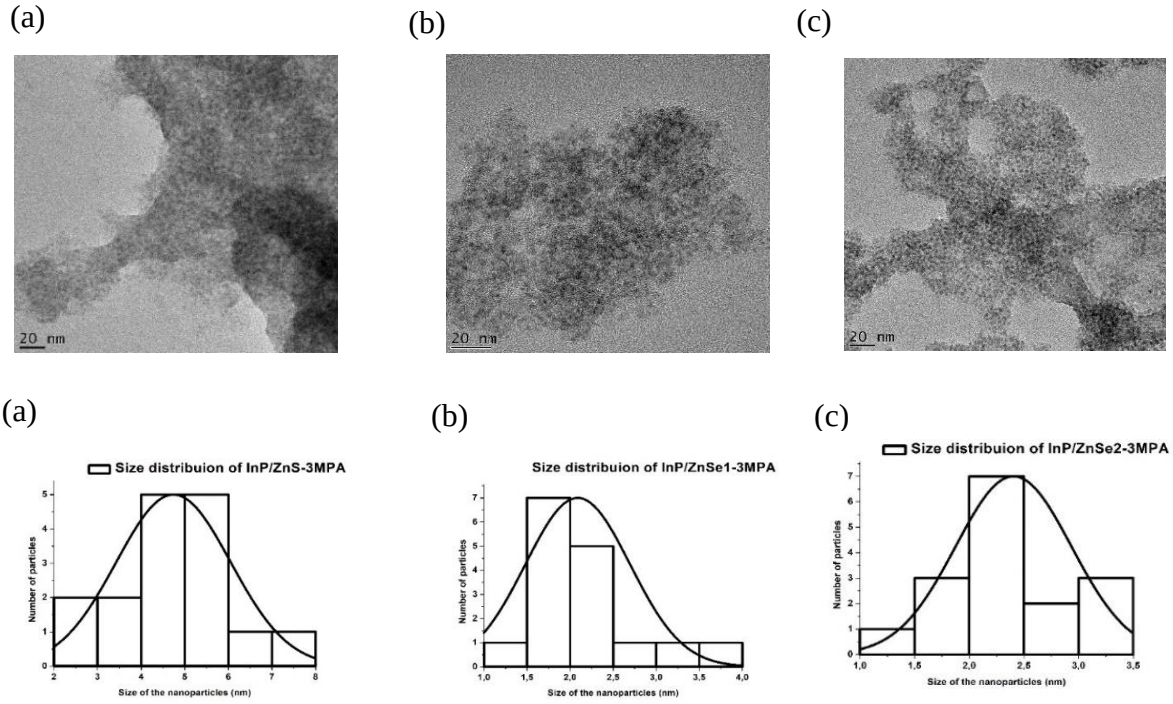


**Figure 4.8.2:** HRTEM micrographs of (a) InP/ZnS-3MPA, (c) InP/ZnSe1-3MPA, (d) InP/ZnSe2-3MPA and their corresponding size distribution curves (a), (b), and (c).

### 4.8.3. HRTEM analysis of chitosan core/shell QDs

Figure 4.8.3 a, b, and c show the HRTEM image of InP/ZnS, InP/ZnSe1, and InP/ZnSe2 capped with chitosan (CHT) with their corresponding size distribution curves. The HRTEM images show that the InP/ZnS, InP/ZnSe1, and InP/ZnSe2 QDs-CHT nanocrystals are spherical in shape. The size is roughly around 4.6 nm, 11.5 nm, and 11.5 nm for InP/ZnS, InP/ZnSe1, and InP/ZnSe2 QDs-CHT respectively. These nanocrystals have a relatively small size compared to the QDs -CHT nanocrystals reported in the literature. Wee bang reported a size of 60 nm for the CdSe/ZnS QDs that were modified with 3MPA and encapsulated with chitosan. Tan *et al.,* prepared CdSe/ZnS -3MPA QDs and capped them with CHT and had a size of 60 nm (Tan, Ning, Huang, & Zhang, 2007). Compared to the CdSe/ZnS-3MPA-CHT nanocrystals reported, the QDs-3MPA-CHT nanocrystals obtained in this report are smaller, which is a positive outcome for the application they were synthesized for. Large nanocrystal size is recommended for single-molecule tracking and counting applications, which demand brilliant, stable, and nonblinking probes to enhance the signal-to-noise ratio for molecular detection and localization at the quickest rate. Physically, smaller probes are desired to increase labelling specificity while

reducing bias. To date, efforts to reduce the QD hydrodynamic size have mostly concentrated on reducing the size of organic surface coatings made of ligands and polymers (Le, *et al.*, 2020).

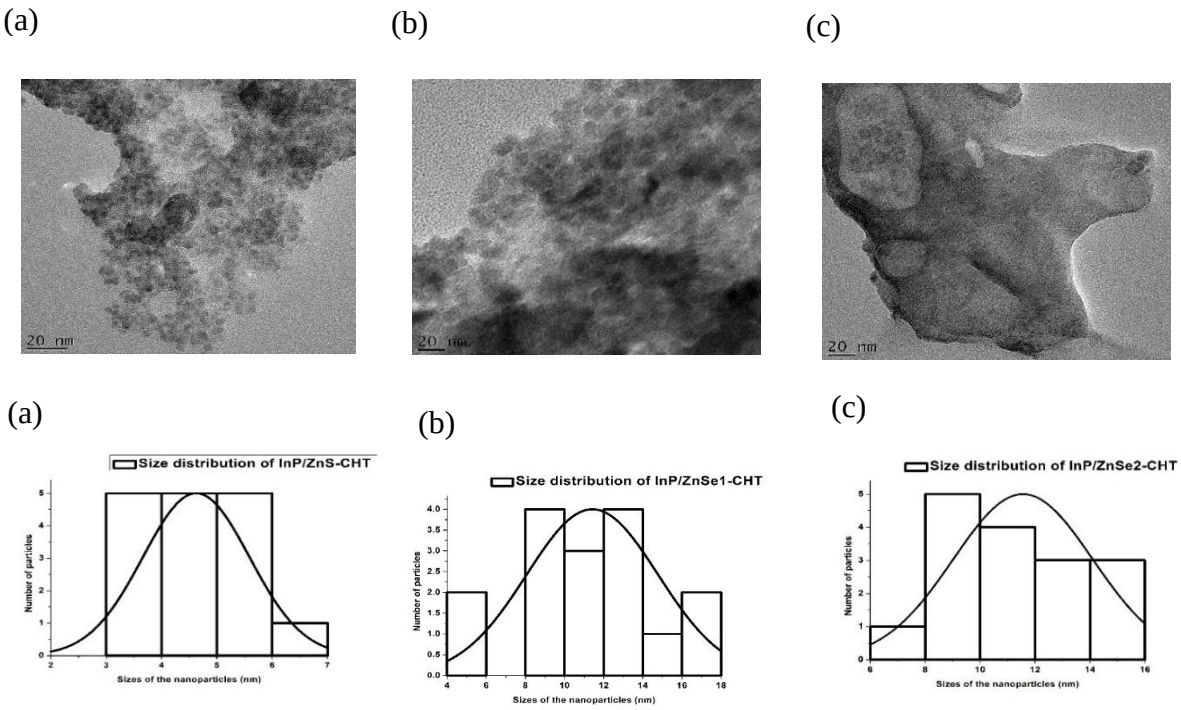


**Figure 4.8.3:** HRTEM pictures of (a) InP/ZnS-CHT, (c)InP/ZnSe1-CHT, and (e) InP/ZnSe2-CHT and their corresponding size distribution curve (a), (b), and (c).

## 4.9. Selected area electron diffraction (SAED) characterization of QDs

### 4.9.1. SAED analysis of the core/shell QDs

The SAED pattern of the synthesized nanocrystals given in Figure 4.9.1 was used to evaluate the sample's crystallographic information and to determine whether they are amorphous, single-crystalline, or polycrystalline. The images of all three synthesized nanocrystals indicate that they are amorphous. This means that these nanocrystals have an irregular pattern of ions, molecules, or atoms, have covalently bonded networks, have a sharp melting point and they are isotropic. Isotropic materials have similar physical properties in all directions because the constituents are arranged in a random manner (no ordered structure) (PSIBERG Team, 2022). The SAED images were analysed using ImageJ software. The rings present in each image were measured giving the radius and d-spacing of each ring present in the SAED image. Table 4.9.1 represents the data retrieved. The SAED image of InP/ZnS has three rings that correspond to 4.337, 1.844, and 1.099 Å respectively. Panzer, *et al.*, reported a synthesis of InP/ZnS QDs where the XRD pattern showed miller indices of (111), (220), and (311) (Panzer, *et al.*, 2017).

Baek, *et al.*, also reported XRD results of the synthesized InP/ZnS QDs. Their results stated that InP/ZnS core/shell QDs had miller indices of (111), (220), and (311) which were likely due to the strain at the interface between InP core and ZnS shell (Baek, *et al.*, 2018). Zhang, *et al.*, said these XRD diffraction peaks of InP/ZnS had 28.20°, 47.50°, and 51.2° angles as shown in Figure 4.9.1 d, the red curve (Zhang, *et al.*, 2020). Therefore, the three d-spacing values of InP/ZnS obtained in this study can be attributed to (111), (220), and (311) hkl values reported in the literature. Zhao, *et al.*, reported XRD results of InP/ZnSe synthesized QDs with miller indices of (111), (220), and (311) as shown in Figure 4.5.4 e, the blue curve (Zhao, *et al.*, 2021).

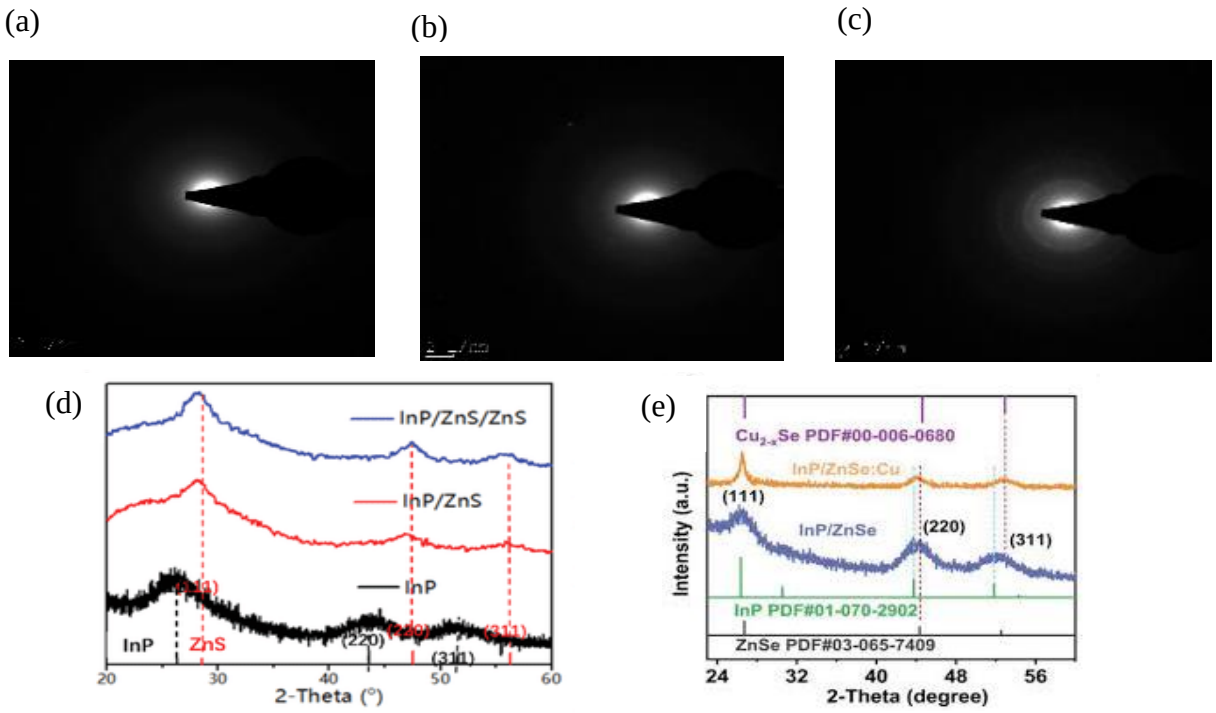


**Figure 4.9.1:** SAED pattern of (a) InP/ZnS, (c) InP/ZnSe1, (e) InP/ZnSe2 QDs, (d) XRD of InP/ZnS (Zhang, *et al.*, 2020), and (e) XRD of InP/ZnSe (Zhao, *et al.*, 2021).

**Table 4.9.1:** Size and d-spacing of Indium-phosphide QDs

| QDs | r (nm) | d- spacing (Å) |
|---|---|---|
| InP/ZnS | 0,433 | 4,337 |
| | 0,184 | 1,844 |
| | 0,109 | 1,099 |
| | | |
| InP/ZnSe1 | 0,195 | 1,947 |
| | 0,105 | 1,053 |
| | | |
| InP/ZnSe2 | 0,334 | 3,336 |
| | 0,204 | 2,043 |
| | 0,177 | 1,768 |
| | 0,112 | 1,118 |

### 4.9.2. SAED analysis of 3MPA core/shell QDs

The SAED picture of 3MPA-capped QDs is shown below. These capped QDs are amorphous same as the uncapped QDs. The rings here are clearer or more visible compared to the uncapped QDs and also increased in number. Table 4.9.2 shows the radius and the d-spacing of the rings in each sample. The fact that there was a difference in the pictures of capped and uncapped QDs means that 3MPA was successfully immobilized on the surface of the QDs. With little to nothing with research on core/shell, 3MPA capped one cannot fully discuss or compare miller indices to literature work.

(a) (b) (c)

**Figure 4.9.2:** SAED of (a) InP/ZnS-3MPA, (b) InP/Znse1-3MPA and (c) InP/Znse2-3MPA

**Table 4.9.2:** Size and d-spacing of 3MPA-capped QDs

| QDs | r (nm) | d- spacing (Å) |
|---|---|---|
| InP/ZnS-3MPA | 0,292 | 2,915 |
| | 0,194 | 1,942 |
| | 0,159 | 1,587 |
| | 0,111 | 1,108 |
| InP/ZnSe1-3MPA | 0.004 | 0.049 |
| | 0.003 | 0.036 |
| | 0.002 | 0.0204 |
| InP/ZnSe2-3MPA | 0.318 | 3.181 |
| | 0.201 | 2.013 |
| | 0.171 | 1.708 |
| | 0.130 | 1.301 |
| | 0.110 | 1.109 |

### 4.9.3. SAED analysis of chitosan core/shell QDs

The SAED pattern of chitosan capped QDs is shown below in Figure 4.7.5. The crystallinity of InP/ZnS-CHT and InP/ZnSe2-CHT is amorphous while InP/ZnSe1-CHT is polycrystalline due to the presence of multiple dots in the SAED pattern. The presence of rotating stacking faults in the measured area is shown by these dots. This results from domain boundaries where domains intersect and have various crystallographic orientations, back folding of edges, inherent rotational stacking defects, overlapping domains, or other factors. (Kumar, *et al.*, 2018).

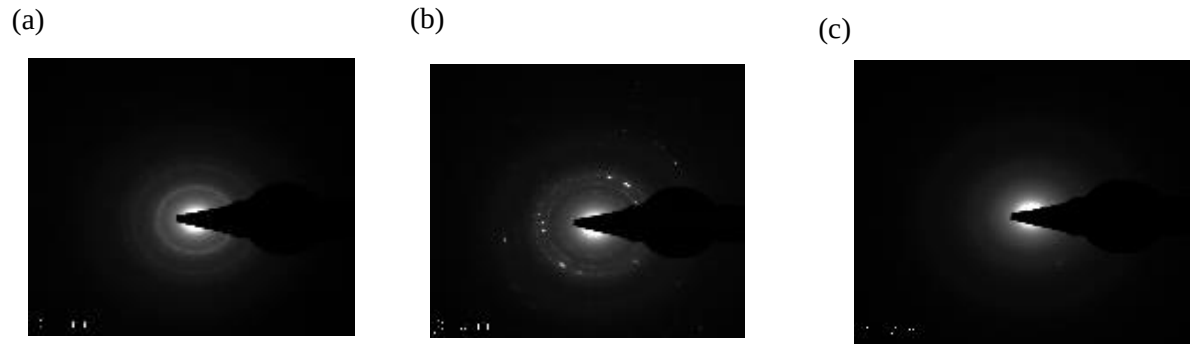


**Figure 4.9.3:** SAED of (a) InP/ZnS-CHT, (b) InP/ZnSe1-CHT and (c) InP/ZnSe2-CHT

**Table 4.9.3:** Size and d-spacing of chitosan-capped QDs

| QDs | r (nm) | d- spacing (Å) |
|---|---|---|
| InP/ZnS-CHT | 0,314 | 3,142 |
| | 0,184 | 1,841 |
| | 0,161 | 1,609 |
| | | |
| InP/ZnSe1-CHT | 0,031 | 0,317 |
| | 0,025 | 0,246 |
| | 0,017 | 0,171 |
| | 0,011 | 0,111 |
| | | |
| InP/ZnSe2-CHT | 0,286 | 2,851 |
| | 0,176 | 1,758 |
| | 0,109 | 1,088 |

## 4.10. Energy dispersive spectroscopy (EDS) analysis

### 4.10.1. EDS of the quantum dots

The EDS spectrum of the synthesized nanocrystals is shown in Figure 4.10.1. The EDS helps to show the elements present in a given sample. The EDS of these nanocrystals is expected to show indium, phosphine, zinc, and sulfur (for InP/ZnS), selenium (for InP/ZnSe-based QDs), and some elements from the starting materials used during the preparation. The EDS of InP/ZnS (Figure 4.10.1 a) shows phosphine, zinc, sulfur, and bromine from one of the starting materials $ZnBr_2$ indicating that this reactant did not react completely. Figure 4.10.1 b shows zinc and phosphine from the expected elements. Bromine is from one of the starting materials $ZnBr_2$ indicating that this reactant did not react completely. Whereas, Figure 4.10.1 c shows zinc, selenium, phosphine from the expected elements, and bromine. The missing peaks of indium and selenium from spectrums can be accounted for because these elements have a concentration below 0.01 wt.% that is not detected by this instrument (Nasrazadani & Hassani, 2016). The carbon and copper peaks visible to both spectrums can be accounted to the carbon-copper grid used when analysing samples. Figures 4.10.1 b and c show unexpected peaks of sodium and oxygen due to possible contamination in the sample.

(a)

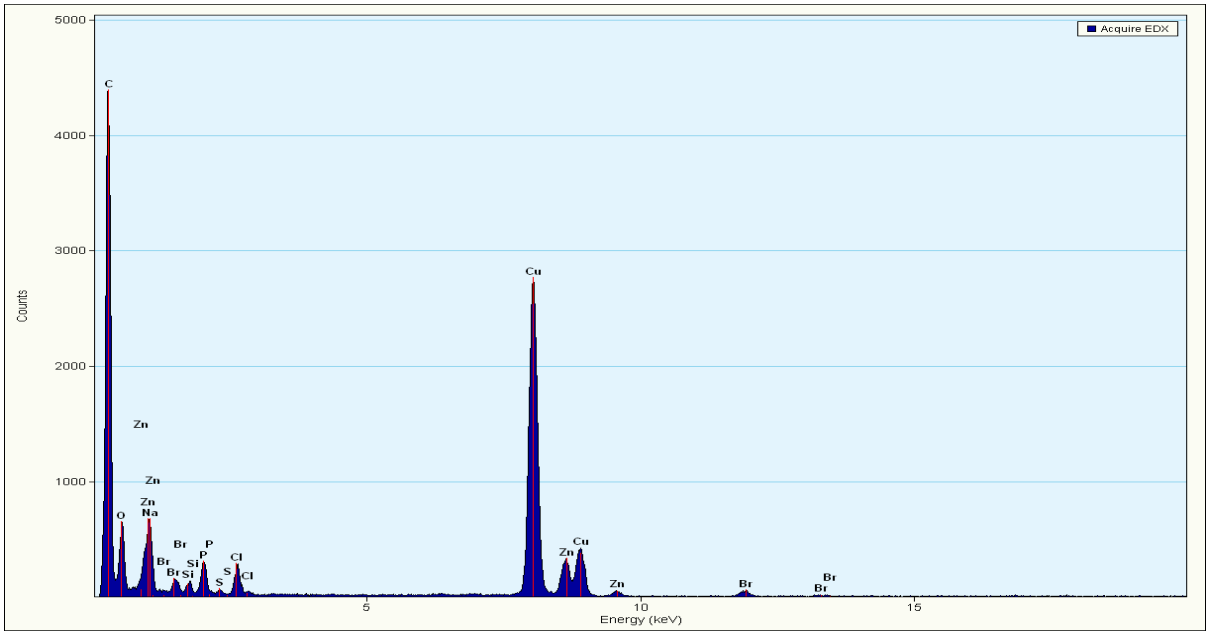
Acquire EDX
Counts
Energy (keV)
C
Zn
O
Na
Br
Si
P
S
Cl
Cu

(b)

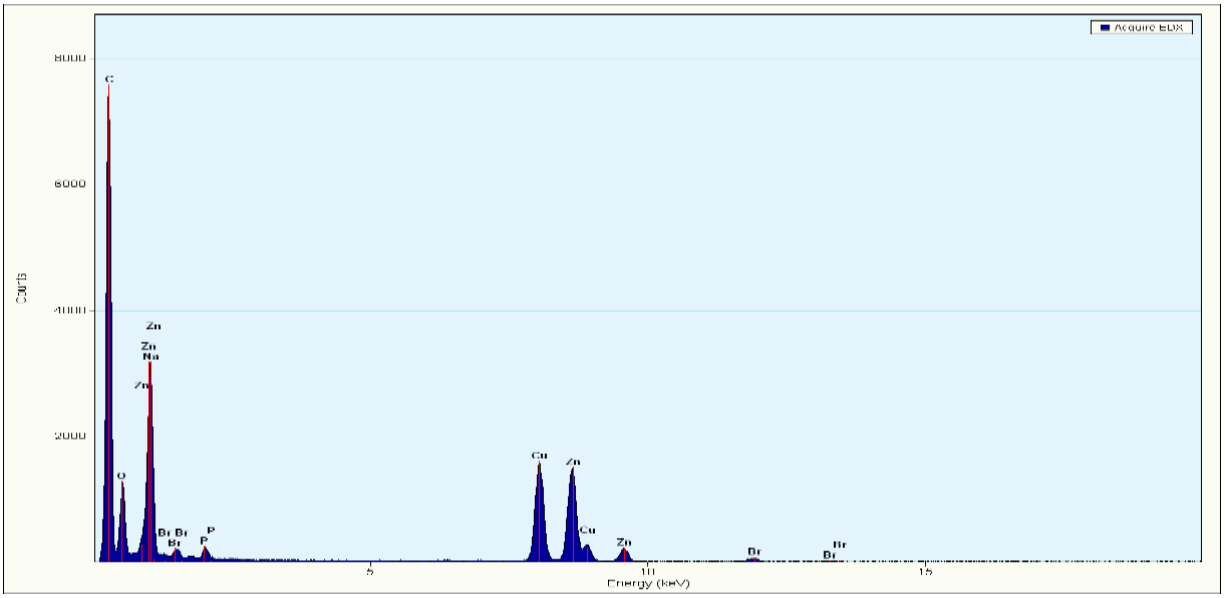
Acquire EDX
Counts
Energy (keV)
C
Zn
Na
O
Br
P
Cu

(c)

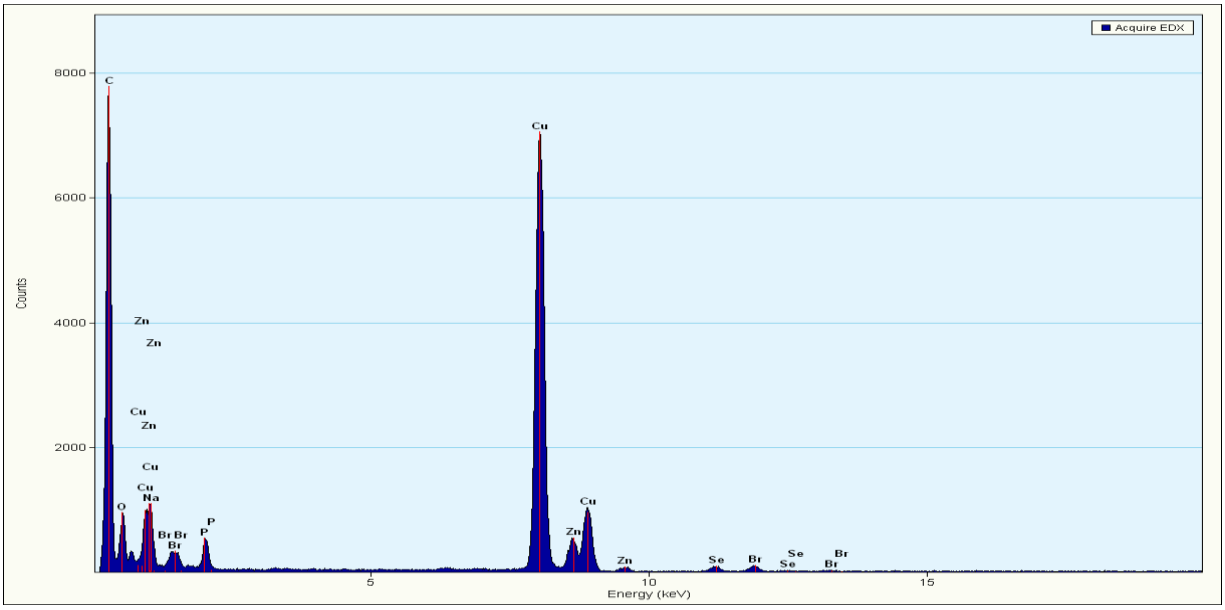
Acquire EDX
Counts
Energy (keV)
C
Cu
Zn
O
Na
Br
P
Se

**Figure 4.10.1:** Energy dispersive spectroscopy spectrum for (a) InP/ZnS, (c) InP/ZnSe1, (e) InP/ZnSe2 QDs.

### 4.10.2. EDS of the 3MPA quantum dots

The energy dispersive spectroscopy (EDS) spectrum of the 3MPA-capped QDs is shown in Figure 4.10.2. The EDS of these nanocrystals is expected to show indium, phosphine, zinc, and sulfur (for InP/ZnS-3MPA), selenium (for InP/ZnSe2-3MPA based QDs), and some elements from the starting materials used during the preparation. The EDS of InP/ZnS-3MPA (Figure 4.6.6 a) shows indium, phosphine, zinc, and sulfur as expected. Same the EDS spectrum of InP/ZnSe1-3MPA and InP/ZnSe2-3MPA show indium, phosphine, zinc, and selenium as expected. The oxygen, chlorine, silicon, and potassium elements in the EDS spectrum of InP/ZnS-3MPA are due to some impurities/ contamination in the sample. The InP/ZnSe2-3MPA spectrum only shows chlorine and oxygen as a contaminant. The carbon and copper present in both spectra are due to the carbon-copper grid used during the analysis of the samples.

(a)

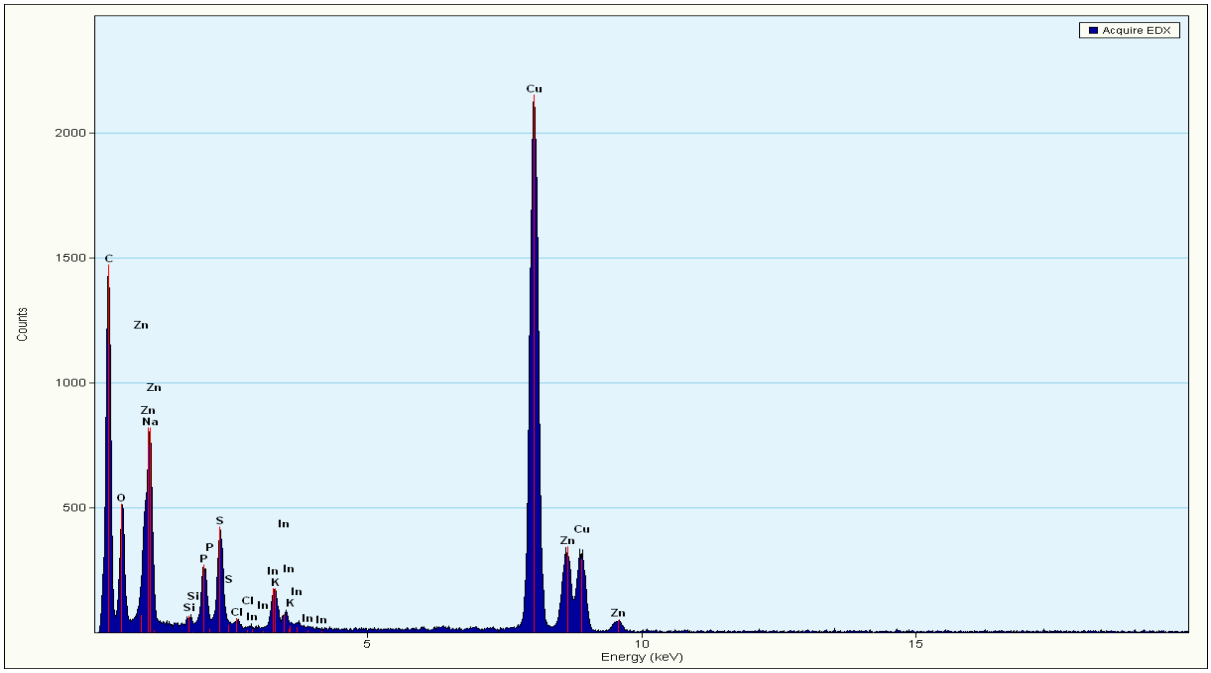

(b)

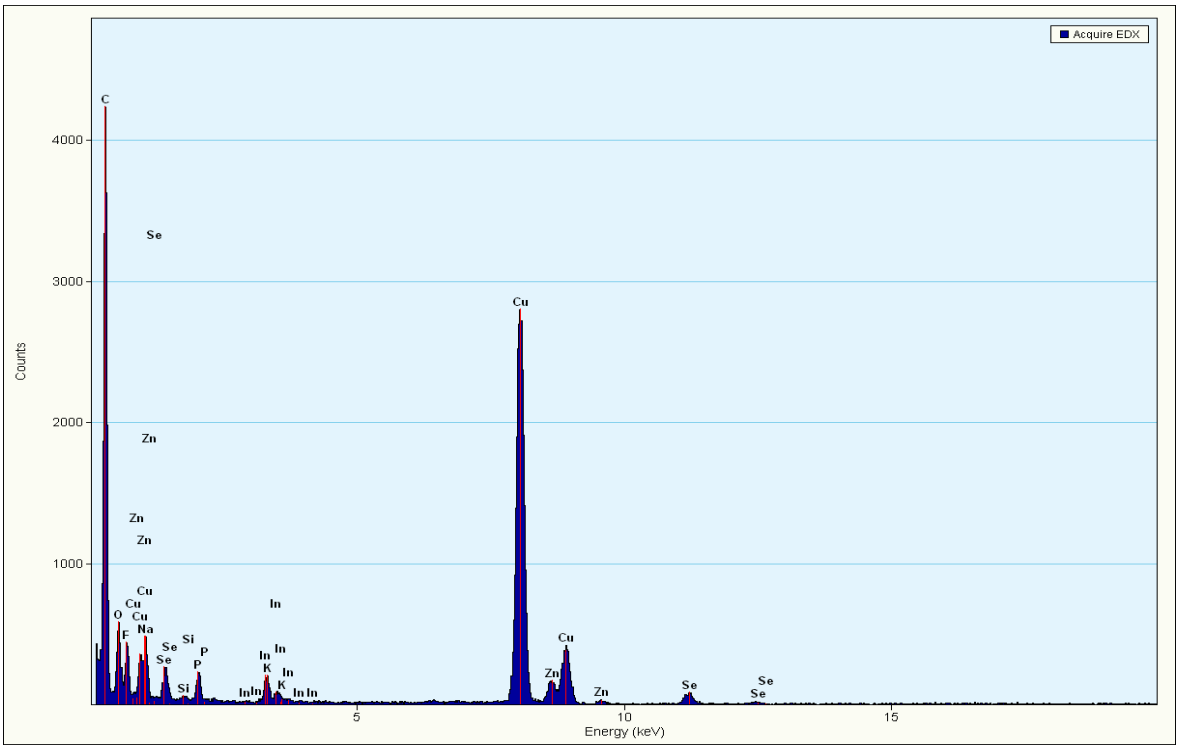


(c)

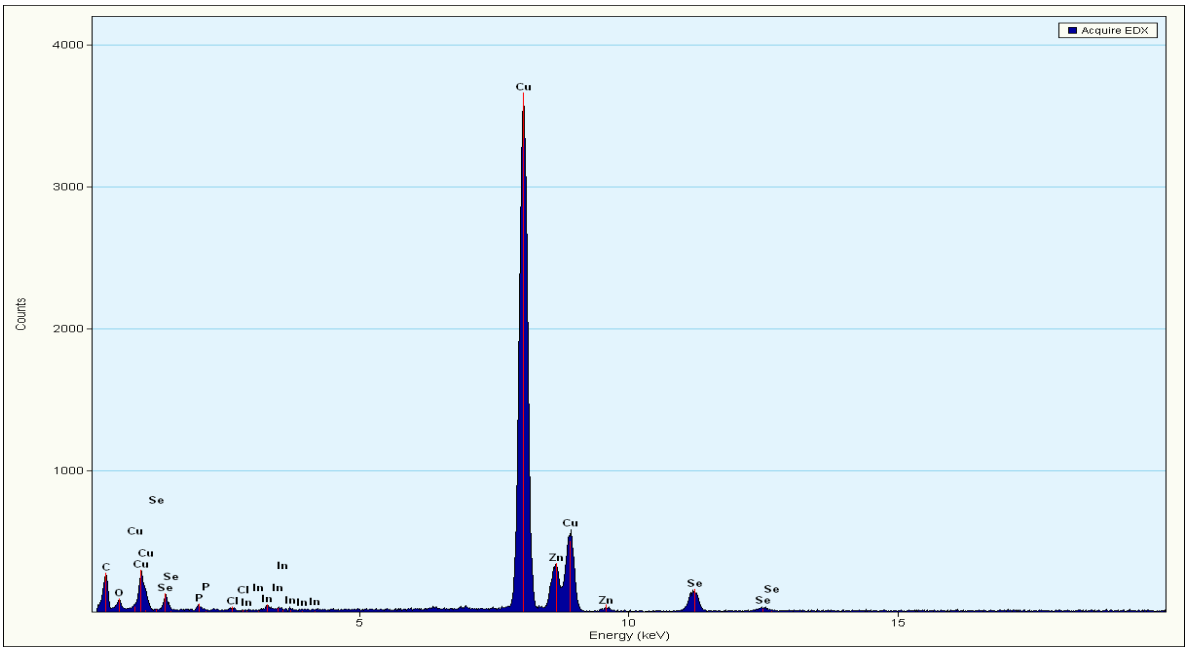


**Figure 4.10.2:** EDS spectra of (a) InP/ZnS-3MPA, (b) InP/ZnSe1-3MPA, and (c) InP/ZnSe2-3MPA QDs.

### 4.10.3. EDS of the chitosan quantum dots.

The chemical composition of the synthesized QDs - CHT nanocrystals was evaluated using EDS. Figure 4.10.3 a, b, and c show the EDS spectra of InP/ZnS-CHT, InP/ZnSe1-CHT, and

InP/ZnSe2-CHT respectively. The spectra of these nanocrystals are expected to show indium, phosphine, zinc, sulfur (InP/ZnS - CHT), and selenium (for InP/ZnSe1-CHT, and InP/ZnSe2-CHT). The InP/ZnS - CHT spectra show all the expected elements present in the sample (Figure 4.6.7 a). InP/ZnSe1-CHT spectra have selenium and sulfur only from the expected elements (Figure 4.10.3 b). While InP/ZnSe2-CHT has indium, phosphine, and selenium (Figure 4.10.3 c). The missing element can be attributed to the fact that EDS analysis only takes images on the focused region of a sample, such that the possibility that a specific chosen region for analysis was not stirred well enough to be uniform before analysis or the particles in the sample were scattered. Also, these elements may have a small concentration such that EDS was not able to pick them. The unexpected elemental peaks such as silicon, oxygen, sodium, and potassium are due to impurities present in the nanocrystal. The presence of copper and carbon in each spectrum is due to the carbon-copper grid used when analysing the samples.

(a)

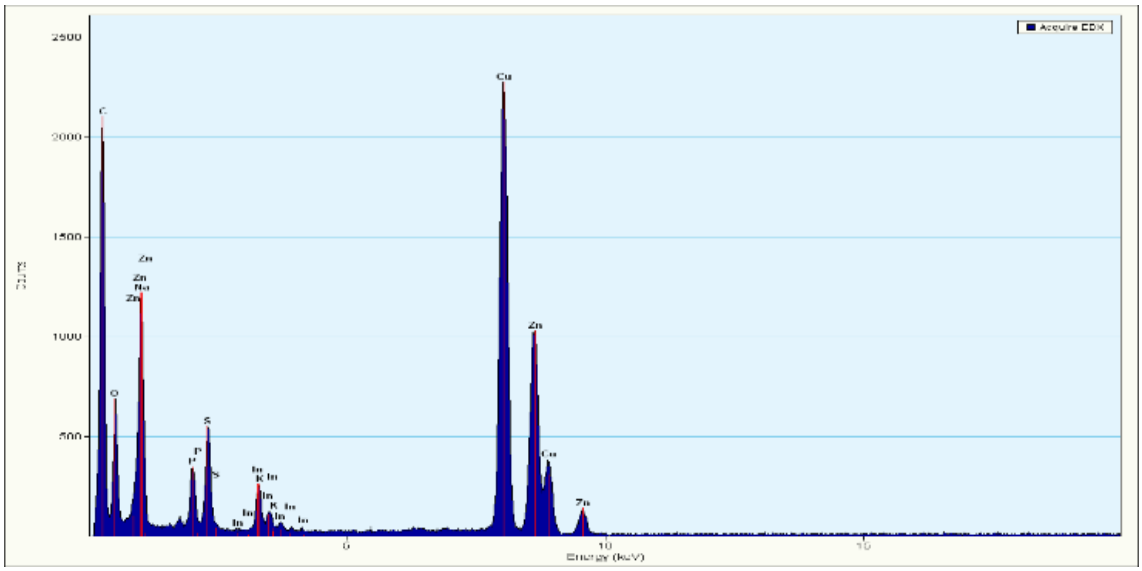


(b)

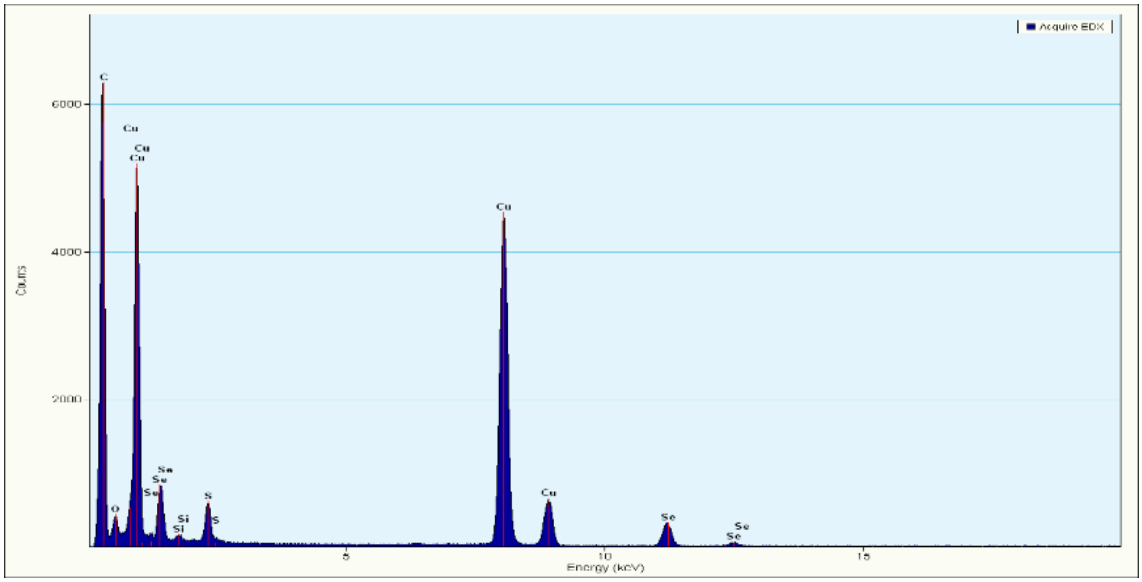

(c)

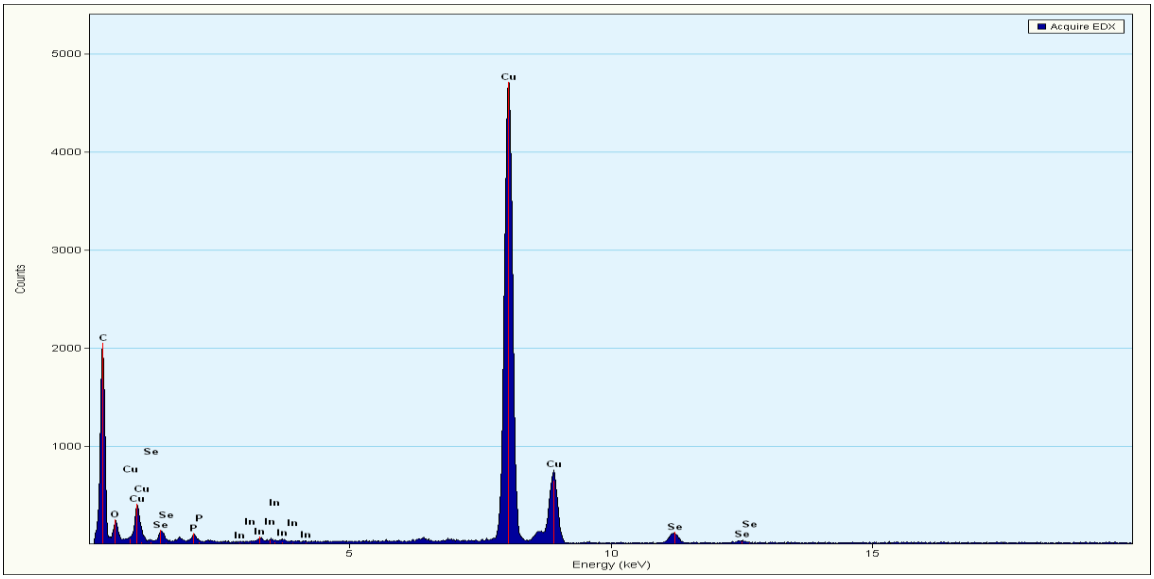


**Figure 4.10.3:** Energy dispersive spectroscopy spectrum for (a) InP/ZnS-CHT, (b) InP/ZnSe1-CHT, (c) InP/ZnSe2-CHT QDs.

## 4.11. Biocompatibility of Quantum dots

QDs have many applications, but in biomedical applications they can serve as drug delivery, therapeutic and most importantly as bioimaging agents (Thovhogi, *et al.*, 2018, Kiplagat, *et al.*, 2016). Their success in this application relies solely in their biocompatibility, especially if they will be used *in vivo* or in humans. Therefore, different synthesis methods and capping of the surface of the QDs have been extensively studied (Kiplagat, *et al.*, 2016), Mushonga, et al., 2013, Zikalala, *et al.*, 2022) . In this venture, the InP-based QDs were reported to be less toxic when compared to the cadmium-based QDs, and that capping the QDs core with biomolecules such as proteins, peptides, polymers, etc.; can enhance the QDs biocompatibility (Mushonga, *et al.*, 2013, Nikazar, *et al.*, 2020). Previous attempts to improve biocompatible of QDs in our laboratory resulted in synthesis and scale-up of water soluble InP/ZnSe (Kiplagat, *et al.*, 2016, Mushonga, et al., 2013). The InP/ZnSe demonstrated dose-dependent cell reduction on non-cancerous human breast (MCF-12A) cell lines, and cytotoxicity on KMST-6 cells at 50 µM (Kiplagat, *et al.*, 2016). In the current study, InP/ZnS-based QDs were synthesized and capped with 3MPA and CHT to improve their biocompatibility. The effects of the six QD variants were investigated on human colon cancer (Caco-2) cells, human non-cancer skin fibroblast (KMST-6) cells and normal rat cardiomyocytes (H9C2) cells using the MTT assay. The working principle behind MTT is that, the tetrazolium salt will be reduced to purple formazan

by metabolically active cells, hence the intensity of the absorption of the dye at 570 nm reflects the number of live cells (Lin, *et al.*, 2012).

The cells were exposed to 0.5mg/ mL of the QDs and their response to the treatments was evaluated after 24 hours. Of the six QDs, InP/ZnS-3MPA and InP/ZnS-CHT showed non-selective cytotoxicity to both normal and cancer cells. Of interest, the InP/ZnS-3MPA/CHT QDs did not show any toxicity towards the normal (KMST-6 and H9C2) cell lines. In fact, an increase in the cell viability was observed which indicated that these QDs can potentially be used in humans without inducing any toxicity to normal cells. In addition to their safety profile, InP/ZnSe2-CHT was able to reduce Caco-2 cell viability to 85%, suggesting that these QDs might also have anti-cancer properties. Other studies also reported on the potential anti-cancer activities of QDs, among others the MPA-capped ZnSe(S) QDs at 36ppm were able to reduce prostate cancer cell viability by 50% after 24 h treatment (Calderón-Ortiz, *et al.*, 2018).

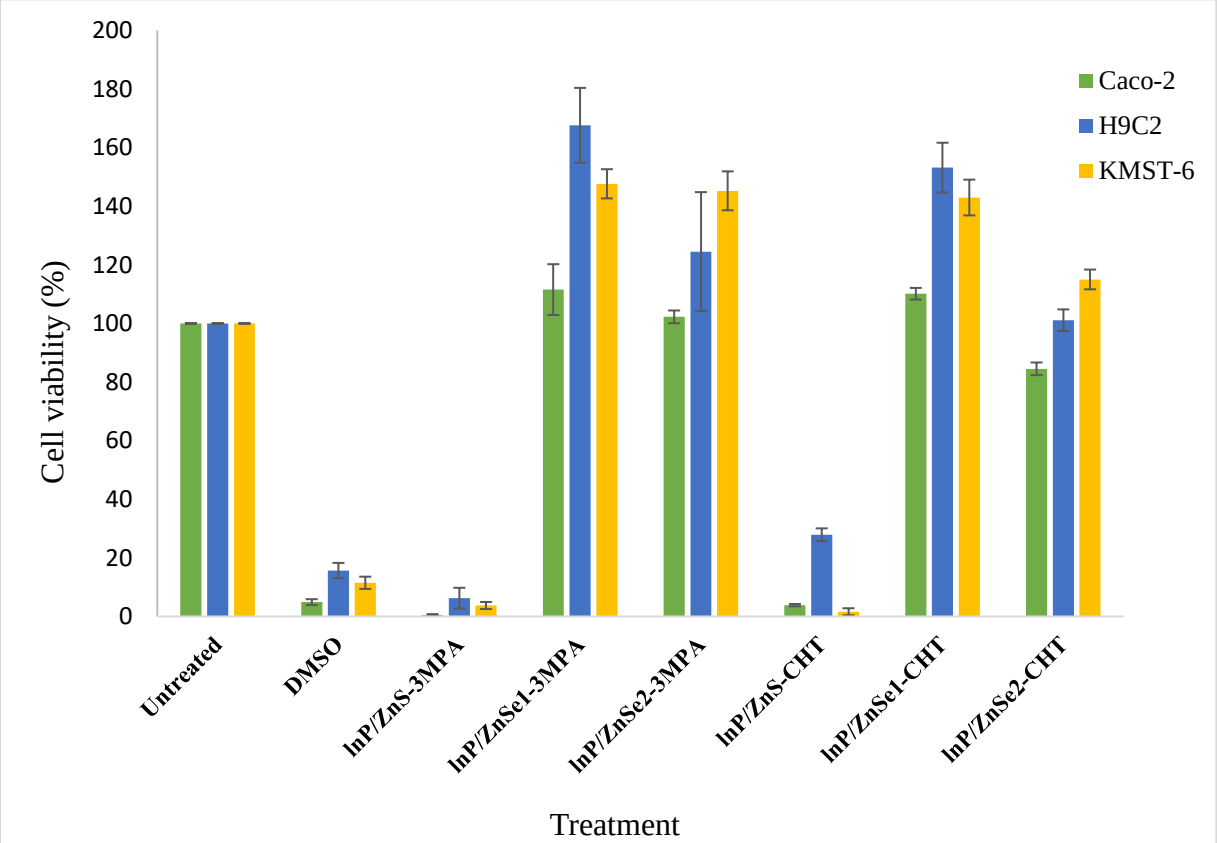


**Figure 11:** Effects of QDs on the cell viability. The cell viability of Caco-2, H9C2 and KMST-6 cells was analysed using the MTT assay. Cells were treated with QDs at 0.5mg/ mL for 24 hours, 6% DMSO was used as a positive control. Results represent one experiment with each

treatment performed in triplicate. A two-way ANOVA test was used to analyse statistical significance and considered statistically significant at $p \leq 0.05$ when compared to the untreated sample. ** = $p \leq 0.01$, *** = $p \leq 0.001$ and **** = $p \leq 0.0001$.

In this study, InP/ZnS-3MPA and InP/ZnS-CHT showed significant toxicity to the cells which was passivated when different sources of phosphorus precursors were used. Using $(DMA)_3P$ and $(DEA)_3P$ (phosphine precursors) in the synthesis of the QDs not only prevented toxicity of the QDs but also generated a biological interesting activity of enhancing cell growth, a widely sought for property in wound healing. Also interesting was the fact that the capping of InP/ZnSe2 with CHT was also able to reduce cancer cell growth while at the same time increasing cell viability on the normal cells, this suggests that these QDs can be used simultaneously as both bioimaging and anti-cancer agents. Thus, more studies are warranted to explore the interesting bioactivities demonstrated by these QDS viz: bioimaging, wound healing and anticancer activities.

The flexibility of QDs to load drugs biomolecules on their surface is especially appealing in medicine and can be exploited for multiplexing; where disease-targeting moieties (such as antibodies, aptamers, etc) or therapeutic agents can be attached to improve drug targeting (Thovhogi, *et al.,* 2018, Nikazar, *et al.,* 2020). By so doing, the bystander effects associated with the conventional therapies can be minimized. Furthermore, drug targeting and drug response can be monitored in real time through the photoluminescence and fluorescent properties of the QDs. However, a lot of work still needs to be done before the QDs can be translated into clinically viable systems.

## 4.12. References


Adeoye, M. D. *et al.,* 2009. Effect of solvents on the electronic absorption spectra of 9,14 dibenzo (a, c) phenazine and tribenzo (a, c, i) phenazine. *Scientific Research and Essay,* pp. 107-111.

Aldana, J., Wang, Y. A. & Peng, X., 2001. Photochemical Instability of CdSe Nanocrystals Coated by Hydrophilic Thiols. *J. Am. Chem. Soc.*, p. 8844–8850.

Allen, P., Walker, B. & Bawendi, M., 2010. Mechanistic insights into the formation of InP quantum dots. *Angewandte Chemie,* pp. 760-762.

Ayabei, K., 2016. Fabrication of luminescent nanocomposites for diagnosis of breast cancer. *UWC Library,* pp. 1-218.

Baek, J. *et al.,* 2018. Multistage Microfluidic Platform for the Continuous Synthesis of III–V Core/Shell Quantum Dots. *Angew. Chem.,* pp. 11081-11084.

Baruah, J. M., Kalita, S. & Narayan, J., 2019. Green chemistry synthesis of biocompatible ZnS quantum dots (QDs) their application as potential thin flms and antibacterial agent. *International Nano Letters,* pp. 1-12.

Beloglazova, N. V. *et al.,* 2017. Fluorescently labelled multiplex lateral flow immunoassay based on cadmium-free quantum dots. *Methods,* pp. 141-148.

Biju, V., Itoh, T. & Ishikawa, M., 2010. Delivering quantum dots to cells: bioconjugated quantum dots for targeted and nonspecific extracellular and intracellular imaging. *Chem.Soc. Rev,* p. 3031–3056.

Brodu, A. *et al.,* 2018. Exciton Fine Structure and Lattice Dynamics in InP/ZnSe Core/Shell Quantum Dots. *ACS Photonics,* p. 3353–3362.

Brunetti, V. *et al.,* 2013. InP/ZnS as a safer alternative to CdSe/ZnS core/shell quantum dots: in vitro and in vivo toxicity assessment. *Nanoscale,* pp. 307-317.

Calderón-Ortiz, E. R. *et al.,* 2018. Evaluation of ZnSe(S) Quantum Dots on the Cell Viability of Prostate Cancer Cell (PC3). *Journal of Electronic Materials,* p. 4361–4365 .

Calvo, P., Remuñán-López, C., Vila-Jato, J. L. & Alonso, M. J., 1998. Novel hydrophilic chitosan-polyethylene oxide nanoparticles as protein carriers. *J. Appl. Polym. Sci.,*, pp. 125-132..

Chandrasekaran, V. *et al.,* 2017. Nearly Blinking-Free, High-Purity Single-Photon Emission by Colloidal InP/ZnSe Quantum Dots. *Nano.Lett,* pp. 6104-6109.

Chandrasiri, H. B., Kim, E. B. & Snee, P. T., 2020. Sterically Encumbered Tris(trialkylsilyl) Phosphine Precursors for Quantum Dot Synthesis. *Inorg. Chem,* p. 15928–15935.

Chan, W. C. W. & Nie, S., 1998. Quantum Dot Bioconjugates for Ultrasensitive Nonisotopic Detection. *Science* , pp. 2016-2018.

Chen, D. *et al.,* 2009. Temperature dependence of "elementary processes" in doping semiconductor nanocrystals. *J Am Chem Soc.*

Drozd, D. *et al.,* 2019. Silanization of quantum dots: Challenges and perspectives. *Talanta,* Volume 205.

Fereshteh, Z. *et al.,* 2012. Synthesis of Nickel Oxide Nanoparticles from Thermal Decomposition of a New Precursor. *Journal of Cluster Science,* pp. 578-583.

Gary, D. C., Glassy, B. A. & Cossairt, B. M., 2014 . Investigation of indium phosphide quantum dot nucleation and growth utilizing triarylsilylphosphine precursors. *Chemistry of Materials,* p. 1734–1744.

Gorji, S. G., Gorji, E. G. & Mohammadifar, M. A., 2015. Effects of pH on turbidity, size, viscosity and the shape of sodium caseinate aggregates with light scattering and rheometry. *Journal of Food Sci and Technol,* pp. 1820-1824.

Grigel, V. *et al.,* 2016. InAs Colloidal Quantum Dots Synthesis via Aminopnictogen Precursor Chemistry. *J. Am. Chem. Soc,* pp. 13485-13488.

Gupta, J. *et al.,* 2022. An electrochemical study of the binding interaction between chitosan and MPA-CdSe QDs for the development of biocompatible theranostic nanoprobe. *Journal of Molecular Liquids,* Volume 358.

Hosseini, M. s. & Pirouz, A., 2013. Study of fluorescence quenching of mercaptosuccinic acid-capped CdS quantum dots in the presence of some heavy metal ions and its application to Hg(II) ion determination. *Luminescence* , pp. 798-804.

Jeong, D.-W.*et al.,* 2019. Influence of interface defects on the optical properties of InP/ZnS quantum dots by low temperature synthesis of InP core. *Applied Surface Science,* pp. 757-760.

Jo, J.-H.*et al.,* 2020. InP-Based Quantum Dots Having an InP Core, Composition-Gradient ZnSeS Inner Shell, and ZnS Outer Shell with Sharp, Bright Emissivity, and Blue Absorptivity for Display Devices. *ACS Appl. Nano Mater.,* p. 1972–1980.

Kim, Y. *et al.,* 2019. Bright and Uniform Green Light Emitting InP/ZnSe/ZnS Quantum Dots for Wide Color Gamut Displays. *ACS Appl. Nano Mater,* p. 1496–1504.

Kiplagat, A. *et al.,* 2016. The cytotoxicity studies of water-soluble InP/ZnSe quantum dots. *Journal of Nanoparticle Research,* pp. 1-12.

Kumar, S., Aziz, S. T., Girshevitz, O. & D.Nessim, G., 2018. One-Step Synthesis of N-Doped Graphene Quantum Dots from Chitosan as a Sole Precursor Using Chemical Vapor Deposition. *J.Phys.Chem.C,* pp. 2343-2349.

Laufersky, G. *et al.,* 2018. Unraveling Aminophosphine Redox Mechanisms for Glovebox-free InP Quantum Dot Syntheses. *Nanoscale,* pp. 1-11.

Le, P. *et al.,* 2020. Optimizing Quantum Dot Probe Size for Single-Receptor Imaging. *ACS Nano.,* p. 8343–8358..

Li, H., Jia, C., Meng, X. & Li, H., 2019. Chemical synthesis and applications of colloidal metal phosphide nanocrystals. *Frontiers in chemistry,* p. 625.

Lin, J.-J., Lin, W.-C., Dong, R.-X. & Hsu, h.-h., 2012. The cellular responses and antibacterial activities of silver nanoparticles stabilized by different polymers.. *Nanotechnology,* pp. 1-13.

Liu, P. *et al.*, 2021. Green InP/ZnSeS/ZnS Core Multi-Shelled Quantum Dots Synthesized with Aminophosphine for Effective Display Applications. *Adv. Funct. Mate,* pp. 1-7.

Massadeh, S., Xu, S. & Nann, T., 2009. Synthesis and Exploitation of InP/ZnS Quantum Dots for Bioimaging. *Proceedings of SPIE - The International Society for Optical Engineering.*

Micic, O. I. *et al.*, 1995. Synthesis and Characterization of InP, GaP, and GaInP2 Quantu Dots. *J. Phys. Chem,* p. 7754–7759.

Mocatta, D. *et al.*, 2011. Heavily doped semiconductor nanocrystal quantum dots. *Science,* 332(6025), pp. 77-81.

Mushonga, P., Onani, M. O., Madiehe, A. M. & Meyer, M., 2013. One-pot synthesis and characterization of InP/ZnSe semiconductor. *Materials Letters,* pp. 37-39.

Nasrazadani, S. & Hassani, S., 2016. Modern analytical techniques in failure analysis of aerospace, chemical, and oil and gas industries. *Handbook of Materials Failure Analysis with Case Studies from the Oil and Gas Industry,* pp. 39-54.

Nikazar, S. *et al.*, 2020. Revisiting the cytotoxicity of quantum dots: an in-depth overview. *Biophys Rev,* pp. 703-718.

Nurul, A. L., Mohd, N. Z. & Mahendran, A. L. S., 2018. Chapter 20 - Engineered Nanomaterial in Electronics and Electrical Industries. *Handbook of Nanomaterials for Industrial Applications,* pp. 324-364.

Panzer, R. *et al.*, 2017. Versatile Tri(pyrazolyl)phosphanes as Phosphorus Precursors for the Synthesis of Highly Emitting InP/ZnS Quantum Dots. *Angew. Chem. Int. Ed,* p. 14737 –14742.

PSIBERG Team, 2022. [Online] Available at: https://psiberg.com/amorphous-vs-crystalline-solids/

R.Harish, *et al.*, 2020. Cytotoxicity assessment of chitosan coated CdS nanoparticles for bio-imaging applications. *Applied Surface Science.*

Reid, K. R. *et al.*, 2018. Chemical Structure, Ensemble and Single-Particle Spectroscopy of Thick-Shell InP–ZnSe Quantum Dots. *Nano Lett.*, pp. 709-716.

Sapsford, K. E., Pons, T., Medintz, I. L. & Mattoussi, H., 2006. Biosensing with Luminescent Semiconductor Quantum Dots. *Sensors* , pp. 925-953.

Tan, W. B., Ning, Huang & Zhang, Y., 2007. Ultrafine biocompatible chitosan nanoparticles encapsulating multi-coloured quantum dots for bioapplications. *Journal of Colloid and Interface Science,* pp. 464-470.

Tessier, M. D. *et al.*, 2015. Economic and Size-Tunable Synthesis of InP/ZnE (E= S, Se) Colloidal Quantum Dots.. *Chem. Mater.*, pp. 4893- 4898.

Tessier, M. D. *et al.*, 2016. Aminophosphines: A Double Role in the Synthesis of Colloidal Indium Phosphide Quantum Dots. *J. Am. Chem. Soc.*, pp. 5923-5929.

Thovhogi, N. *et al.*, 2018. Peptide-functionalized quantum dots for potential applications in the imaging and treatment of obesity. *Int J Nanomedicine,* pp. 2551-2559.

U.Jadhao, N. & B.Naik, A., 2017. Effect of electronegativity on structural; spectrophotometric and thermo-chemical properties of fluorine and chlorine substituted isoxazols by DFT method. *Cogent Chemistry.*

Woo-Seuk, S. *et al.,* 2013. Amine-derived synthetic approach to color-tunable InP/ZnS quantum dots with high fluorescent qualities. *Journal of Nanoparticle Research,* p. 1–10.

Yu, P. *et al.,* 2022. Highly efficient green InP-based quantum dot light-emitting diodes regulated by inner alloyed shell component. *Light Science & Applications,* 11(162).

Zhang, W. *et al.,* 2020. InP/ZnS/ZnS Core/Shell Blue Quantum Dots for Efficient Light-Emitting Diodes. *Adv. Funct. Mater.,* pp. 1-9.

Zhao, H. *et al.,* 2021. Role of Copper Doping in Heavy Metal-Free InP/ZnSe Core/Shell Quantum Dots for Highly Efficient and Stable Photoelectrochemical Cell. *Adv. Energy Mater,* pp. 1-10.

Zikalala, N., Parani, S. & Oluwafemi, O. S., 2022. Aqueous synthesis of Zn-based ternary core/shell quantum dots with excellent stability and biocompatibility against different cell lines. *Journal of Materials Science,* p. 6780–6789.

# Chapter 5: Conclusion and recommendations

## 5.1.Conclusion

Non-cadmium-based QDs were successfully synthesized using one -pot hot injection method. Two different phosphorus precursors were used where InP/ZnS was synthesized with tris(diethylamino)phosphine and InP/ZnSe was synthesized with tris (dimethyl amino) phosphine and tris(diethylamino)phosphine giving InP/ZnSe1 and InP/ZnSe2 respectively. They were further made water soluble by capping them with 3MPA. To render them more stable and less toxic, for the first time, the indium phosphide-based QDs were further capped with chitosan.to confirm and monitor the synthesis as well as determine the physicochemical properties such as shape, size, distribution, etc, various characterization methods were employed. The UV-Vis analysis showed that the synthesized QDs had absorption wavelengths between 448 nm and 474 nm with InP/ZnSe2 having the highest absorption. The 3MPA capped had absorption between 300 nm and 374 nm, which was an expected blue shift compared to the core/shell QDs as the 3MPA molecule quenched the QD's fluorescence. The chitosan capped had absorption between 300 nm and 371 nm, which was also an expected blue shift as this polymer was only being attached to the 3MPA. This polymer is bulky, so it is bound to block lighter than 3MPA. The PL studies of 3MPA and chitosan QDs showed the same emission wavelengths at the same excited wavelengths. The FTIR showed all the expected functional groups in each surface modification step. The uncapped QDs showed no OH group in the region of 3200-2700 cm 1, proving that they are not water-soluble. The 3MPA was successfully attached by showing no thiol functional and proving that the QDs are hydrophilic with OH peaks. The important functional groups for chitosan attachment are amide and amino groups. The amide and amino functional group were at 1652 $cm^{-1}$ and 1553 $cm^{-1}$ for InP/ZnS-CHT respectively, InP/ZnSe1-CHT and InP/ZnSe2-CHT showed these peaks at 1630 $cm^{-1}$ and 1487 cm-1. We never obtained any data for XRD even though the samples were sent for analysis. The InP/ZnS QDs had a size of 5,6 nm, the size decreased as 3MPA, and chitosan was added to 4.7 nm and 4.6 nm respectively. The InP/ZnSe QDs synthesized with $(DMA)_3P$ had a size of 5,4 nm and the ones synthesized with $(DEA)_3P$ had a size of 3,6 nm. When 3MPA was added the size decreased and when chitosan was added the size increased. The InP/ZnSe-based QDs were similar in size in all stages, meaning that the phosphorus precursor had no significant impact on the physicochemical properties of the synthesized InP/ZnSe QDs.

All of the synthesized QDs' physicochemical characteristics were successfully determined, and then the MTT assay was used to assess their cytotoxic activities. The MTT results showed that InP/ZnS-3MPA and InP/ZnS-CHT based QDs were not toxic to normal cell lines (KMST-6 and H9C2). These QDs may be utilized in humans without endangering healthy cells, according to an improvement in cell viability that was seen. InP/ZnSe2-CHT was able to reduce Caco-2 cell viability to 85%, indicating that these QDs might also have anti-cancer effects in addition to their safety profile.

### 5.2.Recommendations

- To synthesize the InP core at different temperatures to investigate the optical properties.
- Fabrication of indium-based QDs should be focused on employing tris (dialkylamino)phosphines as phosphorus precursors. Also, further, investigate their effect on parameters such as optical properties and particle size.
- We recommend doing XRD in the future to further have a concrete discussion of the particle size and the sample's crystallography.
- To do cytotoxicity studies of the synthesized QDs within a month to prevent precipitation of the particles which could lead to toxic NPs.

### 5.3.Future work

- To synthesize the QDs making 3MPA a reagent instead of a capping agent.
- To do surface modification of chitosan at different concentrations to further test the cytotoxicity effects.
- To monitor the pH values of QDs before and after surface modification to study the effects of pH and also to understand the factors that take play in the change of values during characterization.
- To do surface modification with other polymers such as gelatin.
- To work with different shells such as ZnO, and ZnTe instead of the commonly used ones (ZnS and ZnSe).
- The synthesis of InP/ZnS using $(DMA)_3P$ was not done due to the limitation of TOP which was needed for sulfur precursor preparation. In the future, this need to be done so that a thorough discussion of the effect of $(DMA)_3P$ and $(DEA)_3P$ can be expanded.